EMR TEST FACILITIES
EVALUATION OF REVERBERATING CHAMBER LOCATED AT RADC, GRIFFISS AFB ROME, NEW YORK

Myron L. Crawford
Galen H. Koepke
John M. Ladbury

National Bureau of Standards
U.S. Department of Commerce
Boulder, Colorado 80303-3328

December 1987

NBSIR 87-3080

EMR TEST FACILITIES EVALUATION OF REVERBERATING CHAMBER LOCATED AT RADC, GRIFFISS AFB ROME, NEW YORK

Myron L. Crawford
Galen H. Koepke
John M. Ladbury

Electromagnetic Fields Division
Center for Electronics and Electrical Engineering
National Engineering Laboratory
National Bureau of Standards
Boulder, Colorado 80303-3328

December 1987

Sponsored by
Compatibility and Measurements Division
RADC/RBC
Griffiss AFB, New York 13441

U.S. DEPARTMENT OF COMMERCE, C. William Verity, Secretary

NATIONAL BUREAU OF STANDARDS, Ernest Ambler, Director

CONTENTS

LIST OF FIGURES AND TABLES

Electromagnetic Radiation Test Facilities
Evaluation of Reverberating Chamber
Located at RADC, Griffiss AFB, Rome, New York

Myron L. Crawford
Galen H. Koepke
John M. Ladbury

Electromagnetic Fields Division
National Bureau of Standards
Boulder, Colorado 80303

This report describes measurement procedures and results obtained from evaluating the reverberating chamber facility located at the Rome Air Development Center (RADC), Griffiss Air Force Base, Rome, New York. The facility was developed by the RADC for use in measuring and analyzing the electromagnetic susceptibility/vulnerability (EMS/V) of weapon systems and the shielding effectiveness of enclosures and shielding materials. A brief description of the facility, including the instrumentation used for performing its evaluation and calibration by the National Bureau of Standards (NBS), is given. Measurements described include: (1) evaluation of the chamber's transmitting and receiving antennas' voltage standing wave ratios; (2) measurement of the chamber's insertion loss or coupling efficiency versus frequency; (3) measurement of the chamber's tuner effectiveness; (4) determination of the E-field uniformity in the chamber's test zones versus frequency; (5) determination of the absolute amplitude calibration of the test E-fields in the chamber based upon the reference antenna's received power measurements and calibrated dipole probe antenna measurements; (6) comparison of reference standard equipment under test (EUT) responses to test fields established inside the RADC reverberating chamber and the NBS anechoic chamber; and (7) evaluation of the performance characteristics of the reverberating chamber excited by pulsed rf at selected discrete frequencies as a function of pulse width (0.2 - 20 μs) and the chamber's quality factor (Q). Conclusions indicate that the chamber can be used at frequencies down to approximately 150 MHz for cw testing and, for rf pulsed immunity testing with pulse widths as short as 0.3 μs by using rf absorber loading. Immunity testing to pulsed rf fields however has some inherent limitations that are discussed in the report. Estimates of the cw measurement uncertainties derived empirically from the test results are given .

Key words: electromagnetic radiated susceptibility/vulnerability measurements; reverberating chamber.

1.0 Introduction

The use of a reverberating chamber for performing EMS/V measurements is relatively new. Considerable work has been done in the past to evaluate and document methods for using this technique [1-4]. Recently, research work has been done at the National Bureau of Standards (NBS) to carefully evaluate, develop (when necessary), describe, and document the methodology for performing radiated susceptibility/vulnerability (EMS/V) measurements using a reverberating chamber. This effort is described in an NBS publication, NBS TN 1092, and IEEE Proceedings review paper [5,6]. In addition, preliminary work was performed to evaluate the time domain response characteristics of a reverberating chamber with the purpose of determining the feasibility of using such a chamber for pulsed rf immunity testing. This work was published as a progress report to the sponsor [7] dated January 1987. Included as an appendix to the report was a paper, "Preliminary evaluation of a reverberation chamber method for pulsed rf immunity testing " [8], which gives a brief discussion of the theoretical concepts pertinent to the effort.

The incentive for performing this work stems from numerous advantages suggested for the use of a reverberating chamber. These include:

1. Electrical isolation from or to the external environment;
2. Accessibility (indoor test facility);
3. Ability to generate high level fields efficiently over large test volumes;
4. Broad frequency coverage;
5. Cost effectiveness;
6. Potential use for both radiated susceptibility and emission testing with minor instrumentation changes;
7. No requirement of physical rotations of the equipment under test (EUT); and
8. Security.

These advantages are somewhat offset by limitations, which include loss of polarization and directivity information relative to the EMC/EMI profile of the EUT and somewhat limited measurement accuracy. However, this technique does offer a time-efficient, cost-effective way to evaluate the EMS/V performance of large equipment using a shielded enclosure with minor modifications. The measurement concept utilizes the shielded, high-Q, multimoded environment to obtain uniform (time averaged) fields that may simulate "real world", near-field environments. Also, it may well be the only technique by which very high exposure fields can be safely generated for performing EM susceptibility tests required by the Department of Defense for some of their "real world" applications.

These considerations, along with others, motivated RADC to invest in the research and development of this methodology and finally to construct and place into operation the facility whose description and evaluation are given in this report. Measurements described were performed between January 26 and February 16, 1987.

2.0 Description of the RADC Reverberating Chamber Facility and NBS Evaluation Systems

The RADC reverberating chamber is made from a large modular shielded enclosure 3.69 m x 5.18 m x 9.78 m (12.11 ft x 17.03 ft x 32.09 ft) in size. The enclosure is constructed from galvanized steel panels with an integrated panel and joiner system. Cross sectional views of the chamber are shown in figure 2.1. It is equipped with two access doors, a small personnel door located adjoining the shielded instrumentation and operator control room and a large double door located at the end of the chamber. The chamber is equipped with a large tuner shown in figure 2.2 (a). The locations and orientations of the chamber's excitation (transmitting) and reference receiving antennas are shown in figures 2.2 (b) and 2.2 (c). The purpose of these antenna placements (located in the corners of the chamber oriented toward the corners) is to couple the transmitted signal into all possible modes and to monitor the reference received signal from all possible modes as efficiently and uniformly as possible. This must be done without favoring particular modes or transmitting directly into the chamber's test zone, or coupling the signal directly between the transmitting and receiving antennas. This is necessary to obtain a statistically uniform, spatial distribution of the field in the chamber's test zone.

A photograph and the block diagrams of the basic systems used to evaluate the chamber are shown in figures 2.3, 2.4, and 2.5. Figure 2.3 is a photograph showing the NBS equipment used in performing the chamber evaluation tests. Figure 2.4 is the block diagram of the NBS system used for the cw evaluation measurements and figure 2.5 is the block diagram of the NBS system used for the pulsed rf evaluation measurements of the RADC chamber. The test field was established inside the chamber by means of an rf source (cw or pulsed as appropriate for the tests being performed) connected to the appropriate transmitting antenna. Modes excited inside the chamber were then stirred by rotating the tuner which functions as a field-perturbing device. The test zone in the chamber is defined as the chamber's volume minus a minimum separation from the walls and ceiling of approximately 1/2 meter. This assures an ample mode density which is a necessary condition for the validity of the reverberating chamber technique [6]. Placement of an EUT should fall within this volume except, possibly, relative to the floor. The separation distance between the EUT and the floor may be less than 1/2 meter depending upon the EUT intended use configuration relative to the ground plane. Test leads and cables were routed to appropriate monitors, etc., outside the chamber through shielded feed-through connectors and high resistance lines. This was done to prevent leakage of the EM fields to the outside environment or into the instrumentation room. A precision 10 dB attenuator was used whenever possible between the power detector or spectrum analyzer and the receiving antenna. This was done to minimize impedance mismatch with the receiving antenna. For the cw tests, a calibrated bidirectional coupler was used at the input to the transmitting antenna to allow measurements of the net input power. For the pulsed rf tests, only the incident signal was measured. For mode stirred measurements, the input power was measured only at the beginning of the measurement cycle. Details of how the measurement cycles proceed under computer control, and how the data are recorded, managed, and processed for presentation are contained in [5,7].

The chamber was evaluated using two different operational approaches referred to as mode-tuned and mode-stirred.

For the cw mode-tuned tests (100 MHz - 18 GHz), the tuner was stepped at selected, uniform increments, permitting measurements of the net input power supplied to the transmitting antenna, the receiving antenna power, field-measuring probes responses and the EUT response at each tuner position. This allowed corrections to be made for the changes in the transmitting antenna's input impedance as a function of tuner position and frequency. The measurement results were then normalized to a constant net input value (1 watt for these tests). The number of tuner steps used per revolution were 200 (increments of 1.8 deg).

For the cw mode-stirred tests (1.0 - 18.0 GHz), the tuner was continuously rotated while sampling the reference antenna received power, field probe response and the EUT response at rates much faster than the tuner revolution rate. These measurements were made using a spectrum analyzer, diode detectors, and "smart" voltmeters that are capable of data storage and calculation of statistical functions such as mean values and standard deviations. The mode stirred approach allows large data samples (up to 9,999) to be obtained for a single tuner revolution. Tuner revolution rates were adjusted to meet the EUT output monitor and diode probe response time requirements. Typical rates used were approximately 3 to 6 minutes per revolution.

The transmitting and reference receiving antennas used for the cw tests were log periodics (0.1 - 1.0 GHz), and ridged horn antennas (1.0 - 18.0 GHz).

For the pulsed rf tests, the mode-tuned approach was used to optimize measurement accuracy, to obtain complete statistical information for evaluating the time domain response characteristics of the reference antenna's received signal, and to determine total energy content in the received pulse relative to the normalized energy in the transmitted pulse. The mode-stirred approach was used for relative measurements with the digitizing oscilloscope placed in its maximum-hold mode of operation. This approach is much faster than the mode-tuned approach and allows much large data sampling than the mode tuned approach; however, it is less accurate and does not provide complete statistical results since only maximum values are recorded. The approach used was determined by the final results needed. The mode-tuned approach was required for complete statistical data and total energy (transmitted verse received) analysis. The mode-stirred approach was used to analyze relative information such as charge and decay time and chamber loss as a function of amounts of rf absorber placed in the chamber.

For the pulsed rf mode-tuned tests (0.9 - 16.0 GHz), the tuner was stepped at selected, uniform increments, permitting measurements of the transmitting antenna's net input signals' and the reference antenna's received signals' time-domain parameters at each tuner position. This allowed corrections to be made for the changes in the transmitting antenna's input impedance variations as a function of tuner position and frequency so that the results could be normalized to a constant net input value. (This is similar to the approach used for the cw tests.) The wave form data were then processed to determine the statistical parameters as a function of time. For these measurements, 200 tuner steps per revolution were used (1.8 deg increments).

For the pulsed rf mode-stirred tests, the tuner was continuously stepped while sampling the maximum received signal at a rate much faster than the tuner revolution rate. This approach allows large data samples to be obtained for a single tuner revolution.

The transmitting and receiving antennas used for the pulsed rf measurements were a matched pair of rectangular ridged-horns designed to operate from 0.8 GHz to 18 GHz. The instrumentation used for measuring the transmitted and received signals include calibrated diode detectors and a dual channel digitizing oscilloscope. One channel of the digitizer was used to measure the transmitted rf pulse monitored on the sidearm of a calibrated broadband directional coupler and the second channel was used to measure the received signal. The digitizing oscilloscope is capable of measuring signals with rise times in the order of 30 ps at a sampling rate of 50 kHz/s and sample sizes up to 1024/scan.

3.0 Reverberating Chamber CW Evaluation Results

How well a shielded enclosure can be made to operate as a reverberating chamber depends upon a number of interacting considerations. The major requirement is that the enclosure be large compared to the wavelength of the lowest frequency intended for use so that sufficient modes, necessary to obtain statistical spatial field uniformity, exist. This should be true for the RADC chamber described above at frequencies above approximately 100 MHz.

3.1 Antenna Coupling Efficiency and VSWR

The efficiency with which energy can be injected into or coupled out of the chamber via the transmitting and receiving antennas is determined by: (1) the voltage standing wave ratio (VSWR) of the antennas (that is the impedance match between the rf source and the transmitting antenna or between the receiving antenna and its output detector), and (2) the ability of the antennas to couple energy into or out of the particular modes that exist at the test frequencies of interest. Rotating the tuner changes the chamber's boundary conditions and hence shifts the mode excitation frequencies. This changes the characteristics of the field inside the enclosure which in turn influences the effective VSWR of the antennas. Hence the net input power to and the measured received power from the enclosure varies as a function of tuner position. (that is the impedance match between the antennas and their source or termination affects the power transfer between the two.) This can result in errors in determining the amplitude of the field inside the enclosure. Variations, determined statistically, in the VSWR of the transmitting antennas used to excite the RADC chamber are shown in figure 3.1. The receiving antenna's VSWRs should be similar. The figure shows the maximum, average, and minimum VSWR obtained by rotating the tuner through a complete cycle at discrete frequencies from 100 MHz to 18 GHz. Large variations exist, especially at frequencies below 1 GHz. At higher frequencies the variations become comparatively negligible approaching the open field VSWR of the antennas.

The coupling efficiency of the antennas placed inside the chamber is expressed in terms of a ratio of the net input power delivered to the transmitting antenna to the power available at the terminals of the receiving antenna. These ratios, referred to as chamber loss, are shown in figure 3.2. The curves shown in the figure are the average, and minimum losses measured

using the mode-tuned approach, the minimum loss measured using the mode-stirred approach, and the minimum loss determined from rf pulse measurements. The results were determined by rotating the tuner through a complete revolution while recording the transmitted and received power. Impedance mismatch between the power detector used to measure the received power and the receiving antenna have not been accounted for in figure 3.2. As noted from the data shown in figure 3.1, this can contribute to a significant error, especially at frequencies below 1 GHz. The magnitude of this source of error is discussed in [5] and is included in the error estimates given in section 5 of this report.

3.2 Chamber Quality Factor

The chamber's quality factor (Q) influences the operation of the chamber in a number of ways. Examples are tuner effectiveness, rf input power requirements and the accuracy with which test field levels can be established inside the chamber. Another important factor is the time required for the chamber to charge up to a steady state condition after the input signal is applied. This influences, of course, the chamber's response characteristics for pulsed rf testing.

From resonant cavity theory the chamber's "composite Q", ($\tilde{Q}$), can be determined [9] from the equation

$$\tilde{Q} = \frac{3\,V}{2\,S\delta_s} \frac{1}{1 + \frac{3\lambda}{16}\left(\frac{1}{a} + \frac{1}{b} + \frac{1}{c}\right)} , \qquad (1)$$

where V is the volume in m^3, S is the internal surface area in m^2, and $\delta_s = \sqrt{\frac{2}{\omega\mu\sigma}}$ is the skin depth in m, λ is wavelength in m, and a, b, and c are the chamber's internal dimensions in m.

The chamber's composite $\tilde{Q}$ is determined [9] by averaging the 1/Q values of all possible modes within a small frequency interval about the frequency of interest. Equation (1) is considered a maximum or upper bound because it assumes the chamber losses are due only to finite wall conductivity. In reality, some loss will also occur due to leakage from the chamber, loss in antenna support structures, and loss in the chamber's wall coatings.

An alternative means of determining the chamber Q can be achieved by using data obtained for the chamber's loss. Chamber loss is determined experimentally by measuring the difference between the net input power, P_t, delivered to the chamber's transmitting antenna, and the power available, P_r, at the reference antenna terminals. If the energy is uniformly distributed over the volume of the chamber, an empirical value, (Q') can be obtained [10] using the equation

$$Q' = 16\,\pi^2 \frac{V}{\lambda^3} \frac{P_r}{P_t} . \qquad (2)$$

Results obtained by using equation (1) to calculate the composite Q and by using the chamber loss data shown in figure 3.2 and equation (2) to calculate the experimental Q are shown in figure 3.3. Figure 3.3 (a) gives the curves for the calculated values of $\tilde{Q}$ and Q' for the RADC chamber and figure 3.3 (b) shows the ratio of $\tilde{Q}$ to Q'. At frequencies above approximately 1 GHz the ratio approaches a constant value approximately equal to 1.6 or a difference of approximately 2 dB. This indicates that at frequencies where equations (1) and (2) are valid, there are relatively small losses due to contributing sources other than the loss in the chamber walls. At frequencies below approximately 1 GHz, the chamber mode density is insufficient to obtain uniform distribution of the energy over the volume of the chamber. This affects the accuracy with which the empirical value of Q, Q' can be determined. Thus the ratio of $\tilde{Q}$ to Q' increases as the frequency decreases as shown in figure 3.3 (b).

3.3 Tuner Effectiveness

Another consideration in the operation of a reverberating chamber is the effectiveness of the tuner to redistribute the energy in the chamber and hence to obtain complete randomness in the characteristics of the test signal. To achieve this the tuner must be electrically large and be shaped or oriented to distribute energy equally well into all possible chamber modes. A test to determine how well the tuner is functioning is to measure the ratio of the maximum to minimum received power of the receiving antenna as a function of tuner position. This is done while maintaining a constant net input power to the chamber's transmitting antenna. A large ratio indicates that the tuner is, in fact, redistributing the scattered fields inside the chamber effectively. The results of these measurements are given in figures 3.4 and 3.5. Figure 3.4 shows an example of the measured E-field inside the chamber as a function of tuner position at three discrete frequencies. Note how the number of maximum and minimum increase as the frequency increase. Figure 3.5 gives the ratio of the maximum to minimum received power as a function of frequency obtained from data similar to that shown in figure 3.4 over the frequency range 0.1 to 18 GHz. A number of factors, including those referred to earlier and related to the design of the tuner, can influence the magnitude of this ratio. For example, a reduction in this ratio after placing rf absorber and/or an EUT inside the chamber is an indication of the loading effect or reduction of the chamber's quality factor (Q) caused by the absorber and/or the EUT. A minimum ratio of 20 dB is suggested for proper operation of the chamber [5].

3.4 Test Zone E-Field Uniformity

Tests were made to determine the E-field uniformity in the chamber as a function of spatial position and frequency. Ten NBS isotropic probes [11,12,13] designed to operate at frequencies up to 2 GHz were placed inside the chamber as shown in figures 3.6 and 3.7. Each probe has three orthogonally oriented dipoles aligned with the chamber's axes. Measurements were made of the field strength of each orthogonal component at the ten locations for each tuner position (200 steps of 1.8 deg for frequencies 100 - 1000 MHz and 400 steps of 0.9 deg for frequencies 1.0 - 2.0 GHz). These data were normalized for a net input power of 1 W applied at the input terminals of the transmitting antennas. The maximum and average values for each

component and the vector sum (total) of the components were then determined from the complete data sets. The results of these measurements are shown in figures 3.8 (a) and (b). The spread of the data shows the spatial field variation inside the enclosure at the indicated frequencies. The field strength drops significantly at frequencies below approximately 300 MHz. This is due to the low frequency response of the transmitting antenna used and to the lower number of modes available in the chamber at the lower frequencies. Higher density (closer frequency intervals) measurements were made between 100 and 150 MHz to improve the accuracy in determining the spatial field variation at these lower frequencies. The results indicate the chamber is operating properly, but, with rather large spatial variations at the lower frequencies, down to 100 MHz. The spread in the data (spatial distribution) at selected frequencies is summarized in table 3.1. The spread is as great as ± 9 dB at 100 MHz decreasing to approximately ± 3.5 dB at 300 MHz, ± 2.5 dB at 1.0 GHz, and ± 2.0 dB at 2.0 GHz. The average values, determined statistically from the data measured at the ten locations, for the average and maximum E-fields of each component and their composite total are summarized in figure 3.9. The relative amplitudes of the field components are approximately the same and the composite total of the average E-field components is approximately 4.8 dB or a ratio of $\sqrt{3}$ greater than the individual components. This indicates that the measured values of the average of each component are independent of polarization in the chamber. Hence, the average field inside the chambers appears to be randomly polarized. The composite total of the E-field components' maxima (figure 3.9 (b)) is less than 4.8 dB. This indicates that the maximum measured values for each component are not independent ($E_{x(total)}$ is a function of $E_{y(total)}$, etc.). This is similar to the results obtained in the NBS reverberating chamber and appears to be inherent in the reverberating chamber measurement method. The implication is that if multiple receptors are involved in establishing the maximum susceptibility of an EUT (for example in measuring the E-field in the chamber by using an isotropic probe with 3 orthogonal dipoles), the difference between the maximum and average response determined for the EUT may be incorrectly weighted (less than the 7-8 dB anticipated). (See section 2.3 of [5] for the explanation why 7-8 dB difference in signal amplitude between the maximum and average field strengths is anticipated.)

3.5 E-Field Amplitude Calibration

The field strength in the chamber can be determined in two ways. The first is to measure the power received by the reference antennas, and then determine the equivalent power density in the enclosure using the equation [5]

$$\bar{E}_a = \sqrt{\bar{\eta}' \bar{P}_d'} \approx \frac{4\pi}{\lambda} \sqrt{30 \bar{P}_r'} \quad (V/m), \qquad (3)$$

where $\bar{E}_a$ is the equivalent electric field in V/m, $\bar{\eta}'$ is the statistically averaged wave impedance of the chamber in Ω, $\bar{P}_d'$ is the equivalent power density in W/m^2, in the enclosure, λ is the wavelength in m, and $\bar{P}_r'$ is the

average measured received power in W. The averaged wave impedance is assumed to be approximately equal to $120\pi\ \Omega$. The validity of (3) has been verified and is discussed in section 2.3.1 of NBS TN 1092 [5].

The maximum and average electric field strengths inside the RADC chamber determined from the receiving antenna power measurements and (3) are shown in figure 3.10. These data were obtained for 1 W net input power to the chamber's transmitting antenna.

The electric field strength inside the chamber can be determined a second way by measuring it with one or more calibrated probes. Data obtained using a 1-cm dipole probe fabricated at the NBS are also shown on figure 3.10. The probe was calibrated in a planar field using a TEM cell [14] at frequencies up to 500 MHz and in an anechoic chamber at frequencies from 500 MHz to 18 GHz [15]. The assumption is made that the field strength over the aperture of the probe inside the reverberating chamber will approximate the planar field used to calibrate the probe. This is reasonable, at least at frequencies for which the probe is electrically small. Also, the open-space far-field gain of an electrically small dipole is small (1.76 dB). Thus, the probe-measured fields should be equivalent, within approximately 1.76 dB, to the E-fields determined using a receiving antenna. This is true if the equivalent gains for the probe and receiving antenna, after being placed inside the chamber, are assumed to be 1. The agreement shown is typical of the random variations in the data used to determine the field strength inside reverberating chambers.

3.6 Comparison of RADC Reverberating Chamber with NBS Anechoic and Reverberating Chambers

Comparisons of the response or EMS/V characteristics of EUT obtained using an anechoic chamber and a reverberating chamber are typically made in terms of peak values. The main reasons for this are that the EUT's worst case performance or susceptibility is desired and the practical consideration of the difficulty in obtaining a true average response for an EUT from anechoic chamber data. Even determining the EUT's peak response in an anechoic chamber (depending upon how well behaved the EUT receiving pattern characteristic is) can require considerable effort involving complete pattern measurements.

The value of performing these comparisons is to estimate a "correlation factor" between results obtained in the reverberating and the anechoic chambers. This should first be done for reference standard EUTs and then for EUT more typical of operational equipment. For this effort, two reference EUT were used. These were (1) a 1 cm dipole probe antenna referred to earlier (data of figure 3.10) and (2) two ridged horn antennas (one designed to operate in the frequency range, 0.8 - 12 GHz, and one designed to operate in the frequency range, 0.8 - 18 GHz). The measurements were performed in the RADC reverberating chamber and in the 4.9 m x 6.7 m x 8.5 m (16.1 ft x 22.0 ft x 27.9 ft) NBS anechoic chamber located in Boulder, Colorado.

A comparison of the peak output response data obtained for the 1.0 cm dipole is given in figure 3.11. The probe's output response in the anechoic chamber is greater, in general by an average of approximately 2.0 dB than its output in the reverberating chamber. This is as expected since this corresponds approximately to the gain of the electrically short dipole from

measured inside the anechoic chamber. The suggested correlation factor between EUT EMS/V (response) measurements is the free-space gain of the EUT [5].

Comparison measurements of the peak response of a ridge-horn antenna designed to operate in the frequency range, 0.8 - 12 GHz, were made using the RADC reverberating and NBS anechoic chamber. The results are shown in figure 3.12. For the anechoic chamber measurements, the horn was bore-site aligned with the transmitting antenna to obtain the peak response. The horn's response (figure 3.12 (a)) is greater in the anechoic chamber than in the reverberating chamber. The horn was calibrated to determine its free-space gain, in dB, which was then subtracted from the anechoic chamber measured response. These results are shown in figure 3.12 (b). The results agree, in general, as expected.

Figure 3.13 shows the comparison of the peak response of the two similar type ridged-horn antennas to the same level test field inside the RADC reverberating chamber. The results shown are as expected since the response of the antennas should be similiar. (The effective gain of both antennas is 1 inside the reverberating chamber).

It is of value to compare evaluation results obtained for different reverberating chambers, for example, the NBS and RADC reverberating chambers. Such a comparison was made to answer two significant questions: First, can the input power requirements of a uncalibrated chamber be estimated from its measured Q relative to a second calibrated chamber, and second, are susceptibility test results obtained for the same EUT in different reverberating chambers comparable?

Recall from theory that the power density inside a second chamber can be estimated from a calibrated first chamber by using the equation [5],

$$\frac{P_{d_1}}{P_{d_2}} = \frac{V_2 Q_1}{V_1 Q_2} = \left(\frac{E_{a_1}}{E_{a_2}}\right)^2 , \qquad (4)$$

where P_d is the power density and E_a is the electric field for the particular chamber (1 or 2). If we assume the first chamber is the NBS chamber with a volume, $V_1 = 38.19\ m^3$ and the second chamber is the larger, RADC chamber with a $V_2 = 186.94\ m^3$, the ratio, V_2/V_1, is 4.89. The ratio of the experimentally determined Qs, Q_1'/Q_2' for the two chambers is approximately 0.17. This gives a calculated value for the ratio of E_{a_1}/E_{a_2} of approximately -0.8 dB or the RADC chamber should require approximately 0.8 dB less input power to generate the same test field level as compared with the NBS chamber.

We might expect at first, because the NBS chamber is considerably smaller than the RADC chamber, that the NBS chamber would require less power to generate the same test field level than the RADC chamber. This is not so because of the difference in the Qs of the two chambers resulting from the difference in the surface coating used inside the chambers. The RADC chamber

is coated with galvanized zinc over steel and the NBS chamber is coated with nonconductive epoxy over steel. The zinc surface, with its higher conductivity than steel, results in a much higher Q for the RADC chamber than the NBS chamber. Results shown in figures 3.14 compared with figure 3.10 verify these calculations and hence answer the first question affirmatively. Figure 3.14 shows the fields inside the NBS chamber calculated from the chamber's reference antenna received power measurements and also measured by the calibrated 1 cm long dipole probe. These data are similar to the data shown in figure 3.10, obtained for the RADC chamber. The net input power was normalized to one watt for both chambers. The fields inside the two chambers (RADC and NBS) are approximately the same, consistent with the small (0.9 dB) predicted difference. Thus the answer to the first question (Can the input power requirements of a chamber relative to a second calibrated chamber be estimated from its measured Q?) is yes.

Figure 3.15 shows the response of the NBS 1 cm dipole measured inside the NBS reverberating and anechoic chambers. These data can be compared with figure 3.11 showing the same type data for the RADC chamber. Again the agreement is well within the uncertainties estimated for the two measurement techniques and different facilities. Thus the answer to the second question (Are susceptibility test results obtained for the same EUT in different reverberating chambers comparable?) is also yes.

4.0 Reverberating Chamber Pulsed RF Evaluation Results

4.1 Background

Because of the significant potential of the reverberating chamber method for performing cw EMS/V testing of an EUT, there is considerable interest in using this technique also for pulsed rf EMS/V testing. Work was performed to evaluate the RADC chamber's response to pulsed rf excitation to determine the feasibility of using it in this mode of operation and to determine estimates for correction factors necessary to correlate results obtained to a free-space environment.

Parameters of electromagnetic interference (EMI) signals that can contribute to upset in electronic equipment include: (a) total energy, (b) peak amplitude, and (c) transient time characteristics. All these parameters are modified, relative to free space, for signals transmitted inside a reverberating chamber. Their characterization inside a reverberating chamber, particularly for pulsed rf fields, provides information required to determine correction factors as a function of the input pulse parameters. It also provides insight into the inherent limitations associated with using this complex environment for pulsed rf EMS/V testing. Obviously, these factors are influenced by the Q factor of the chamber, since, the time required for the pulsed wave's amplitude to rise to its steady state value inside the chamber and to decay to zero after the input signal is removed is a function of the chamber's Q. These "charge and decay" times can be reduced by artificially lowering the chamber's Q, for example, by inserting small amounts of rf absorber. However, this reduces the accuracy in determining the test field amplitude. Results of work to evaluate the response characteristics of the chamber when excited by pulsed rf of various pulse widths and frequencies, and with the chamber loaded with various amounts of absorber are contained in this section.

4.2 Evaluation of Pulsed RF Measurement Results

Measurements were made, using the mode-stirred approach, to determine the effect of lowering the reverberating chamber's Q on the charge/decay time of the rf pulsed field excited inside the chamber. Varying amounts of pyramidal rf absorber were placed in the center of the chamber on top of a 15 cm high platform of plastic foam. Measurements were first made at 900 MHz (the lowest test frequency) since data obtained previously, of the NBS reverberating chamber's response to pulsed rf, indicated the response time increases as the frequency decreases. Results of these measurements are given in figures 4.1 (a - i). Each figure shows two traces. The top trace is the input pulse applied to the chamber's transmitting or excitation antenna. The bottom trace is the time-domain signal received by the chamber's reference receiving antenna but with the polarity reversed to separate the two traces. The spread in the top traces (input signal) is due to the variations in the input signal amplitude caused by movement of the chamber's tuner. The magnitude of this variation is frequency dependant, decreasing as the frequency increases as indicated in figure 4.2. Figure 4.1a was obtained with the chamber empty (no absorber). Figures 4.1b - 4.1f are for increasing amount of absorber starting with a 1/2 piece (12" x 24") of 3" thick rf absorber, ending with 4 pieces (24" x 24") of 24" thick rf absorber. The influences on both the amplitude and response time are obvious. Figures 4.2a - 4.2c show data similar to figures 4.1a - 4.1i but at selected frequencies from 0.9 GHz to 16 GHz. Data for three amounts of absorber loading are given: with no absorber, with 1 piece of 5" x 24" x 24" rf absorber and with 1 piece of 24" x 24" x 24" rf absorber. Again the effect of absorber loading on both the amplitude and time-domain response is apparent.

It is interesting to compare the chamber's response time (charge or decay), obtained by calculation from the experimentally determined Q values, to the measured response time. Recall from [8] that the response time is approximately $2Q/\omega_0$ for the signal to rise or fall (1-1/e) to 63 % of the steady state amplitude. These results are shown in tables 4.1 and 4.2. Table 4.1 gives the measured average chamber losses, the associated calculated Q factors, and the calculated charge/decay times determined at 900 MHz for the varying amounts of absorber. These data were derived from the results shown in figures 4.1 (a - i) normalized with the results of figures 4.3 sheets 1 -10. Table 4.2 gives the measured average chamber losses, the associated calculated Q factors, the calculated charge/decay times, and the measured charge/decay times at the selected frequencies for the chamber empty, with 1 piece of 5" x 24" x 24" rf absorber, and with 1 piece of 24" x 24" x 24" rf absorber. The calculated and measured response times for the chamber differ somewhat, but are still within the margin of error expected for these type of measurements.

The mode-tuned measurement approach, as previously defined, was used to determine: (a) chamber loss for rf pulse excitation compared to cw excitation thus allowing a comparison of the total energy available in the test field for cw or pulsed rf testing, and (b) the ratio of the received pulse amplitude verses input pulse amplitude as a function of time after the input pulse is turned on. (These are two of the three parameters that are important in assessing potential upset due to EMI of EUT for EMS/V testing.) Again, measurements were made with the chamber empty (no absorber) and with

the chamber loaded with 1 piece of 5" x 24" x 24" rf absorber and with 1 piece of 24" x 24" x 24" rf absorber. Measurements were made to determine the ratio of energy received by the chamber's receiving antenna to the energy transmitted by the transmitting antenna for pulsed rf signals. The total energy received was determined by using numerical integration to determine the energy (amplitude x time) of the received signal relative to the transmitted pulse energy (amplitude x time) as a function of pulse width and rf frequency. Sample results were shown in figure 3.2 for a transmitted pulse width of 1 μs. This pulse width should have the maximum deviation from cw signal chamber loss for rf pulse widths of interest, (1 - 10) μs since the shorter the pulse width, the less time the chamber has to respond (charge up). The cw and rf pulse chamber losses agree within 2 dB at all frequencies. One can conclude for these measurements that even with significant pulse dispersion as a function of time, as shown in figures 4.1 and 4.2, the energy associated with the field inside the chamber is approximately the same as for cw testing. (The chamber loss, cw or rf pulse, is approximately the same.)

Sheets 1-10 in figure 4.3 give the results of the mode-tuned received pulse amplitude measurements data presented statistically as a function of time. These graphs give an indication of the time required for the chamber to charge up to its steady state amplitude and to decay to zero after the pulse is turned off. The results indicate an obvious dependence on frequency and the chamber's Q. Charge-up time results from the time required for the input signal, radiated from the source antenna, to complete all significant multiple reflections that contribute to the final field inside the chamber. Each graph shows two curves, one for the maximum and one for the average received signals. Smooth curves have been added to some graphs to provide estimates for calculating ratios of the transmitted signal amplitude to the received signal amplitude as a function of time, as referred to earlier. By examining these data at the selected frequencies, the approximate charge or decay times can be determined as a function of frequency for the empty chamber and for the chamber loaded with the two different size pieces of rf absorber. These results are shown in figures 4.4 and 4.5. The results are given in terms of the time required for the received signal to rise 63 and 90 percent of the maximum amplitude. The implication of figures 4.4 and 4.5 is that the input pulse duration, at the frequencies of interest, should be above the respective curves for the pulsed rf test field amplitude to be greater than 63 or 90 percent of the maximum steady state or cw amplitude. The steady state amplitude is achieved if the input pulse width is sufficient for the chamber to charge up 100 percent, or to its maximum output for a given input pulse amplitude.

If the transmitted input pulse duration is not longer than the charge time of the chamber, an error will result in terms of establishing a known peak amplitude of the test signal in the chamber. An estimate of a correction factor to apply for this condition can be found by calculating the ratio of the received signal amplitude to the transmitted signal amplitude as a function of time after turning on the transmitted pulse. Figure 4.6 (sheets 1 - 3) gives these results, determined from the data of figure 4.3 sheets 1 - 10. The corrections shown are the ratio of the received signal amplitude as a function of time, after the input pulse is turned on, to the steady state amplitude of the signal. The data are projected down to input pulse durations as low as 0.2 μs. Note the significant reduction in the correction obtained by loading the chamber with rf absorber. The assumption

is that the data shown in the graphs of figure 4.6 can be used to correct for test field signal amplitude reductions due to insufficient transmitted pulse duration times. This assumption needs to be experimentally verified by comparing the measured responses of a well characterized EUT to cw fields and to pulsed rf fields of varying pulse widths, at the same frequencies, using both an anechoic chamber and an evaluated (calibrated) reverberating chamber.

Figure 4.7 is another way to display the data shown in figure 4.6. The correction factors are shown for discrete input pulse widths as a function of frequency rather than for discrete frequencies as a function of input pulse width. The dots are the actual data extracted from figure 4.6 and the solid curves are the smooth approximations for this data.

5.0 Summary of CW Measurement Uncertainty

5.1 Estimate of Uncertainty in Establishing CW E-Field Amplitude Inside the Chamber

As indicated in section 3, EMS/V test fields established inside the chamber can be determined two ways: either using a reference receiving antenna or a calibrated probe. If a reference receiving antenna is used, the field is determined in terms of "equivalent" power density or "equivalent" electric field strength by using (3). If a calibrated E-field probe is used, the field strength is measured relative to an equivalent probe response in a known planar field. An estimate of the uncertainties in each of these methods can be determined by analyzing the contributing parameters involved in each method. The significant sources of error are summarized in tables 5.1 and 5.2 for the mode-tuned and mode-stirred approaches respectively, within their appropriate frequency bands. Four major categories are identified. The first is the uncertainty in determining the received power measured by the reference antennas (1a. tables 5.1 and 5.2), or in measuring the E-field with the calibrated probe (1b. tables 5.1 and 5.2). The uncertainty in determining the received power is broken up into five components: cable loss, attenuator calibration, reference antenna efficiency, power meter or spectrum analyzer measurement uncertainties, and impedance mismatch. Values shown for the first four components are typical of estimated uncertainties stated for these types of measurements and instruments. The fifth component, impedance mismatch is the uncertainty in determining the actual power delivered to the detector (load) attached to the antenna (source) relative to the power available. The actual or measured power is a function of the impedance match between the source and load, with maximum power transfer occurring when a conjugate impedance match exists.

Power transfer between a source and a load is given as

$$P_f = \begin{array}{c}\text{fraction of maximum} \\ \text{available power absorbed} \\ \text{by the load}\end{array} = \frac{(1 - |\Gamma_S|^2)(1 - |\Gamma_L|^2)}{|1 - \Gamma_S\Gamma_L|^2}, \qquad (5)$$

where Γ_S and Γ_L denote complex reflection coefficients for the source and load respectively. The magnitudes, $|\Gamma_S|$ and $|\Gamma_L|$ can be obtained from the appropriate VSWR by the expressions

$$|\Gamma_i| = \frac{VSWR - 1}{VSWR + 1} , \qquad i = S \text{ or } L . \tag{6}$$

The VSWRs for the reference antennas (sources) and power detectors (loads) used in the RADC reverberating chamber are given in table 5.3. These values were used to calculate the estimated uncertainties shown for the mismatch errors in tables 5.1 and 5.2. Both the statistical average and maximum values are given.

Discussions of the uncertainty in calibrating E-field probes in planar fields can be found in [14,15]. Their response to fields inside a reverberation chamber has been shown to be less than their response in a planar field. The difference is proportional to their free-space gain [5]. Typical probes used are electrically short dipoles over most of the frequency range. Sometimes, however, they are used beyond their resonance frequency (for example the 1 cm dipole probe at frequencies above 15 GHz). The corrections needed to correlate results obtained in the reverberating chamber with those obtained in free-space or in anechoic chambers then correspond to from 1.76 dB to 2.6 dB. The total estimated uncertainties of using the NBS 1 cm dipole probe to measure E-field amplitudes in the reverberating chamber are shown on tables 5.1 and 5.2 (see 1b).

The second category of error, referred to as mixing or sampling efficiency, is divided into two parts. The first part relates to the ability to obtain a uniform spatial field distribution (statistically) inside the chamber and to effectively destroy the polarization characteristics of the exposure field. (The statistically determined response characteristics of the EUT and chamber reference antenna are independent of their directional properties.) The second part is the uncertainty due to limiting the number of tuner positions per revolution when performing the measurement. This source of uncertainty is different when determining the average as compared to the maximum field as shown in the tables. Data contained in [5] (figure 2.27 and table 6.4) were used in obtaining these estimates.

The third category of uncertainty relates only to determining the equivalent E-field strength in the chamber from the equivalent power density. Recall that equation (3) assumes that the equivalent wave impedance inside the chamber is 120π Ω. In reality this is not true as has been shown [5]. However, data shown in [5] can be and were used to provide an estimate for this error. These data indicate that a wave impedance as great as 1600 ohms can exist at frequencies below 500 MHz when the maximum E-field is measured. This corresponds to approximately 6 dB of correction. However, a significant amount of data obtained to date, indicates that a well behaved relationsnip (7-9 dB difference) exists between the measured peak and average values of the E-field. This suggests, at least at frequencies above a few hundred megahertz where the chambers are highly moded, that the peak value of the wave impedance for the maximum measured E-field inside the chambers decreases as the frequency increases. In the limit, it should approach 120π Ω. Thus this source of error decreases as frequency increases. These observations are reflected in the uncertainty estimates shown in the tables.

The fourth source of error occurs if corrections for net input power variations due to the loading effect of the chamber on the VSWR of the source

antennas are not applied. These corrections are made when using the mode-tuned approach and hence are not included in table 5.1. They are not made however, when using the mode-stirred approach and hence are shown in table 5.2.

The total worst-case uncertainties for each method (receiving antenna and calibrated probe) of determining the E-field for both the mode-tuned and mode-stirred approaches are shown at the bottom of the appropriate table. These uncertainties should be regarded as a conservative estimate. The probability of the true value of amplitude of the test field being near an extreme is small. This is because the probability of all error sources being at their extreme value in the worst possible combination is almost zero.

A more realistic method of combining uncertainties is the root-sum-of-the-squares (RSS) method. The RSS uncertainty is based on the assumption that the errors are statistically independent of each other and hence combine like random variables.

Finding the RSS uncertainty requires that each individual uncertainty be expressed in fractional form. The method of calculation follows the name (that is, square the components, add those squares and then take the square root). The results for both methods of determining the E-fields are shown at the bottom of tables 5.1 and 5.2.

5.2 General Comments

Some general comments on interpreting uncertainties of immunity measurement results based upon the above experimental error analysis are appropriate.

1) The mismatch error at frequencies below 2 GHz, (particularly if corrections are not made for the transmitting or receiving antennas mismatches looking into their source or load), will cause the field determination inside the chamber to be low. This also causes the EUT response results to be lower than they actually are. For example, the low frequency data of figures 3.10, 3.11, 3.14, and 3.15 should be corrected (response increased) proportionally to the systematic offset error estimates shown in tables 5.1 and 5.2.

2) The wave impedance, when the peak response of an EUT is measured, appears to be higher than 120π Ω, especially for frequencies lower than 500 MHz. This means that if the free space wave impedance of 120π ohms is used in determining the corresponding peak amplitude of the exposure field, there will be a systematic offset error resulting in too low a calculated E-field exposure value. Since the actual E-field is higher than the calculated value, this results in too high a EUT response indication for a specified E-field exposure. If the E-field is determined using a calibrated E-field probe, there still remains a degree of uncertainty since the wave impedance is different in the calibration environment as compared to the reverberating chamber environment. For this reason, this source of error was included in calculating the total and RSS uncertainties in establishing the E-field using the probe method.

3) The spatial variation in the measured, statistically determined E-field in the chamber resulting from a complete revolution of the tuner(s) decreases from as great as ± 9 dB at 100 MHz to less than ± 2 dB at 2.0 GHz. This variation should continue to decrease as the frequency increases. However, high variations exist in the response data obtained for the reference standard EUTs (1 cm dipole and ridged horn) at frequencies where the spatial E-field variation are small. This is due to the other contributing sources of error as discussed in 5.1. A way to reduce this problem is to increase the number of frequencies at which data are taken (clustered around a frequency of interest) or increase the number of reference receiving antennas or probes used to determine the exposure field and then average the data (for example as was done in figure 3.9).

6.0 Summary and Conclusions

1. The practical lower frequency limit recommended for using the RADC chamber is approximately 150 MHz.

2. Spatial variations in the E-field maximum and average values determined in the chamber test volume are shown in table 3.1. These data were determined using the mode-tuned approach with 200 tuner increments at 100 to 1000 MHz and 400 tuner increments at 1000 to 2000 MHz for one complete tuner revolution. The limitation for determining the spatial E-field variation is most likely due to the increasing mode density and hence field complexity in the chamber as a function of frequency. The limited sample size then becomes insufficient to determine the actual maximums with greater accuracy. In reality, the spatial E-field variations should continue to decrease (less than ± 2.0 dB) above 2 GHz if sufficiently large data samples are taken and the measurement instrumentation has adequate dynamic range and precision.

3. Antennas used within the chamber for transmitting energy or for determining the test E-field amplitude should not be used outside their recommended frequency range.

4. The mode-tuned approach is recommended for use with the chamber at frequencies below 1 GHz. Either mode-tuned or mode-stirred can be used from 1 to 2 GHz. The mode-stirred approach is recommended for use above 2.0 GHz. This allows for some overlap in the measurement approach selected. Based upon antenna VSWR and EUT response data obtained from the evaluation measurements, the following approaches and number of samples per tuner(s) revolution are suggested for performing EMS testing.

Frequency Range	Method	# Tuner Positions or Samples
0.15 - 1.0 GHz	Mode-Tuned	200
1.0 - 2.0 GHz	Mode-Tuned	400
1.0 - 4.0 GHz	Mode-Stirred	> 3000
4.0 - 18.0 GHz	Mode-Stirred	> 5000

5. The maximum E-field is approximately 8 dB greater than the average E-field established inside the chamber.

6. The theory for predicting input power requirements for a second unknown chamber based upon the known requirements of a first chamber appears to be valid.

7. Results of reference standard EUT response measurements made using the RADC reverberating chamber are approximately the same as for the NBS reverberating chamber. Hence EMS/V data obtained for an EUT in similarly operated, but different reverberating chambers should be approximately the same.

8. The "correlation factor" between free-space (anechoic chamber) EMS/V results and reverberating chamber obtained results appears to be the free-space (far-field) gain of the EUT. This implies that susceptibility criteria determined for an EUT using a reverberating chamber must include an additional factor proportional to the EUT's open-field estimated gain as a function of frequency.

9. Item 8 also implies that the directional characteristics of an antenna or EUT placed inside a reverberating chamber are lost, resulting in their equivalent gain of unity in this complex environment.

10. If the chamber is used for pulsed rf EMS/V testing and the width of the input pulse to the chamber is not longer than the chamber's charge time, an error will result in terms of establishing a known peak amplitude of the test signal. An estimate of the correction factors to apply for this condition is found in figures 4.6 and 4.7.

11. Use of rf absorber significantly reduces the chamber's charge time and can be used to improve the fidelity of the rf pulsed exposure field for EMS/V testing. However, the amount of absorber should not add more than approximately 6 dB loss to the chamber (reduce the reference antennas received power by more than 6 dB) and/or it should not reduce the tuner effectiveness below 20 dB.

12. Additional work is needed to experimentally verify the correction factors shown in figures 4.6 and 4.7. This could be done by comparing the measured responses of a well characterized EUT to cw and pulsed rf exposure fields as a function of frequency and pulse widths using both an anechoic chamber and an evaluated (calibrated) reverberating chamber.

7.0 Acknowledgments

Work described in this report was sponsored by the RADC, Griffiss AFB, Rome, New York, with Charles Blank as project monitor. The authors wish to acknowledge his assistance in making this project possible. The authors also wish to acknowledge the assistance of William Quinn, Rome Research Corporation, Rome, New York, and John Workman and Darleen Agee, NBS for their help and cooperation in performing the measurements discussed in this report. In addition, the authors express appreciation to Mark Ma, NBS, for his support, helpful comments and editorial review.

8.0 References

[1] Mendes, H.A. A new approach to electromagnetic field-strength measurements in shielded enclosures. Wescon Tech. Papers, Los Angeles, CA. 1968 August.

[2] Cummings, J.R. Translational electromagnetic environment chamber, a new method for measuring radiated susceptibility and emissions. Proc. IEEE Int. Symp. on EMC; 1975; San Antonio, TX.

[3] Corona, P.; Latmiral, G.; Paolini, E.; Piccioli, L. Performance of a reverberation enclosure for power measurements in the microwave range. 2nd Symp. Tech Exhibition on EMC; 1977; Montreux, Switzerland).

[4] Bean, J.L.; Hall, R.A. Electromagnetic susceptibility measurements using a mode-stirred chamber. Proc. IEEE Int. Symp. on EMC; 1978; Atlanta, GA.

[5] Crawford, M.L.; Koepke, G.H. Design, evaluation and use of a reverberation chamber for performing electromagnetic susceptibility/vulnerability measurements. Nat. Bur. Stand. (U.S.) Tech. Note 1092; 1986 April. 148 p.

[6] Ma, M.T.; Kanda, M.; Crawford, M.L.; Larsen, E.B. A review of electromagnetic compatibility/interference measurement methodologies. Proc. of IEEE; Vol. 73, No. 3; 1985 March.

[7] Project Progress Report - Final Report FY86 "EMR test facilities - Evaluation of reverberation chamber method for performing EMC measurements", Prepared for RADC/RBCM, Griffiss AFB, NY. by NBS, Boulder, CO. Report NO. SR-723-1-87. 1987 January.

[8] Crawford, M.L.; Koepke, G.H. Preliminary evaluation of reverberation chamber method for pulsed rf immunity testing. IEEE Int. Symp. on EMC; 1986; San Diego, CA.

[9] Liu, B.H.; Chang, D.C.; Ma, M.A. Eigenmodes and the composite quality factor of a reverberating chamber. Nat. Bur. Stand. (U.S.) Tech Note 1066; 1983 August.

[10] Corona, P.; Latmiral, G.; Paolini, E. Performance and analysis of reverberating enclosures with variable geometry. IEEE Trans. on EMC; EMC-22. 1980 February.

[11] Larsen, E.B.; Ries, F.X. Design and calibration of the NBS isotropic electric-field monitor [EFM-5], 0.2 to 1000 MHz. Nat. Bur. Stand. (U.S.) Tech. Note 1033; 1981 March.

[12] Kanda, M.; Driver, L.D. An isotropic electric-field probe with tapered resistive dipoles for broad-band use, 100 kHz to 18 GHz. IEEE Trans. on MT&T. Vol. MTT-35(2); 1987 February.

[13] Bensema, W.D.; Reeve, G.R.; Koepke, G.H. A multisensor automated EM field measurement system. Proc. IEEE IMTC/85 Conf; 1985; Tampa, FL.

[14] Crawford, M.L. Generation of standard EM fields for calibration of power density meters: 20 kHz to 1000 MHz. Nat. Bur. Stand. (U.S.) NBSIR 75 804; 1975 January. 40 p.

[15] Bowman, R.R. Calibration techniques for electromagnetic hazard meters: 500 MHz to 20 GHz. Nat. Bur. Stand. (U.S.) NBSIR 75-805; 1976 April. 33 p.

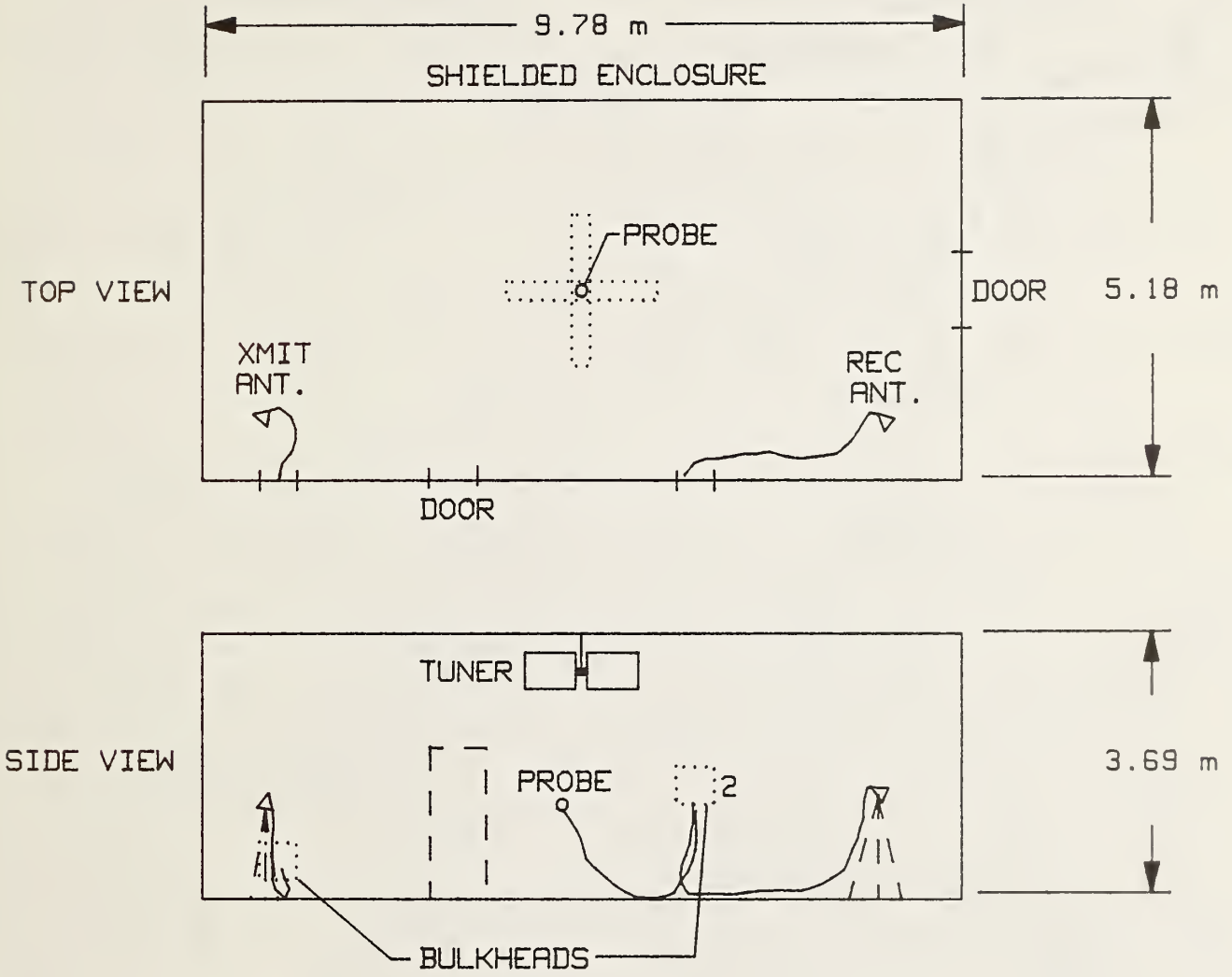

Figure 2.1. Cross sectional views of RADC reverberating chamber showing placement of tuner, transmitting and receiving antennas, and probe used to evaluate E-field amplitude inside the chamber.

Figure 2.2a. Photograph of interior of RADC reverberating chamber showing tuner mounted from ceiling and transmitting antenna mounted on tripod in northeast corner of chamber.

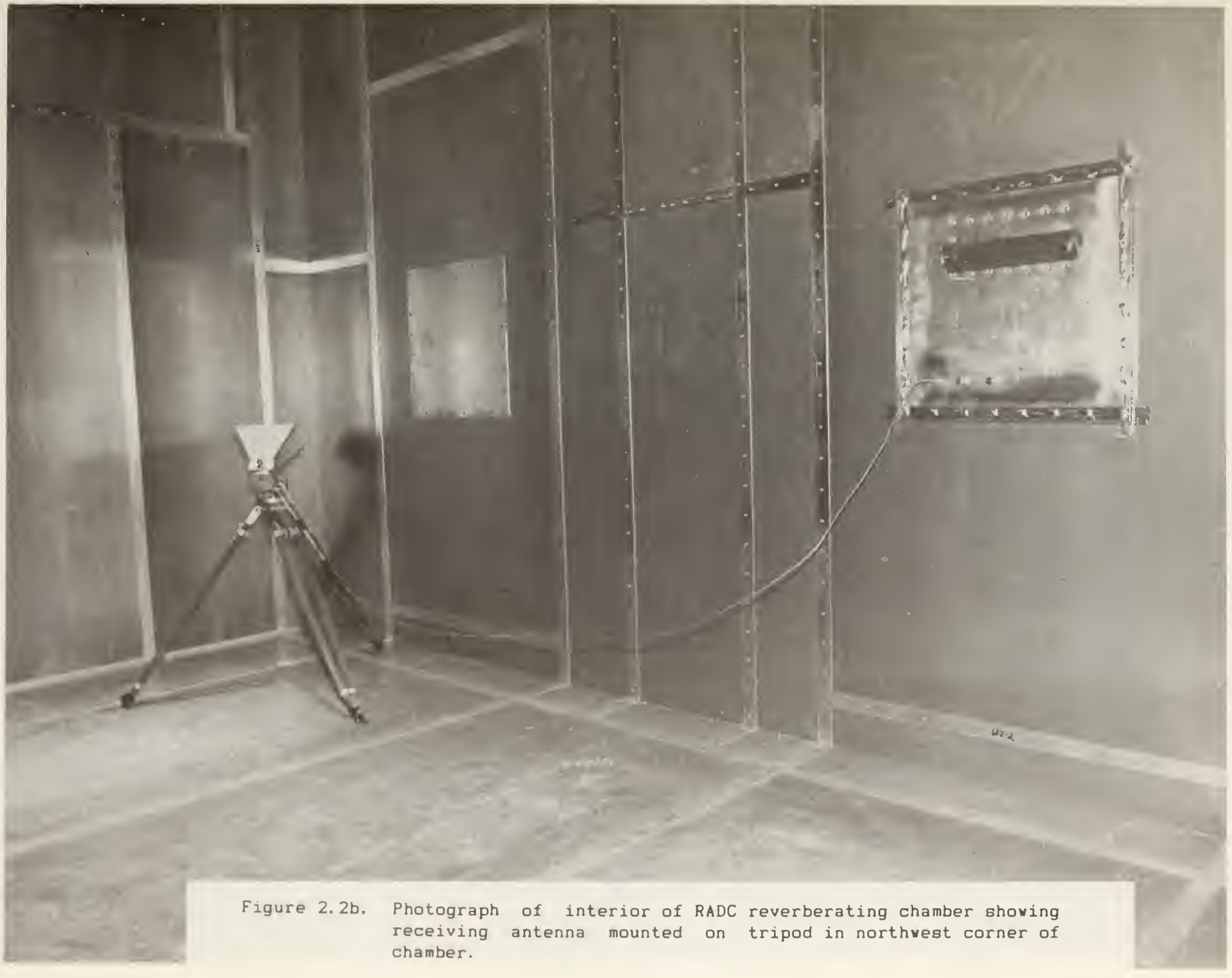

Figure 2.2b. Photograph of interior of RADC reverberating chamber showing receiving antenna mounted on tripod in northwest corner of chamber.

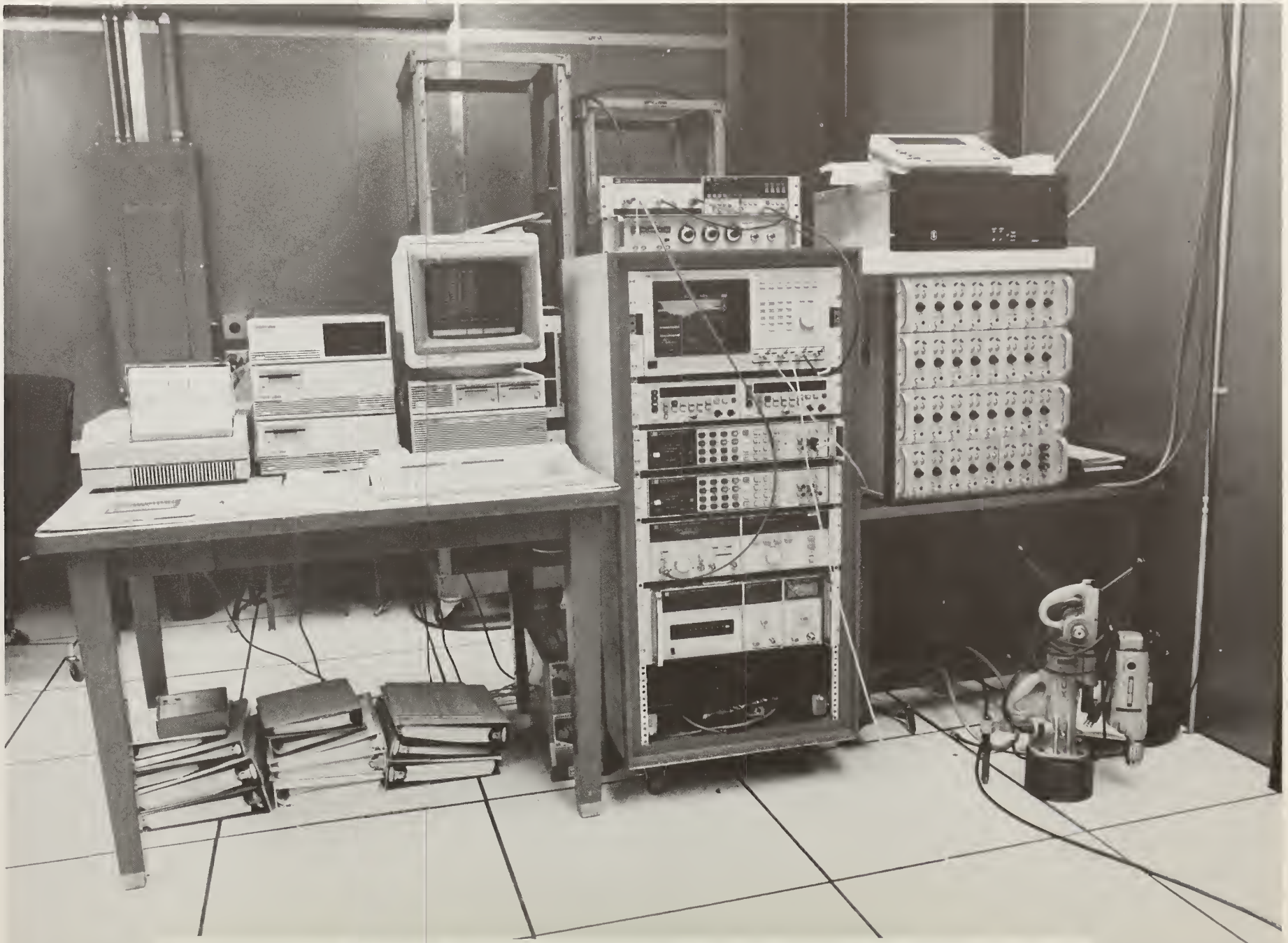

Figure 2.3. Photograph showing NBS equipment used in performing chamber evaluation.

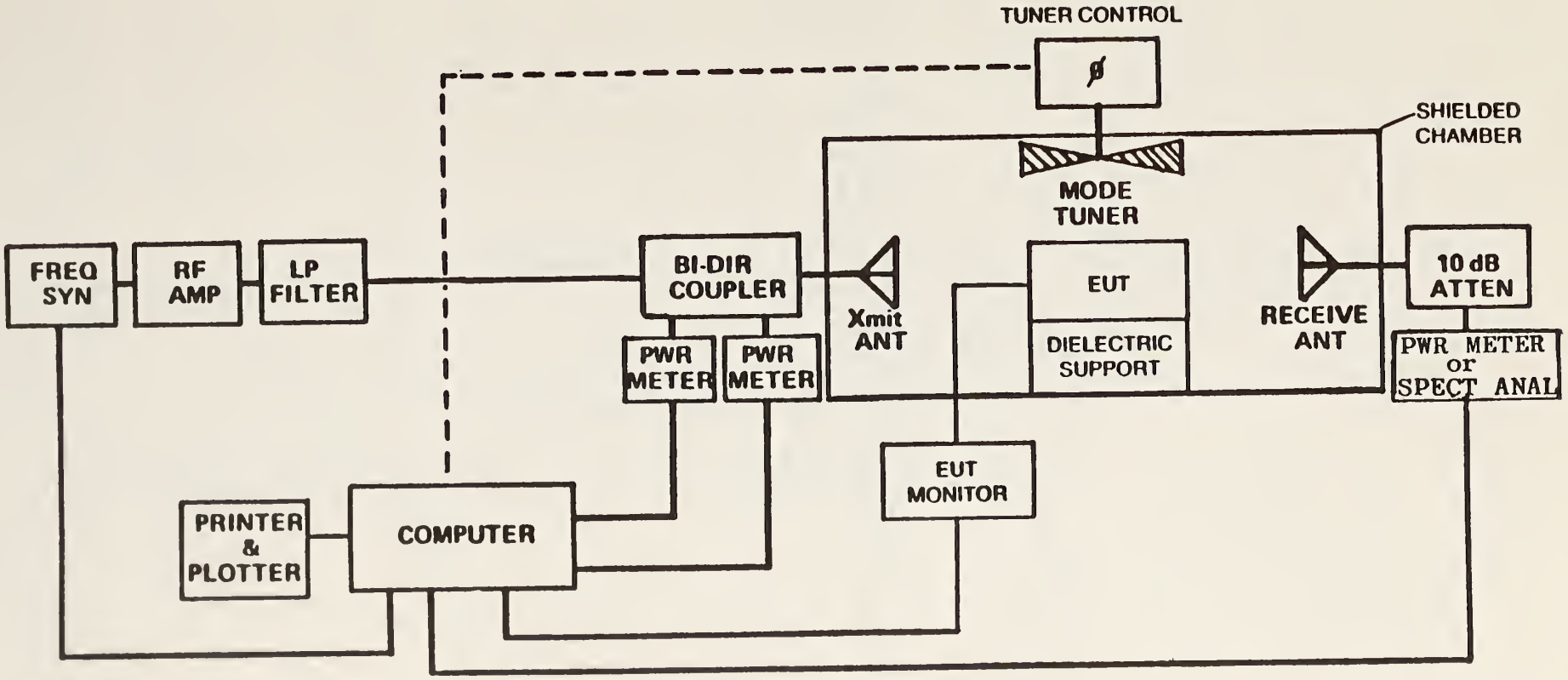

Figure 2.4. Block diagram of NBS system used in cw evaluation of RADC reverberating chamber.

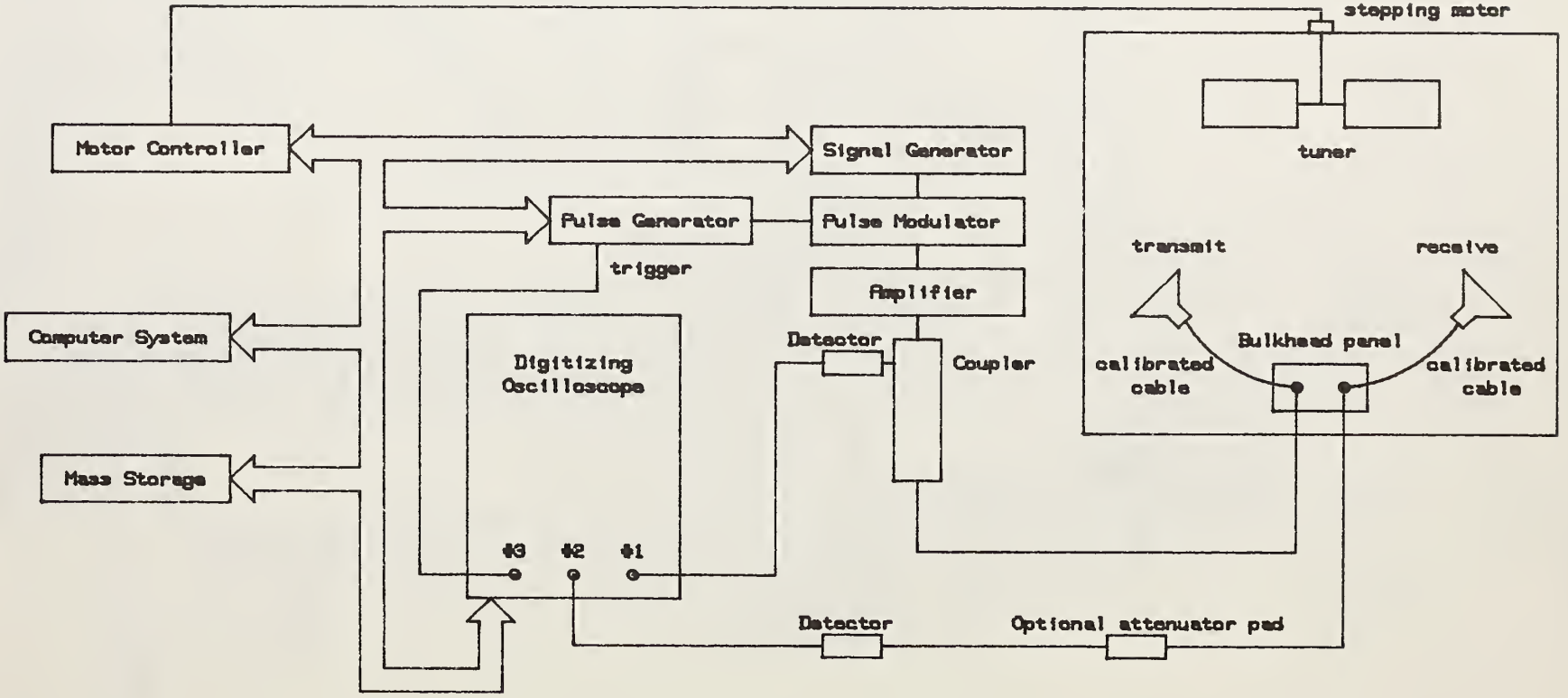

Figure 2.5. Block diagram of system used for evaluating pulsed rf response characteristics of RADC reverberating chamber.

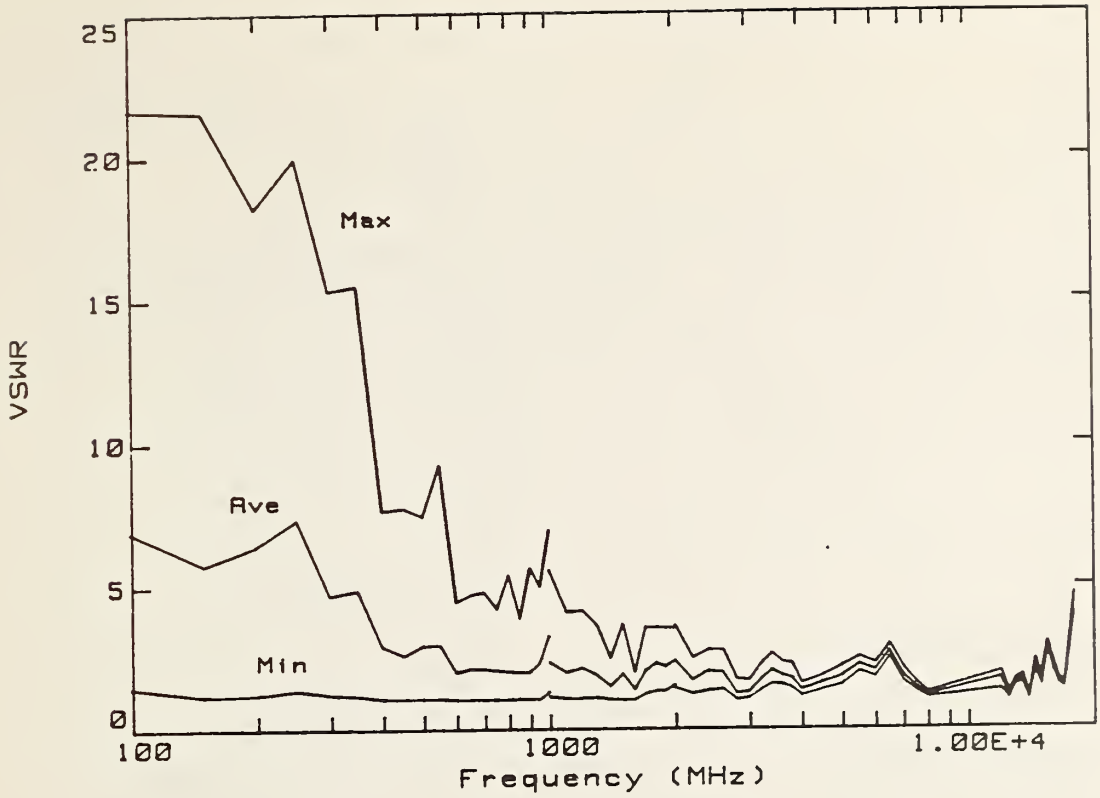

Figure 3.1. Statistical representation of the composite VSWR of the transmitting antennas used to launch the fields inside the RADC reverberating chamber.

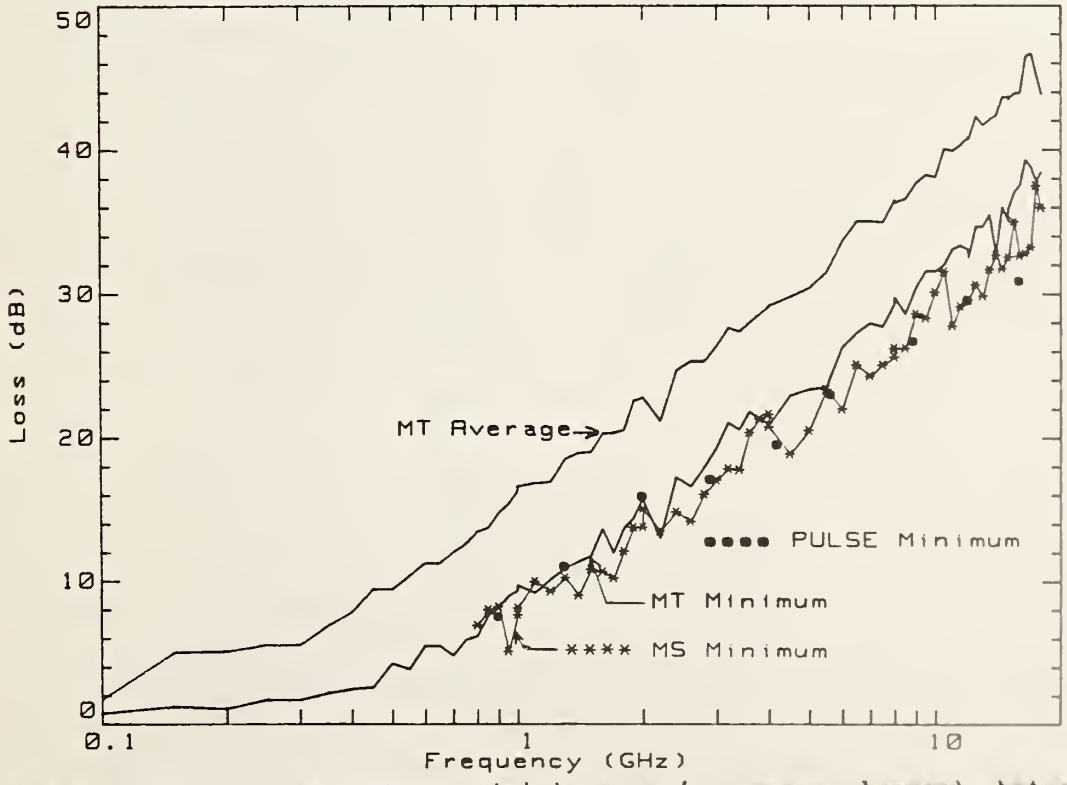

Figure 3.2. Coupling efficiency (minimum and average losses) between transmitted and received powers measured at antenna's terminals inside RADC reverberating chamber. Losses determined for (a) cw measurements using mode-tuned, (b) cw measurements using mode-stirred and (c) from pulsed rf measurements.

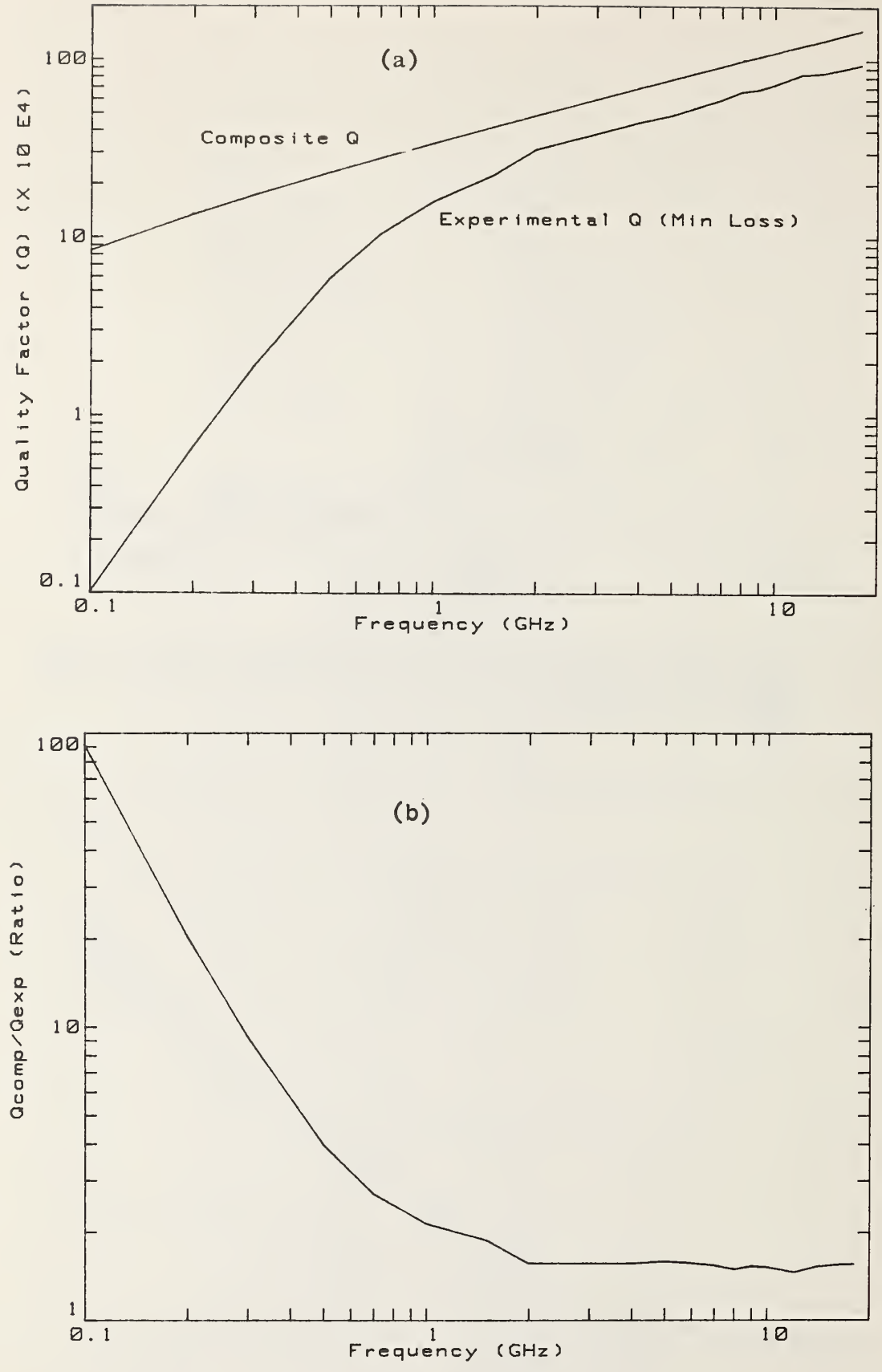

Figure 3.3. Theoretical composite $\tilde{Q}$ and experimental Q' determined for RADC reverberating chamber. (a) Theoretical and experimental values of Q as a function of frequency. (b) Ratio of the theoretical composite $\tilde{Q}$ to experimental Q' as a function of frequency.

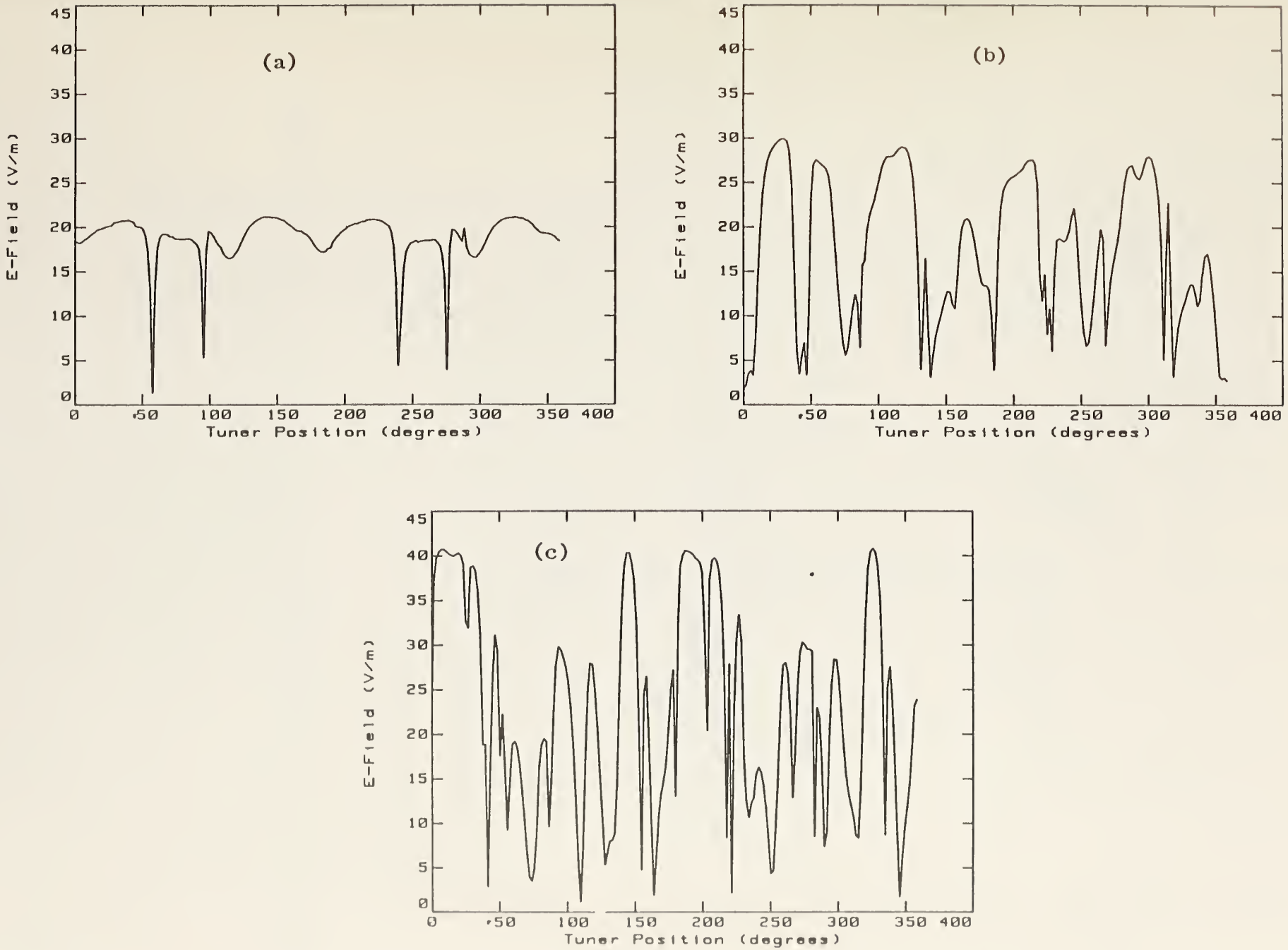

Figure 3.4. Examples of E-field inside the chamber as a function of tuner position for 1 watt net input power. (a) 100 MHz, (b) 150 MHz, and (c) 200 MHz.

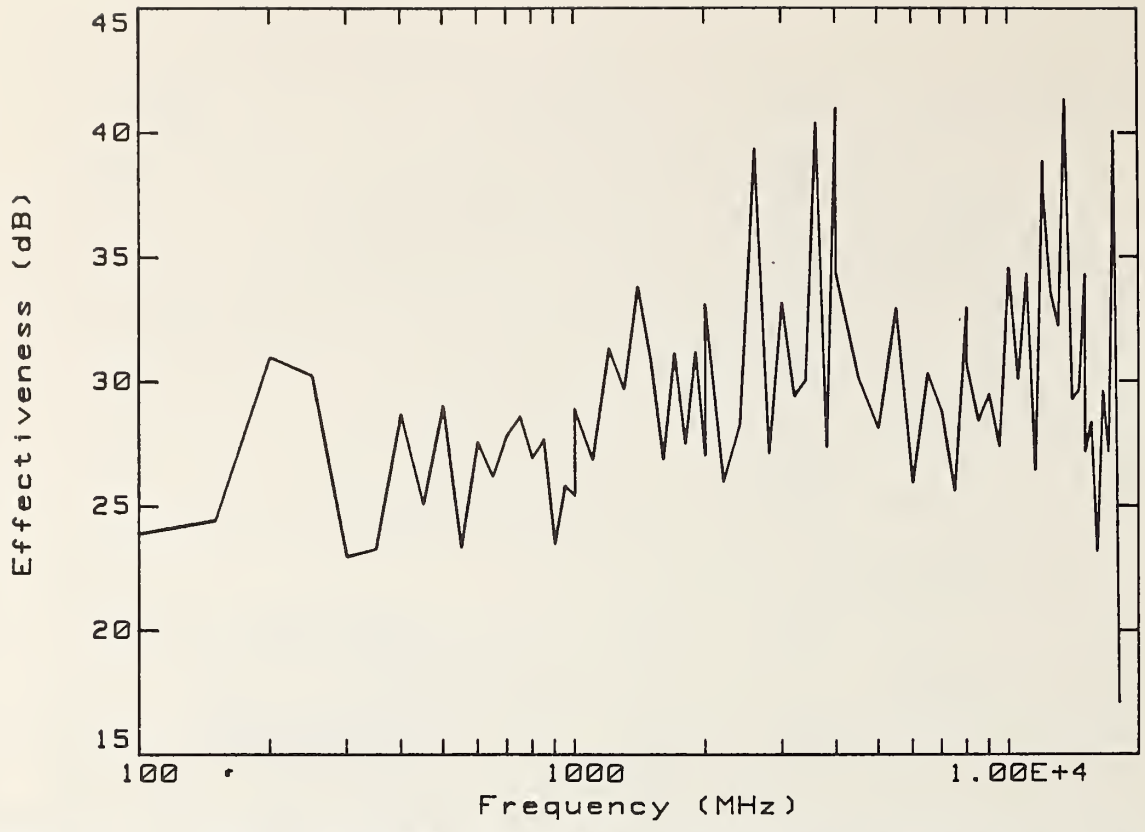

Figure 3.5. **Ratio of maximum to minimum received power obtained by rotating tuner in the frequency range 100 MHz to 18 GHz inside the RADC reverberating chamber.**

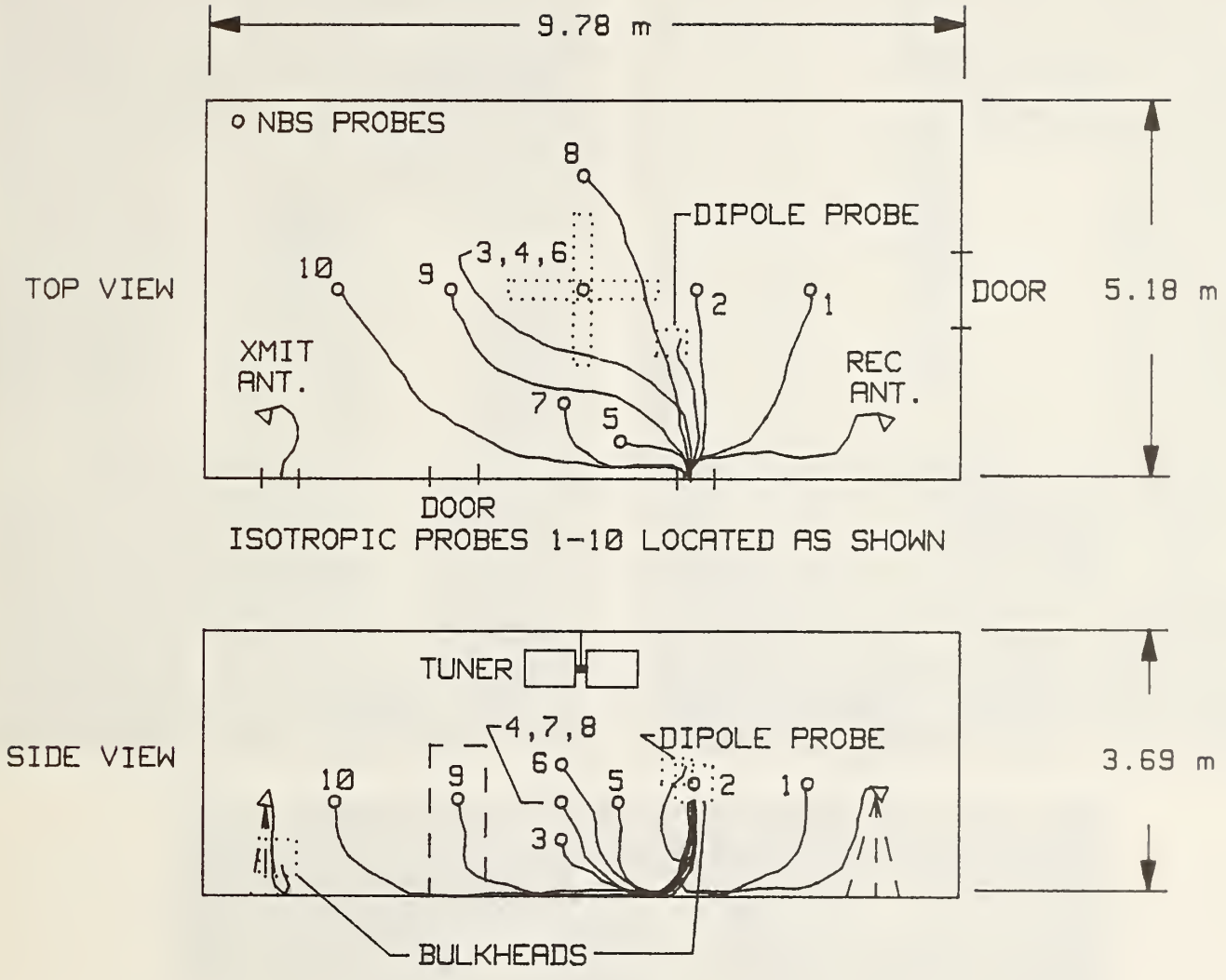

Figure 3.6. Cross sectional views of RADC reverberating chamber showing placement of NBS isotropic probes for evaluation of spatial distribution of E-fields.

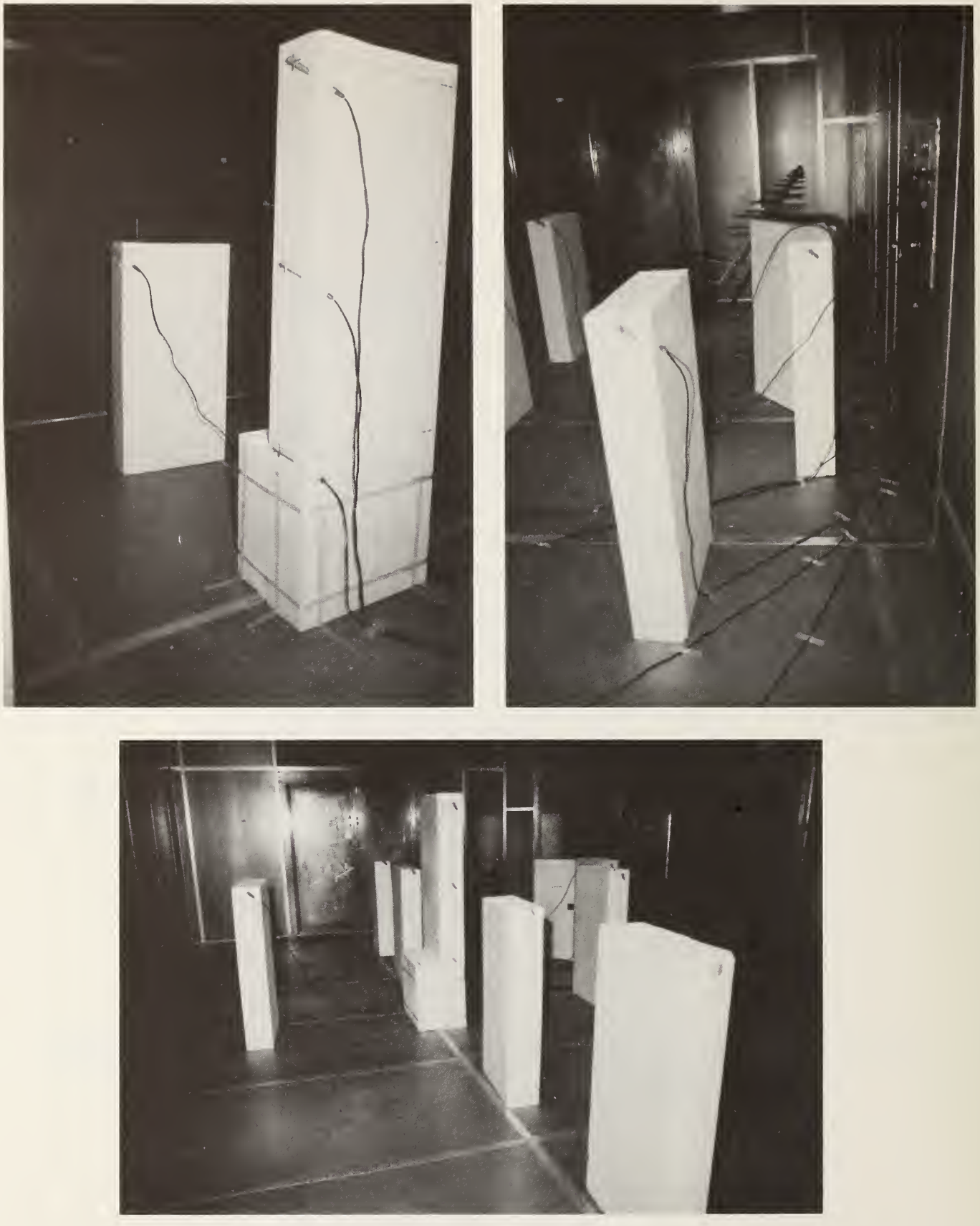

Figure 3.7. Photographs of interior of RADC reverberating chamber showing placement of NBS isotropic probes for evaluation of spatial distribution of E-fields.

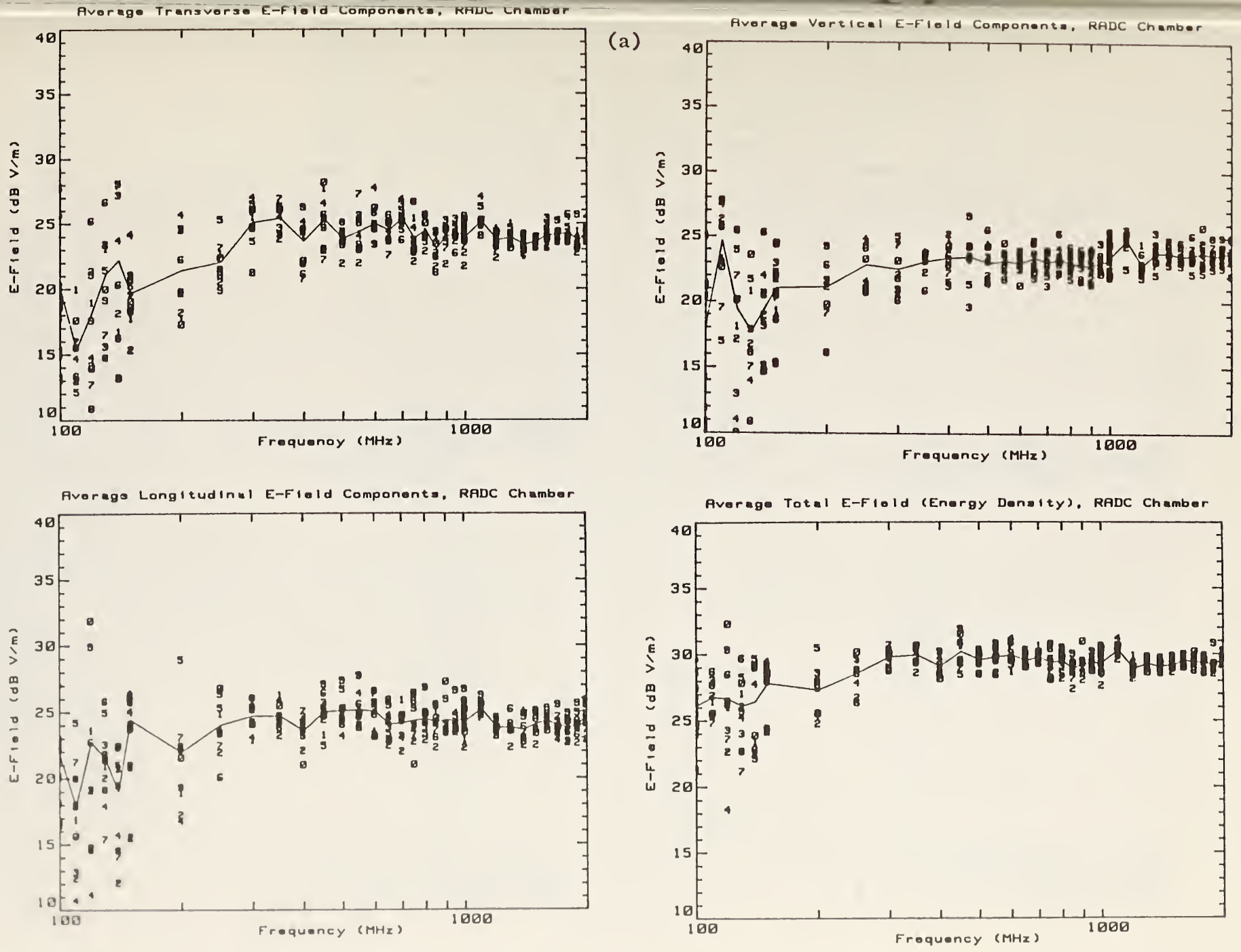

Figure 3.8. Sheet 1 of 2. Average values of three orthogonal components and square root of sum of squares of the components (Total).

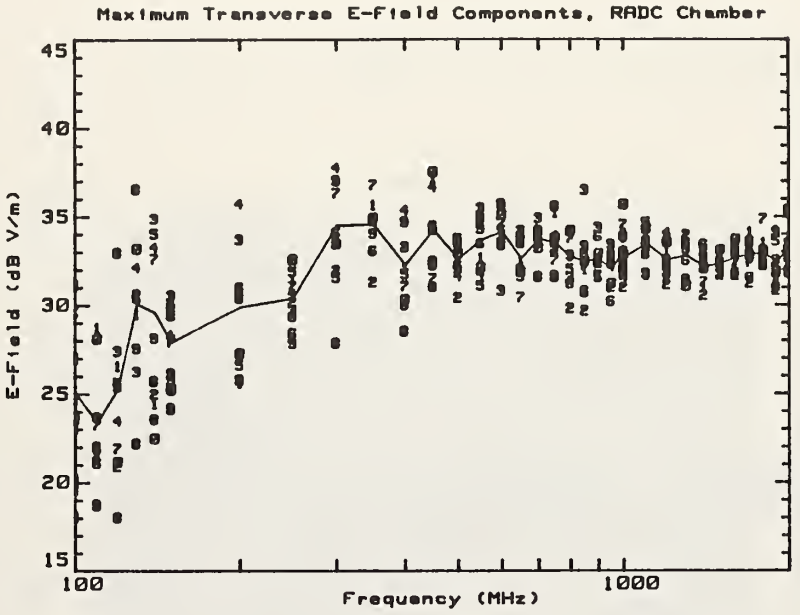

(b)

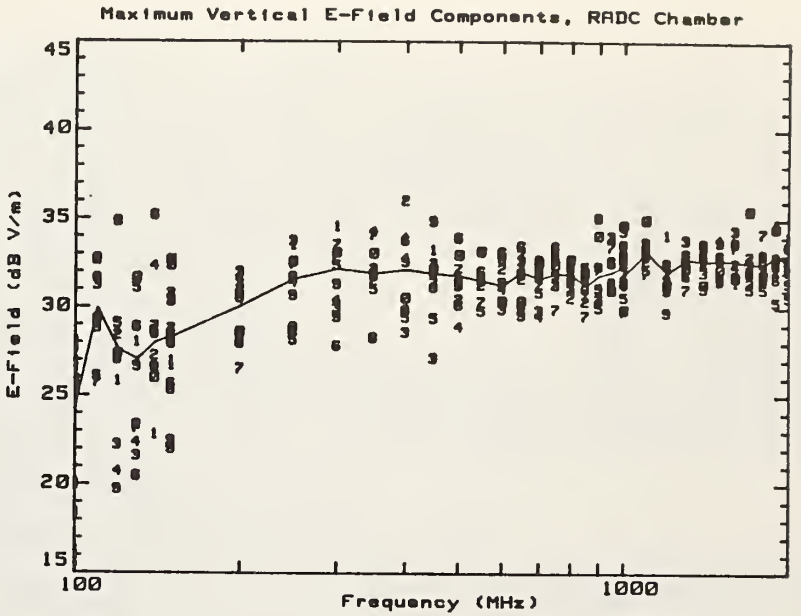

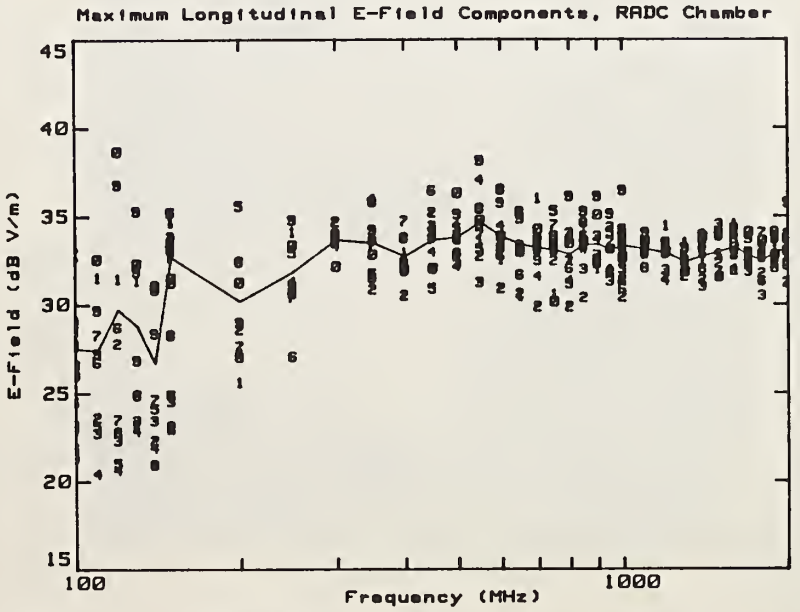

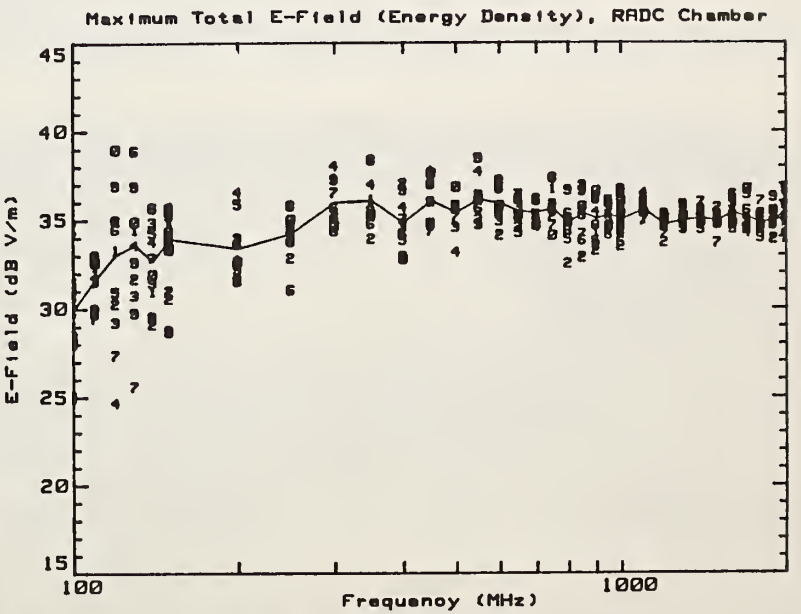

1587,

Figure 3.8. Sheet 2 of 2. Maximum values of three orthogonal components and square root of sum of squares of the components (Total).

Figure 3.8. Spatial distribution of the E-field measured inside the RADC reverberating chamber using array of 10 NBS isotropic probes: (a) average, and (b) maximum. Net input power normalized to 1 watt. Transmitting antennas are log periodic, 0.1 GHz to 1.0 GHz, and ridged horn, 1.0 GHz to 2.0 GHz.

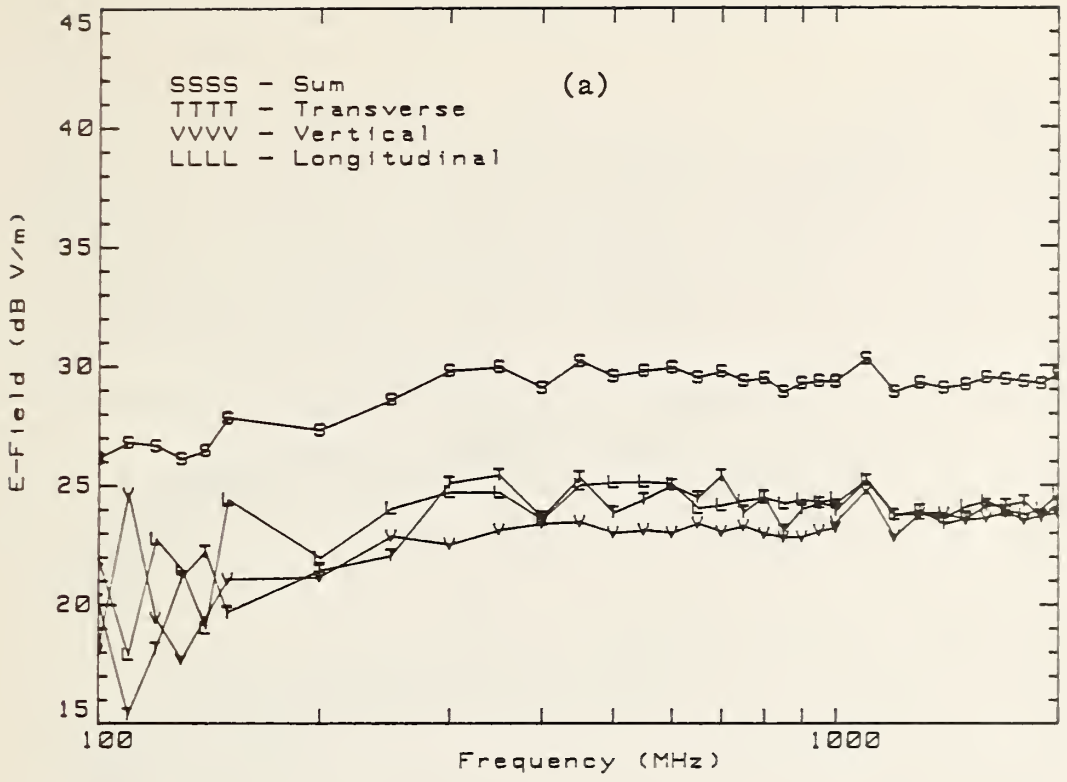

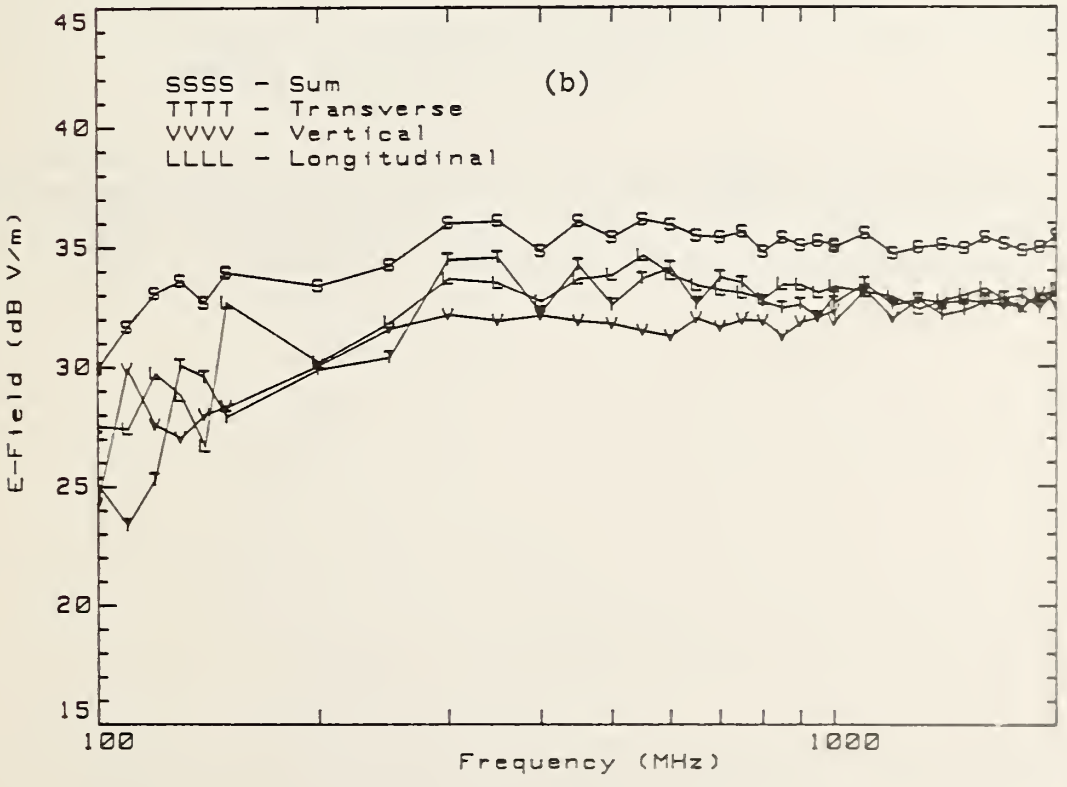

Figure 3.9. Average values of the E-field strength measured inside RADC reverberating chamber using array of 10 NBS isotropic probes with 1 watt net input power: (a) average of the averages, (b) average of the maximums. Transmitting antennas same as figure 3.8.

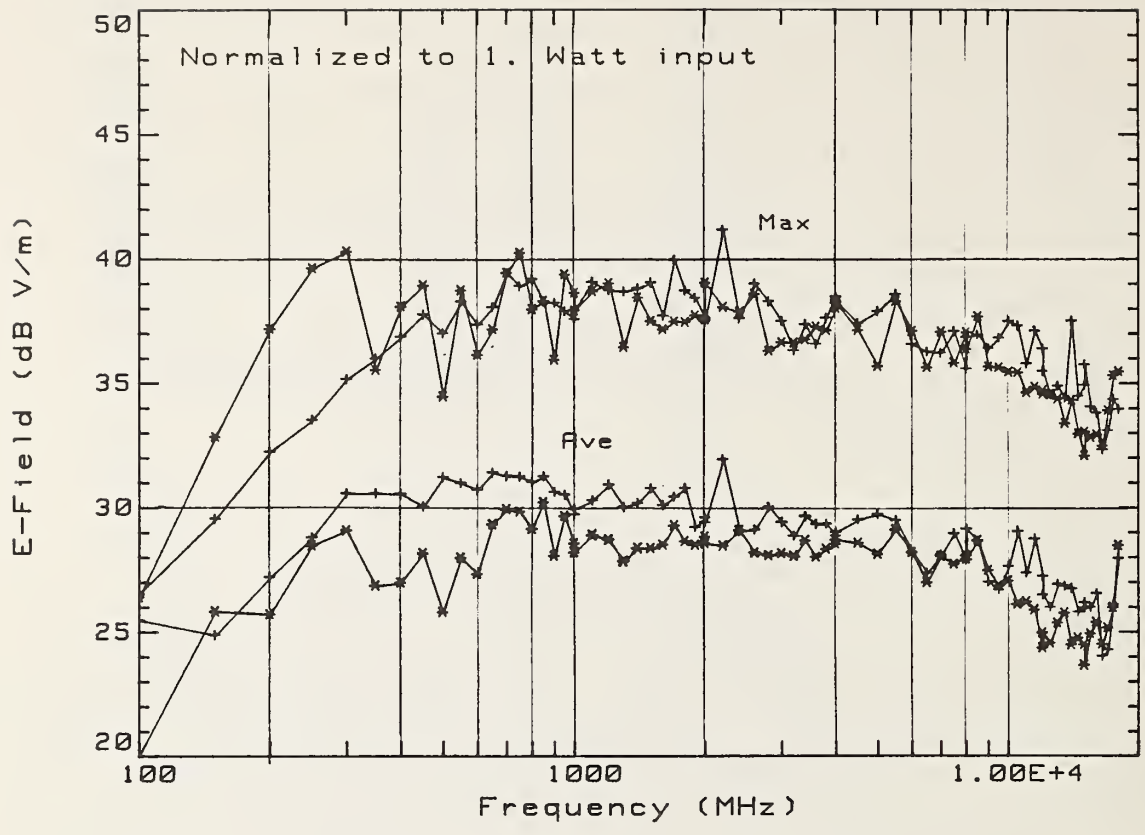

Figure 3.10. Average and maximum E-field strengths determined inside RADC reverberating chamber using: (1) reference antenna's received power measurements (++++), and (2) calibrated 1-cm dipole probe measurements (****). Net input power normalized to 1 watt.

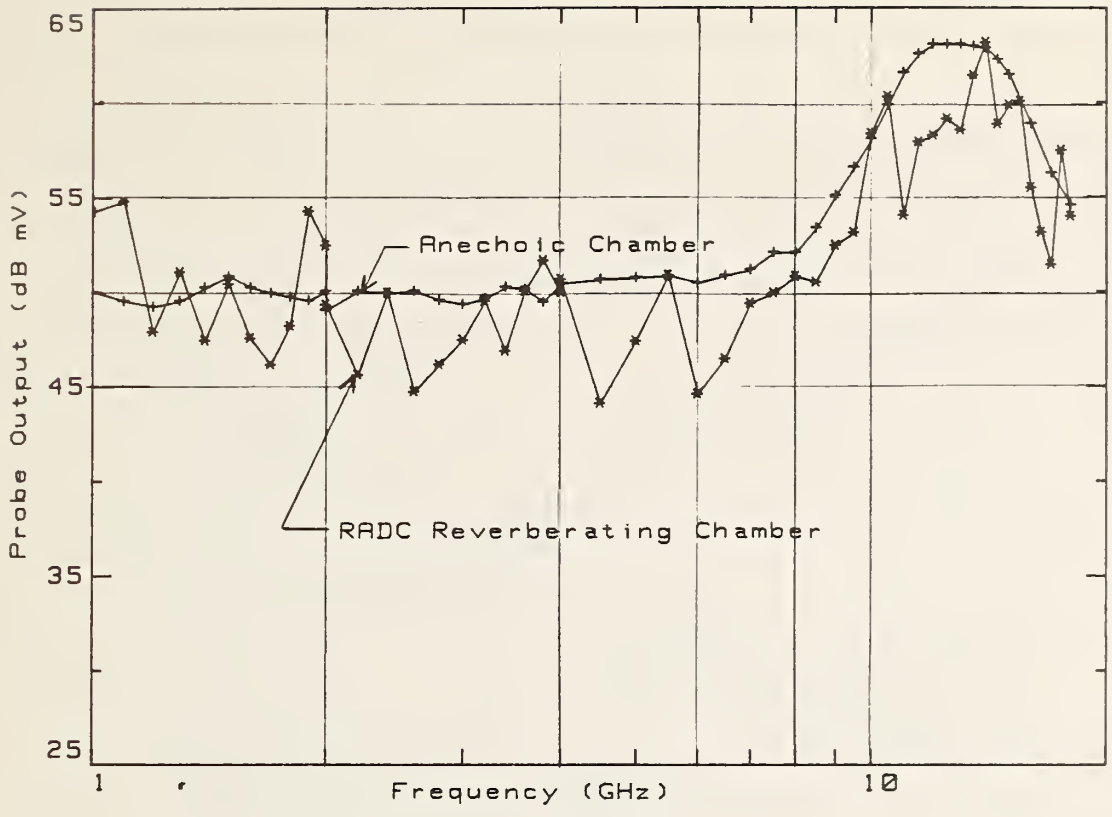

Figure 3.11. Comparison of the peak responses of NBS 1-cm dipole probe to normalized E-field of 37 dB V/m determined using RADC reverberating chamber and NBS anechoic chamber.

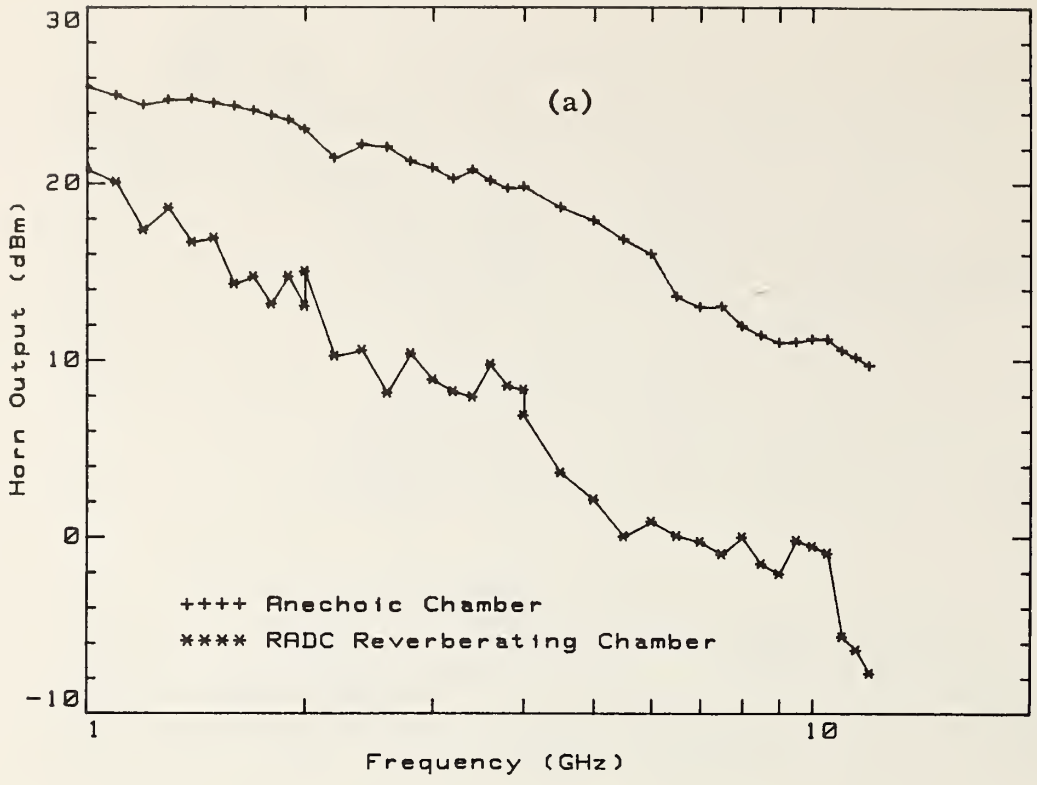

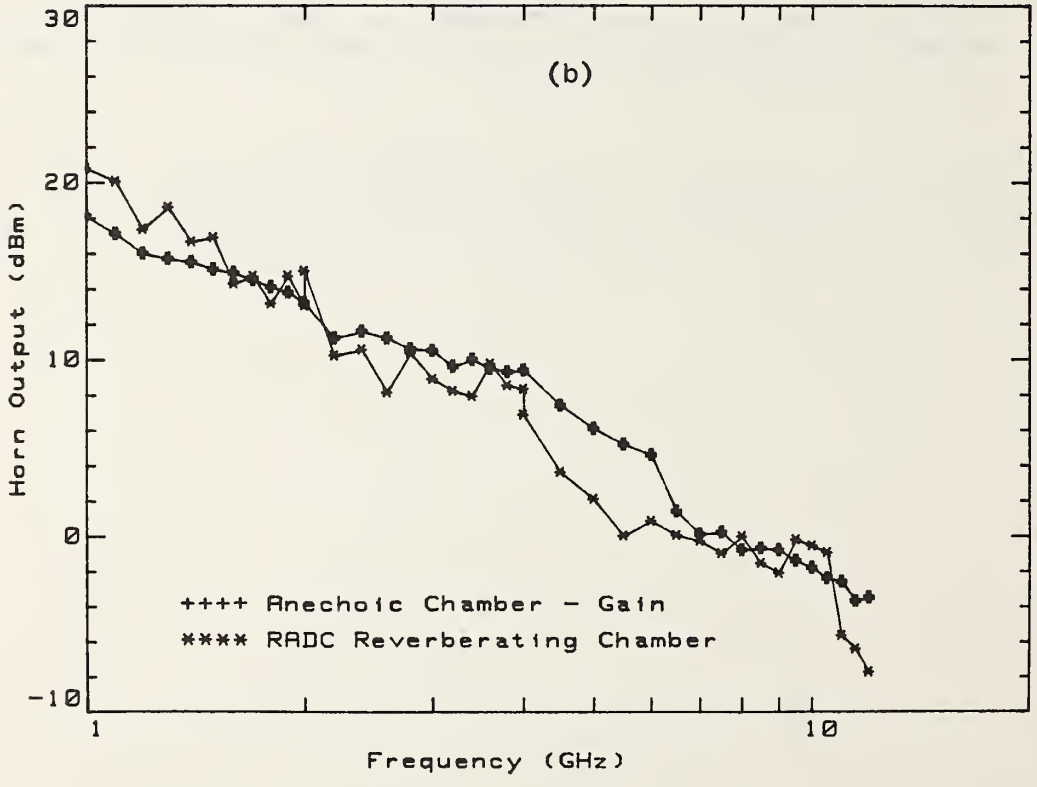

Figure 3.12. Comparison of (1-12 GHz) ridged horn's peak responses to normalized E-field of 37 dB V/m established inside RADC reverberating chamber and inside NBS anechoic chamber. (a) antenna output versus frequency, (b) Comparison of responses with horn's free-space gain subtracted from anechoic chamber results.

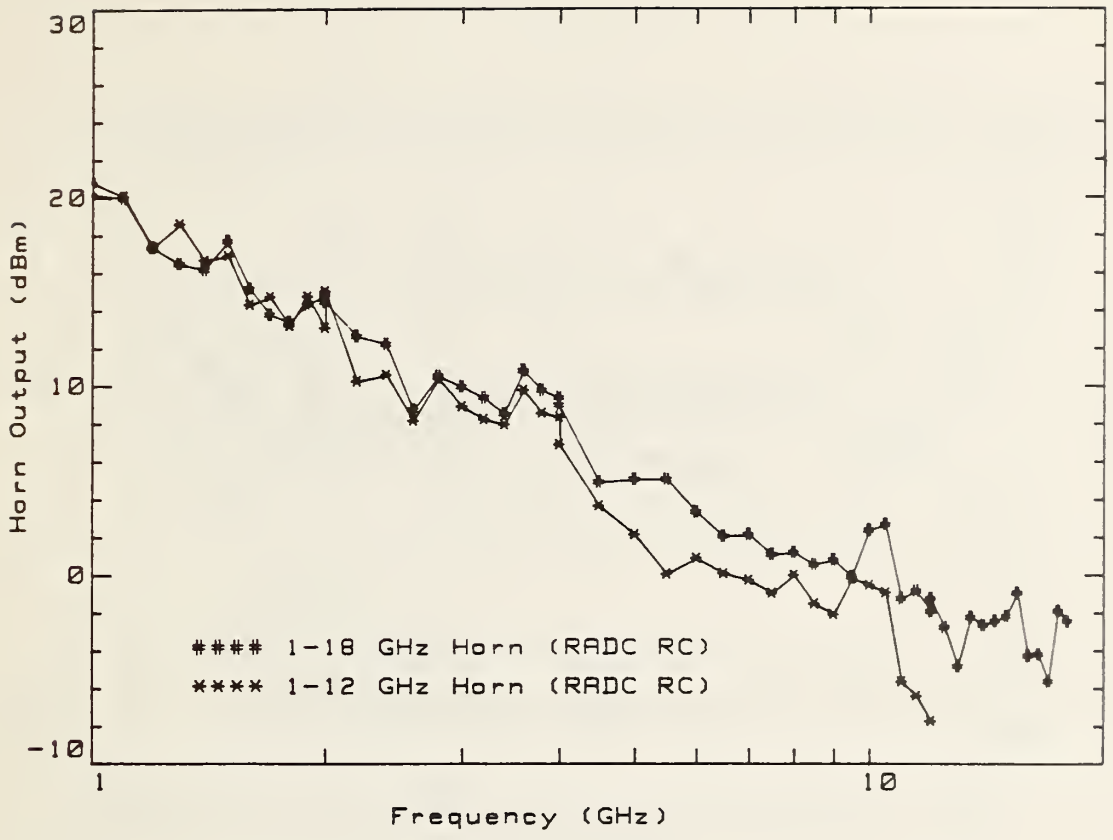

Figure 3.13. Comparison of peak response of (1-18 GHz) and (1-12 GHz) ridged horn antennas to 37 dB V/m normalized E-fields established inside RADC reverberating chamber.

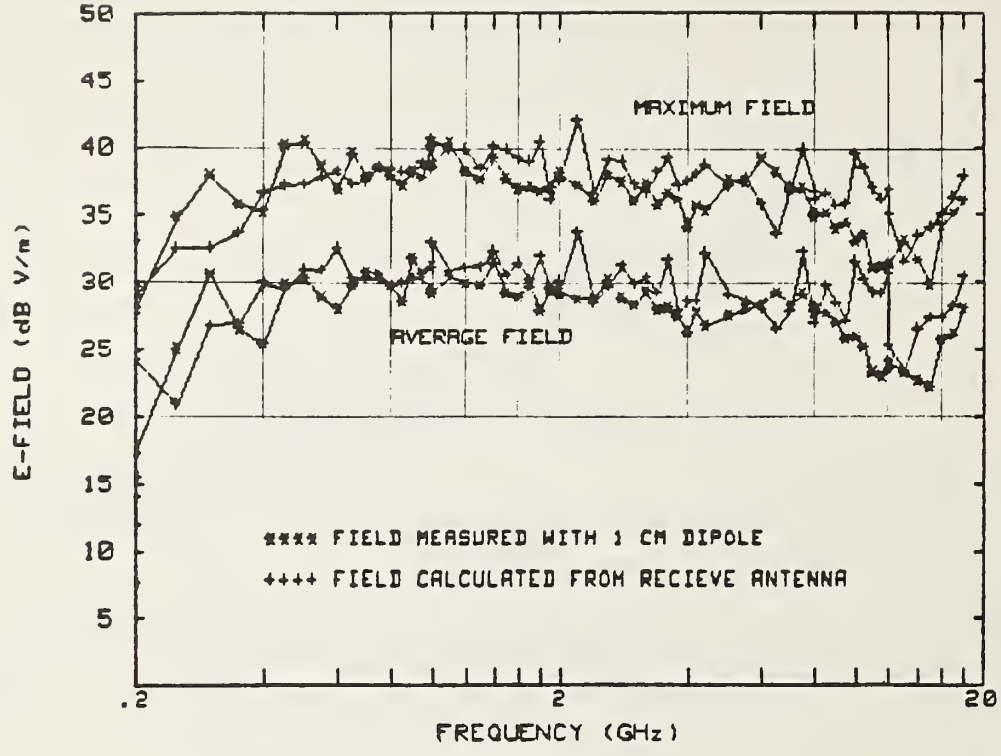

Figure 3.14. Average and maxumum E-field strengths inside empty NBS reverberating chamber for 1-W net input power determined from: a) reference antenna's received power measurements, and b) calibrated 1-cm dipole probe measurements.

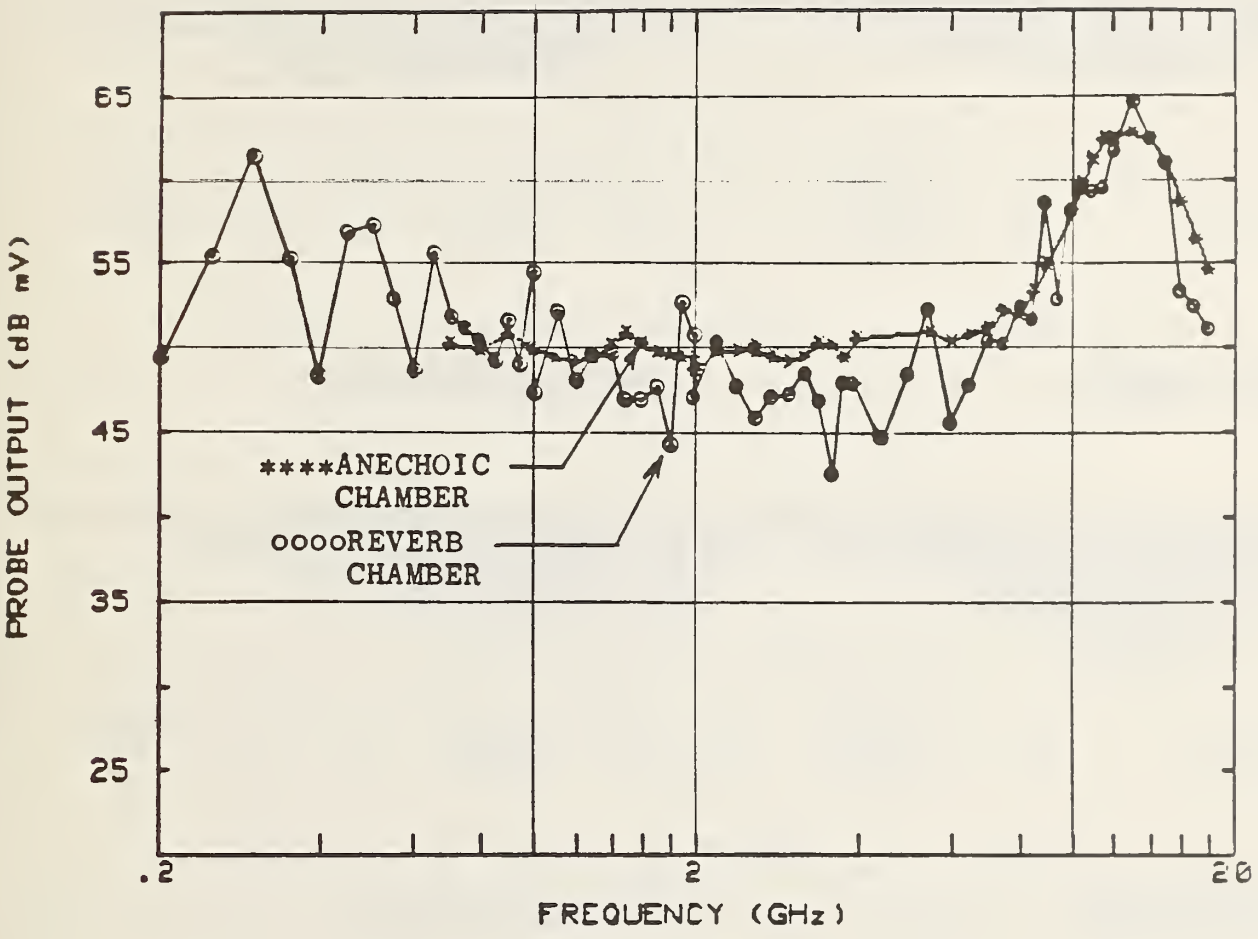

Figure 3.15. Comparison of 1-cm dipole probe's peak response to EM field established inside NBS reverberating and anechoic chambers. Output normalized to E-field exposure of 37 dB V/m.

(a) No Absorber

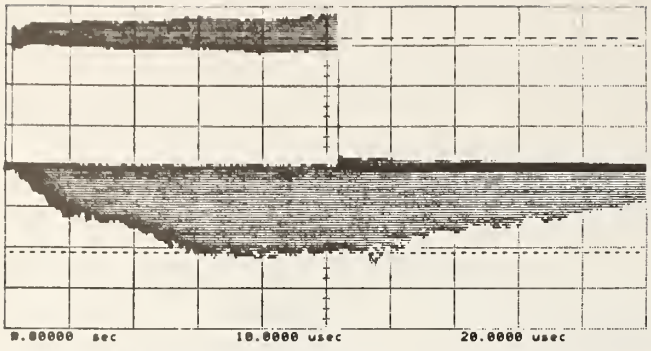

Function1 = 50.00 mvolts/div
Ch. 2 = 100.0 mvolts/div
Timebase = 2.00 usec/div
Delta V = -372.0 mvolts
Vmarker1 = 160.0 mvolts
Offset = 0.000 volts
Offset = 0.000 volts
Delay = 0.00000 sec
Vmarker2 = -212.0 mvolts

(b) 1/2 Pc. 3" Absorber

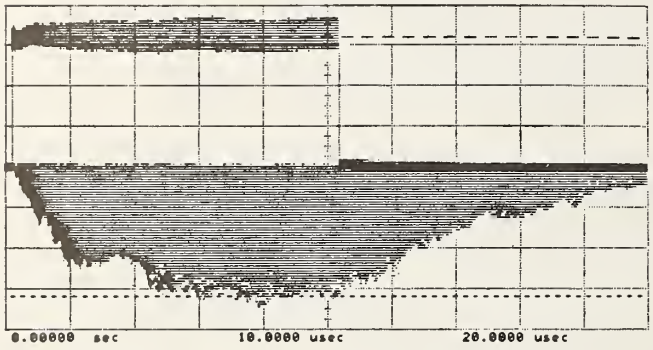

Function1 = 50.00 mvolts/div
Ch. 2 = 50.00 mvolts/div
Timebase = 2.00 usec/div
Delta V = -320.0 mvolts
Vmarker1 = 160.0 mvolts
Offset = 0.000 volts
Offset = 0.000 volts
Delay = 0.00000 sec
Vmarker2 = -160.0 mvolts

(c) 1 Pc. 3" Absorber

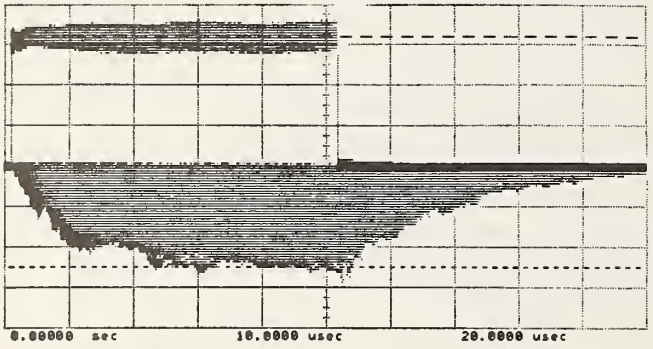

Function1 = 50.00 mvolts/div
Ch. 2 = 50.00 mvolts/div
Timebase = 2.00 usec/div
Delta V = -205.0 mvolts
Vmarker1 = 160.0 mvolts
Offset = 0.000 volts
Offset = 0.000 volts
Delay = 0.00000 sec
Vmarker2 = -125.0 mvolts

(d) 1 Pc. 5" Absorber

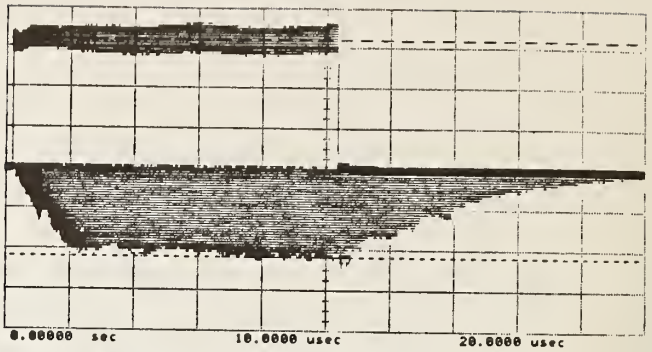

Function1 = 50.00 mvolts/div
Ch. 2 = 50.00 mvolts/div
Timebase = 2.00 usec/div
Delta V = -270.0 mvolts
Vmarker1 = 160.0 mvolts
Offset = 0.000 volts
Offset = 0.000 volts
Delay = 0.00000 sec
Vmarker2 = -110.0 mvolts

(e) 1 Pc. 8" Absorber

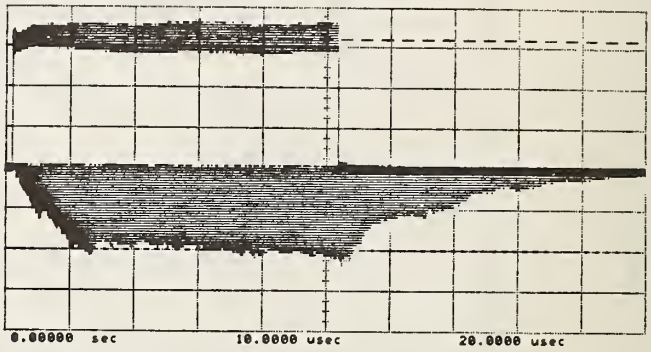

Function1 = 50.00 mvolts/div
Ch. 2 = 50.00 mvolts/div
Timebase = 2.00 usec/div
Delta V = -260.0 mvolts
Vmarker1 = 160.0 mvolts
Offset = 0.000 volts
Offset = 0.000 volts
Delay = 0.00000 sec
Vmarker2 = -100.0 mvolts

(f) 1 Pc. 11" Absorber

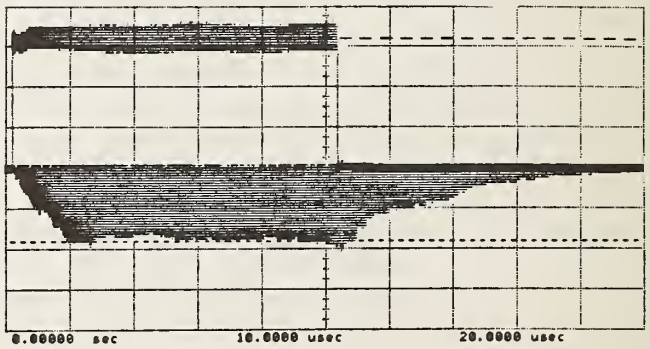

Function1 = 50.00 mvolts/div
Ch. 2 = 50.00 mvolts/div
Timebase = 2.00 usec/div
Delta V = -250.0 mvolts
Vmarker1 = 160.0 mvolts
Offset = 0.000 volts
Offset = 0.000 volts
Delay = 0.00000 sec
Vmarker2 = -90.00 mvolts

Figure 4.1. Sheet 1 of 2.

(g) 1 Pc. 24" Absorber

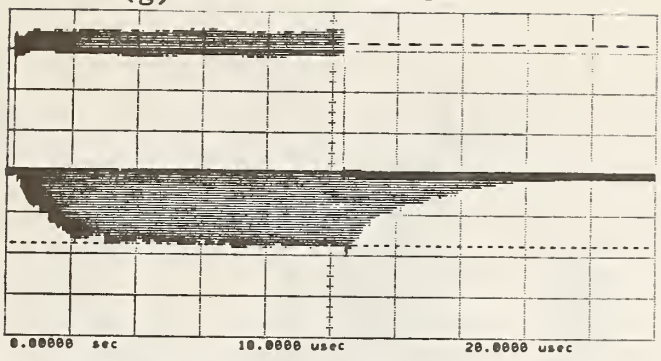

Function1 = 50.00 mvolts/div
Ch. 2 = 50.00 mvolts/div
Timebase = 2.00 usec/div
Delta V = -247.0 mvolts
Vmarker1 = 160.0 mvolts

Offset = 0.000 volts
Offset = 0.000 volts
Delay = 0.00000 sec
Vmarker2 = -87.00 mvolts

(h) 2 Pcs. 24" Absorber

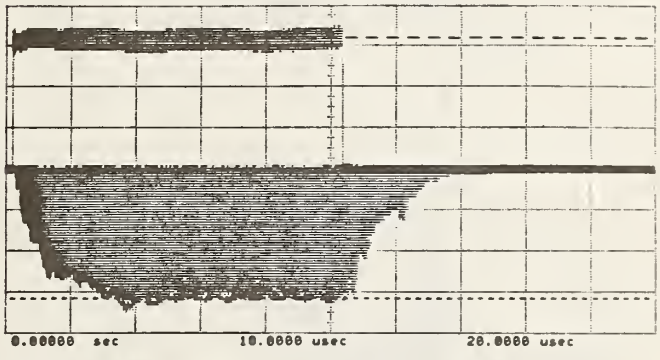

Function1 = 50.00 mvolts/div
Ch. 2 = 20.00 mvolts/div
Timebase = 2.00 usec/div
Delta V = -223.2 mvolts
Vmarker1 = 160.0 mvolts

Offset = 0.000 volts
Offset = 0.000 volts
Delay = 0.00000 sec
Vmarker2 = -63.20 mvolts

(i) 4 Pcs. 24" Absorber

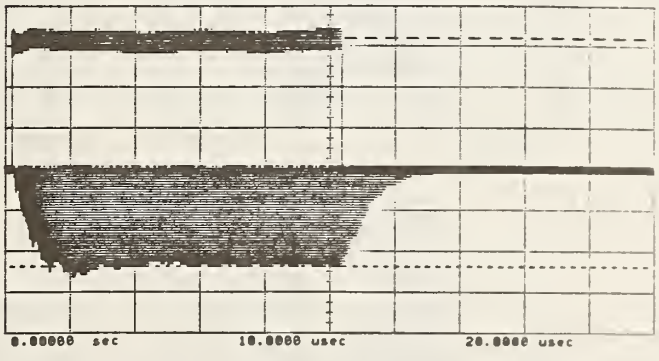

Function1 = 50.00 mvolts/div
Ch. 2 = 20.00 mvolts/div
Timebase = 2.00 usec/div
Delta V = -207.2 mvolts
Vmarker1 = 160.0 mvolts

Offset = 0.000 volts
Offset = 0.000 volts
Delay = 0.00000 sec
Vmarker2 = -47.20 mvolts

Figure 4.1. Sheet 2 of 2.

Figure 4.1. Maximum received rf pulse waveforms inside RADC reverberating chamber determined with increasing amounts of rf absorber loading at 0.9 GHz. Measurements were made using dual channel digitizing oscilloscope.

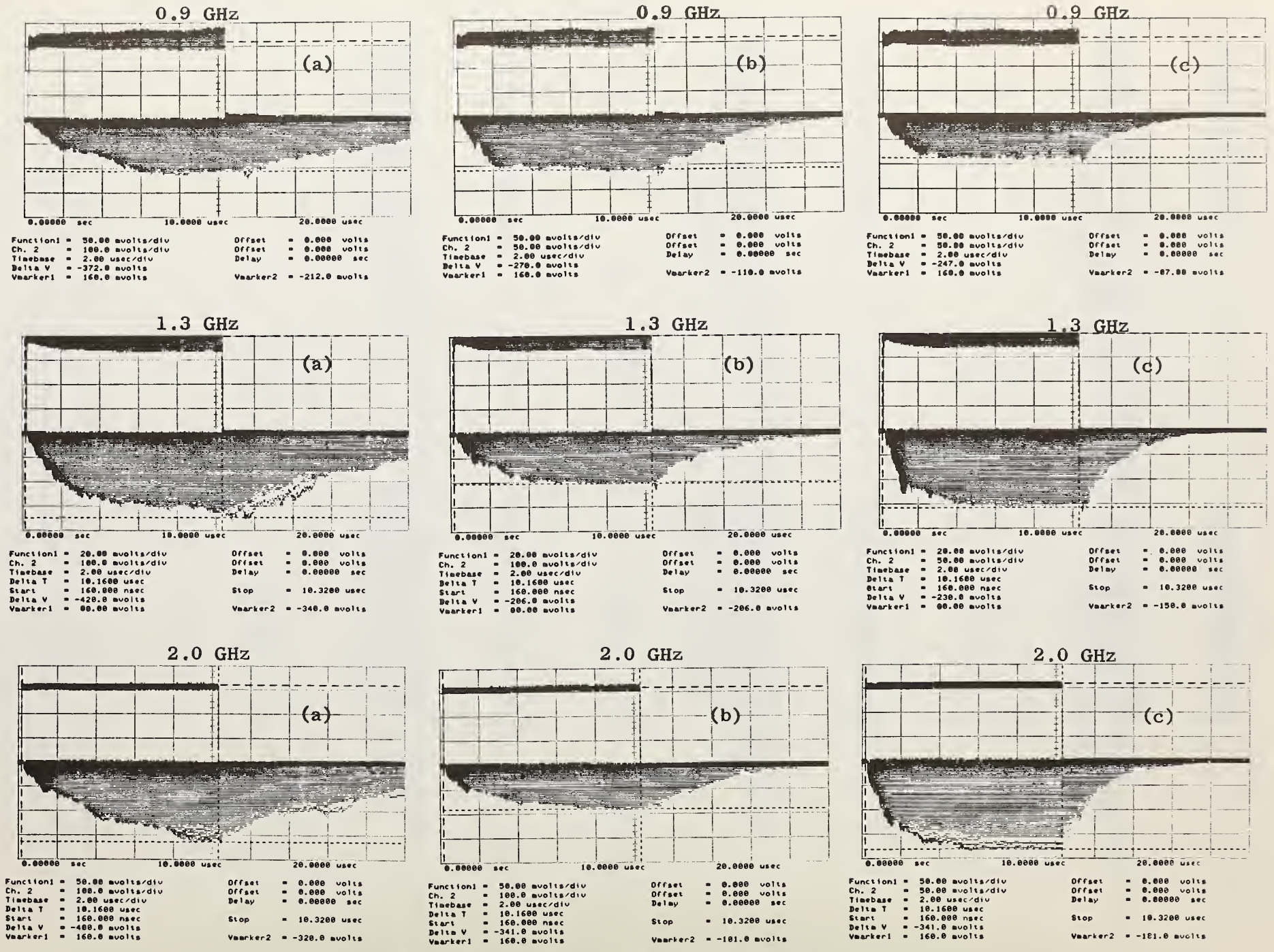

Figure 4.2. Sheet 1 of 3, (0.9, 1.3, 2.0)GHz.

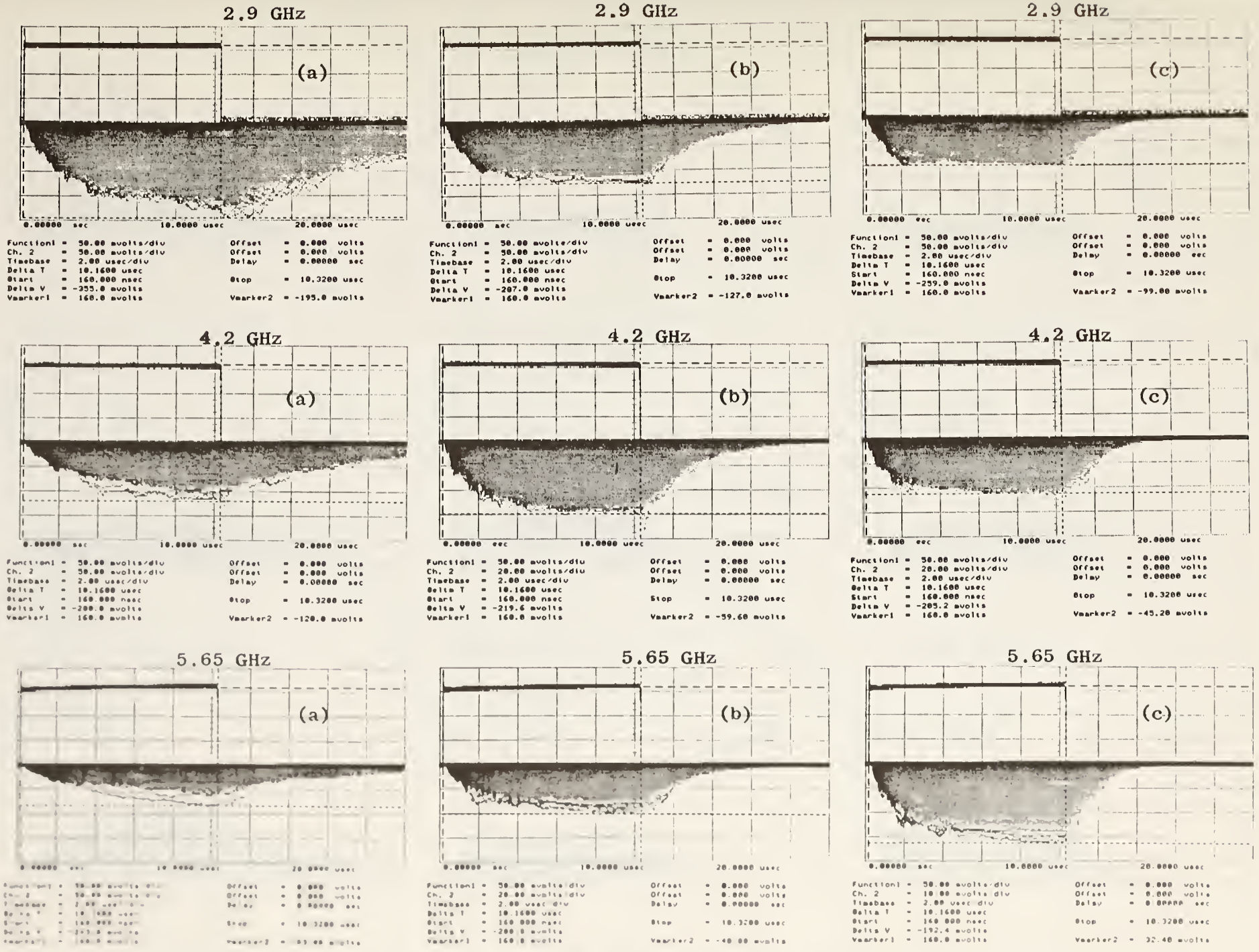

Figure 4.2. Sheet 2 of 3, (2.9, 4.2, 5.65)GHz.

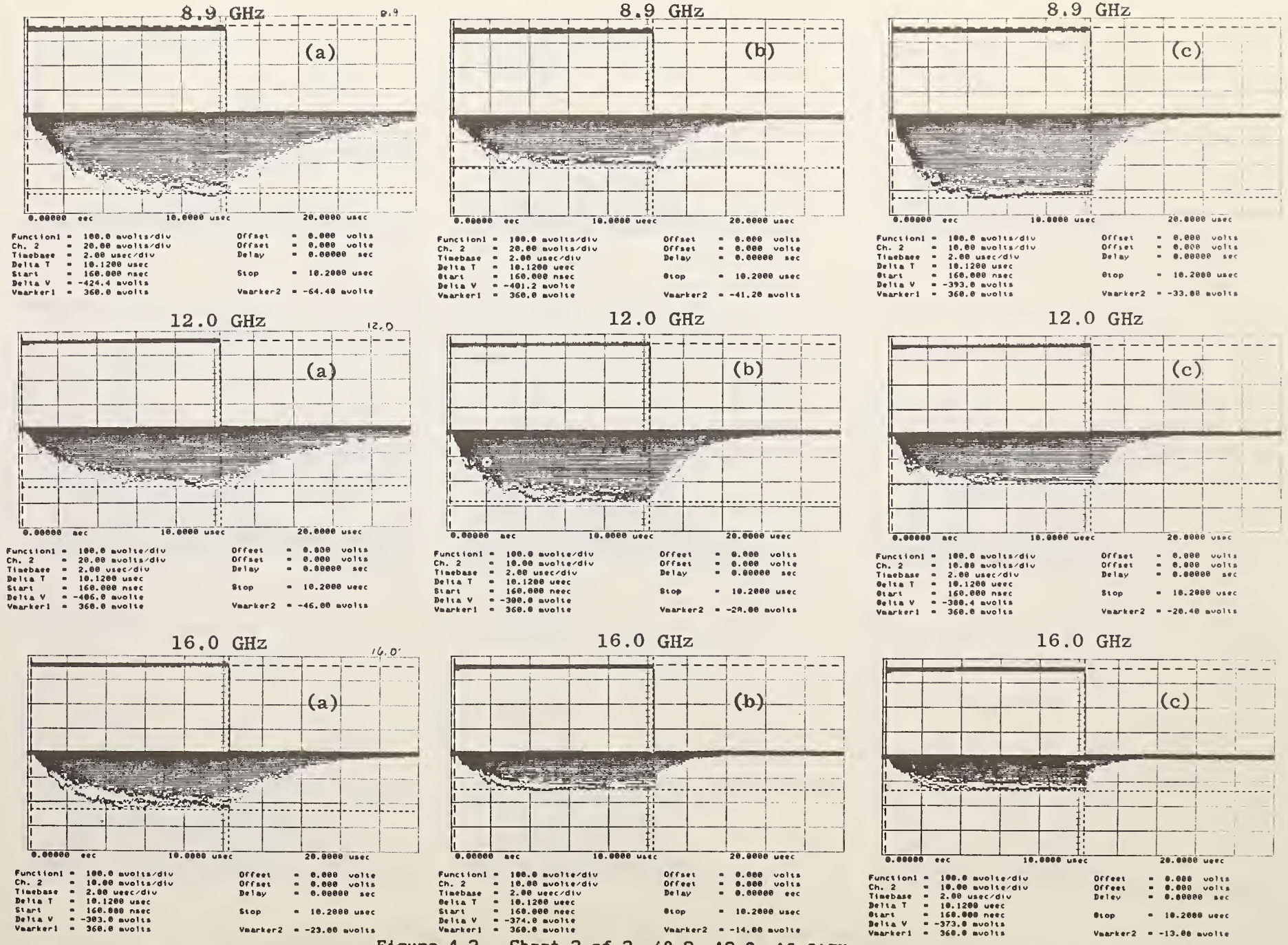

Figure 4.2. Sheet 3 of 3, (8.9, 12.0, 16.0)GHz.

Figure 4.2. Maximum received rf pulse waveforms inside RADC reverberating chamber with (a) no absorber, (b) 1 piece 5" x 24" x 24" rf absorber and (c) 1 piece 24" x 24" x 24" rf absorber at selected frequencies. Measurements were made using dual channel digitizing oscilloscope.

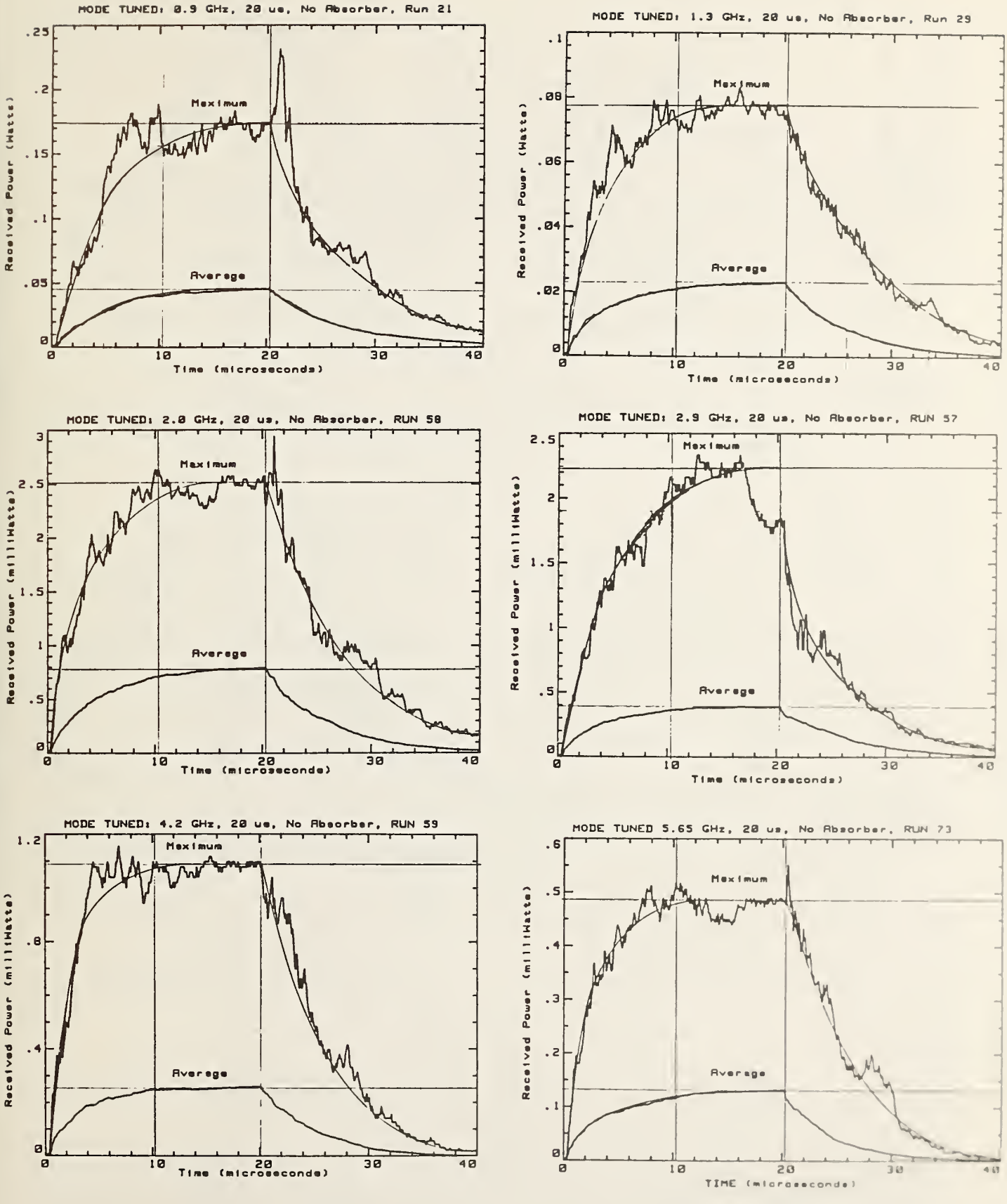

Figure 4.3. Sheet 1 of 10. Input pulse width is 20 μs. Input pulse amplitude is 1 W. at 0.9 and 1.3 GHz and 0.1 W at 2.0, 2.9, 4.2 and 5.65 GHz.

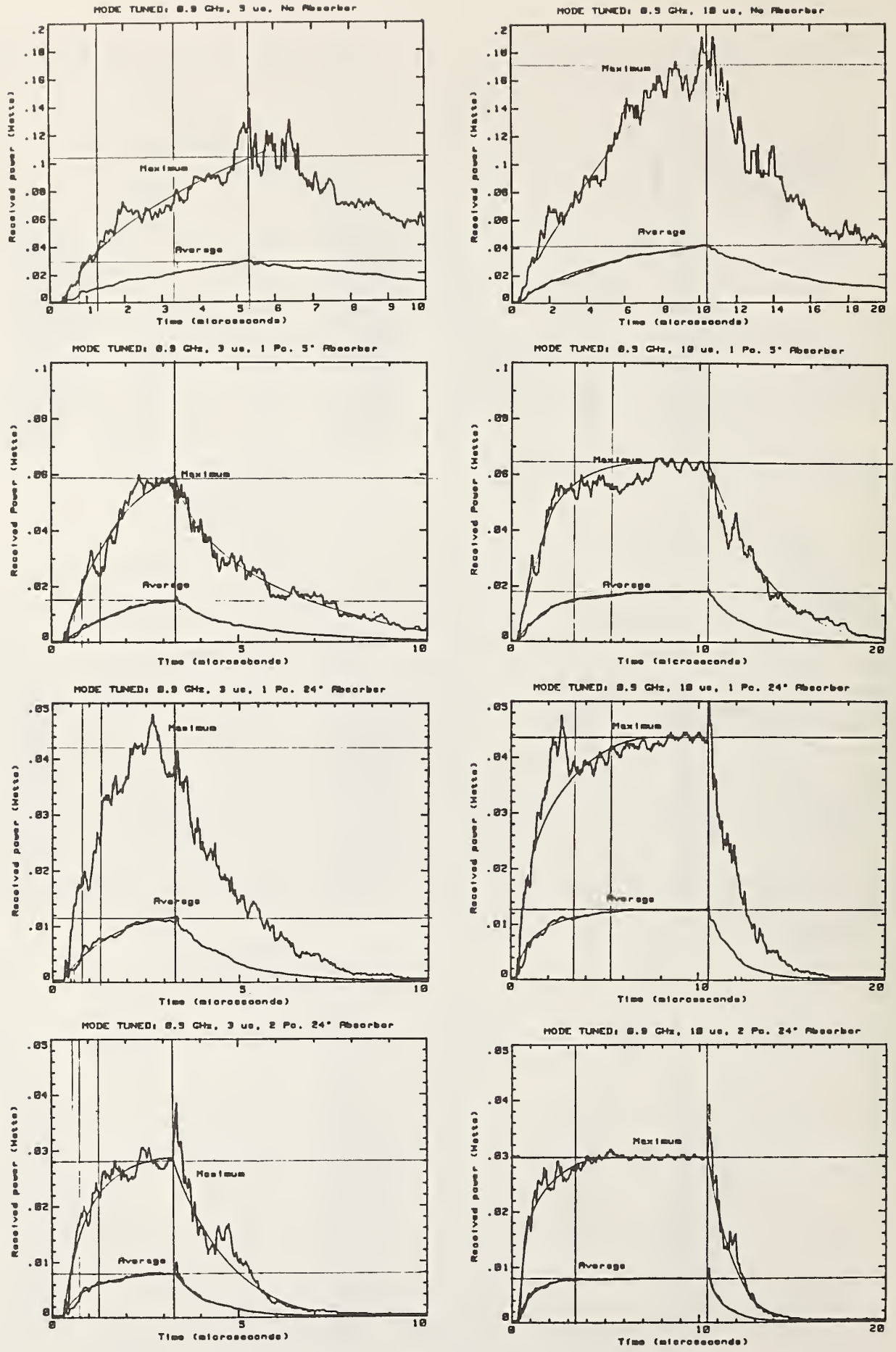

Figure 4.3. Sheet 2 of 10. Frequency = 0.9 GHz, input pulse amplitude is 1 W.

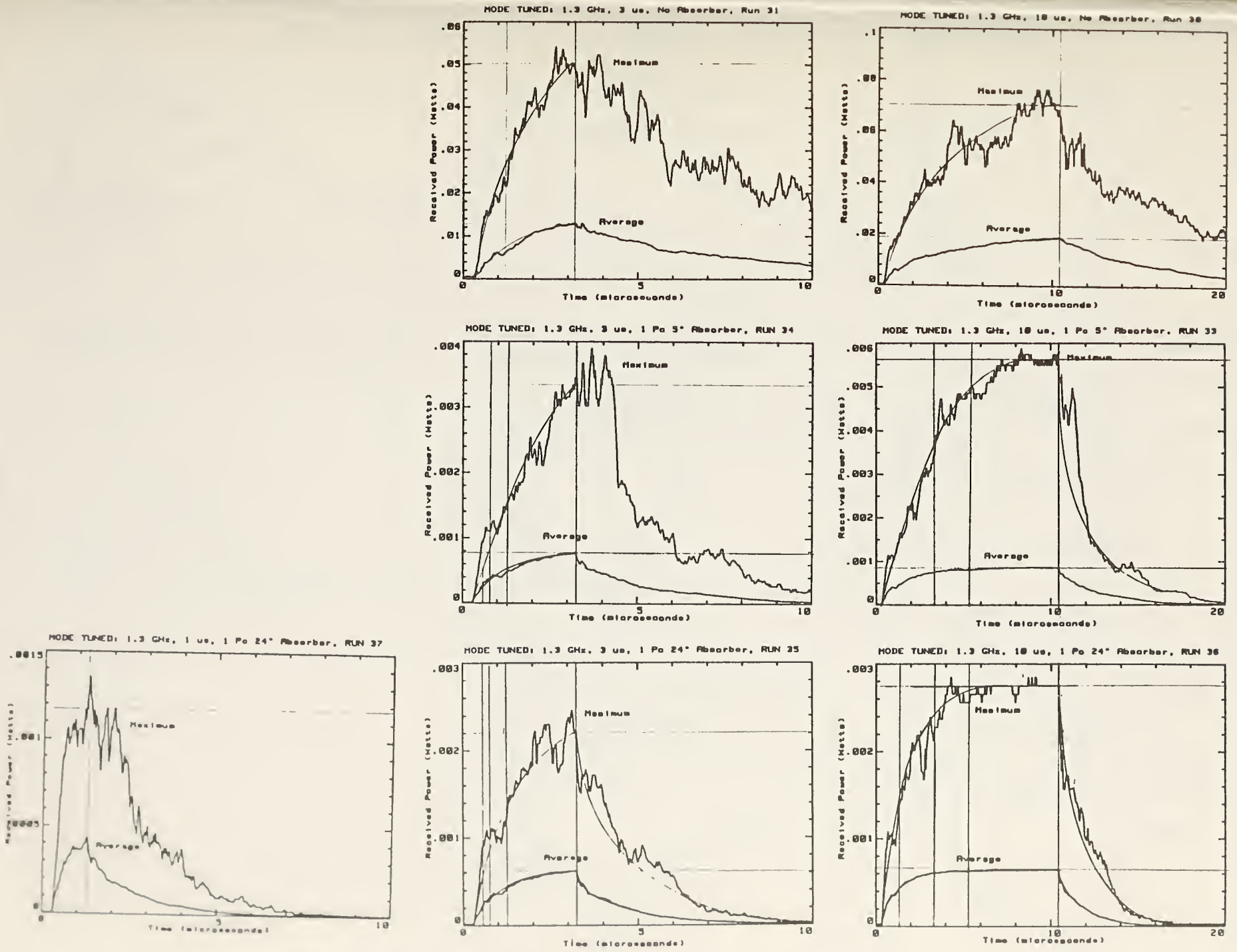

Figure 4.3. Sheet 3 of 10. Frequency = 1.3 GHz, input pulse amplitude is 1 W for no absorber loading and 0.1 W for absorber loading.

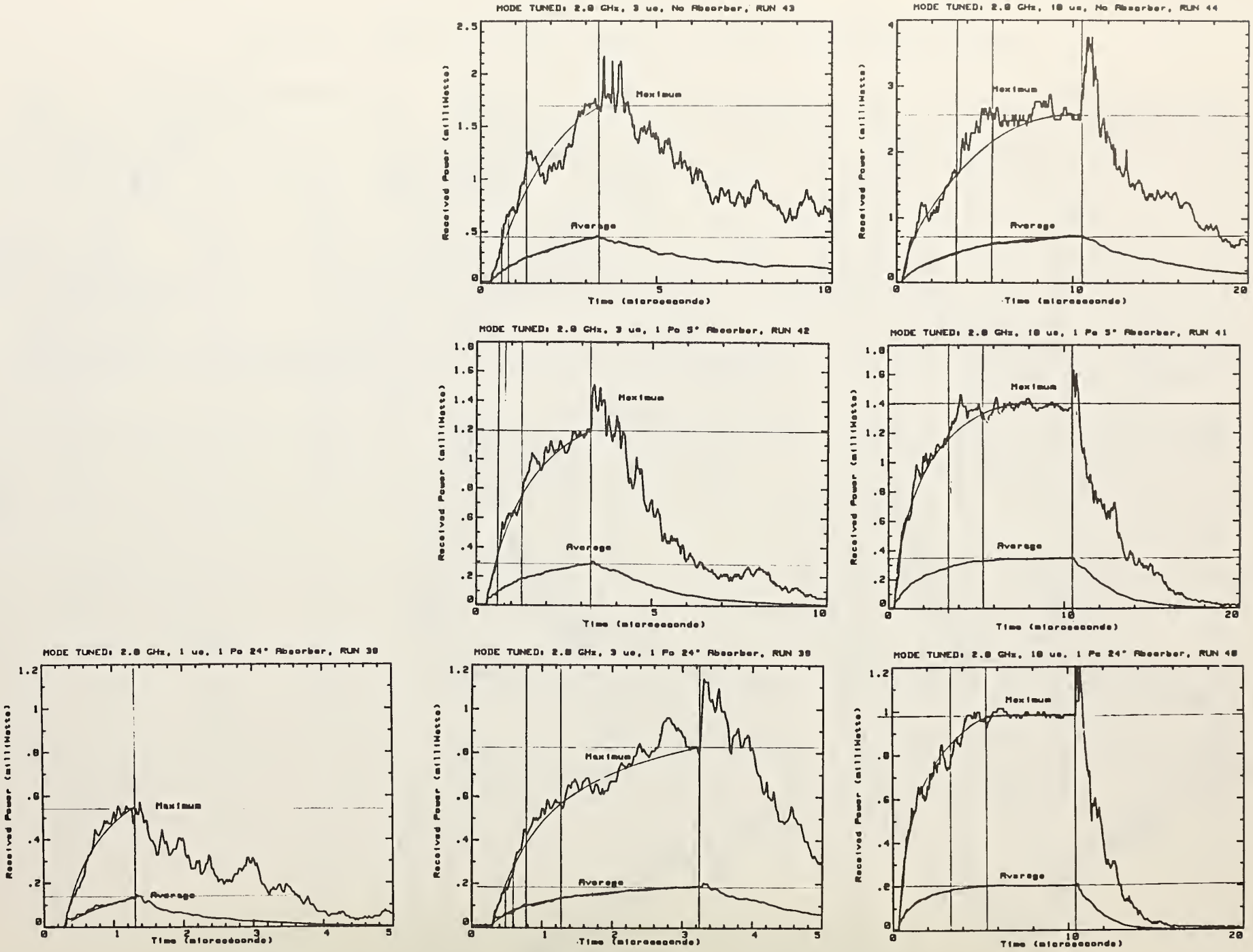

Figure 4.3. Sheet 4 of 10. Frequency = 2.0 GHz, input pulse amplitude is 0.1 W.

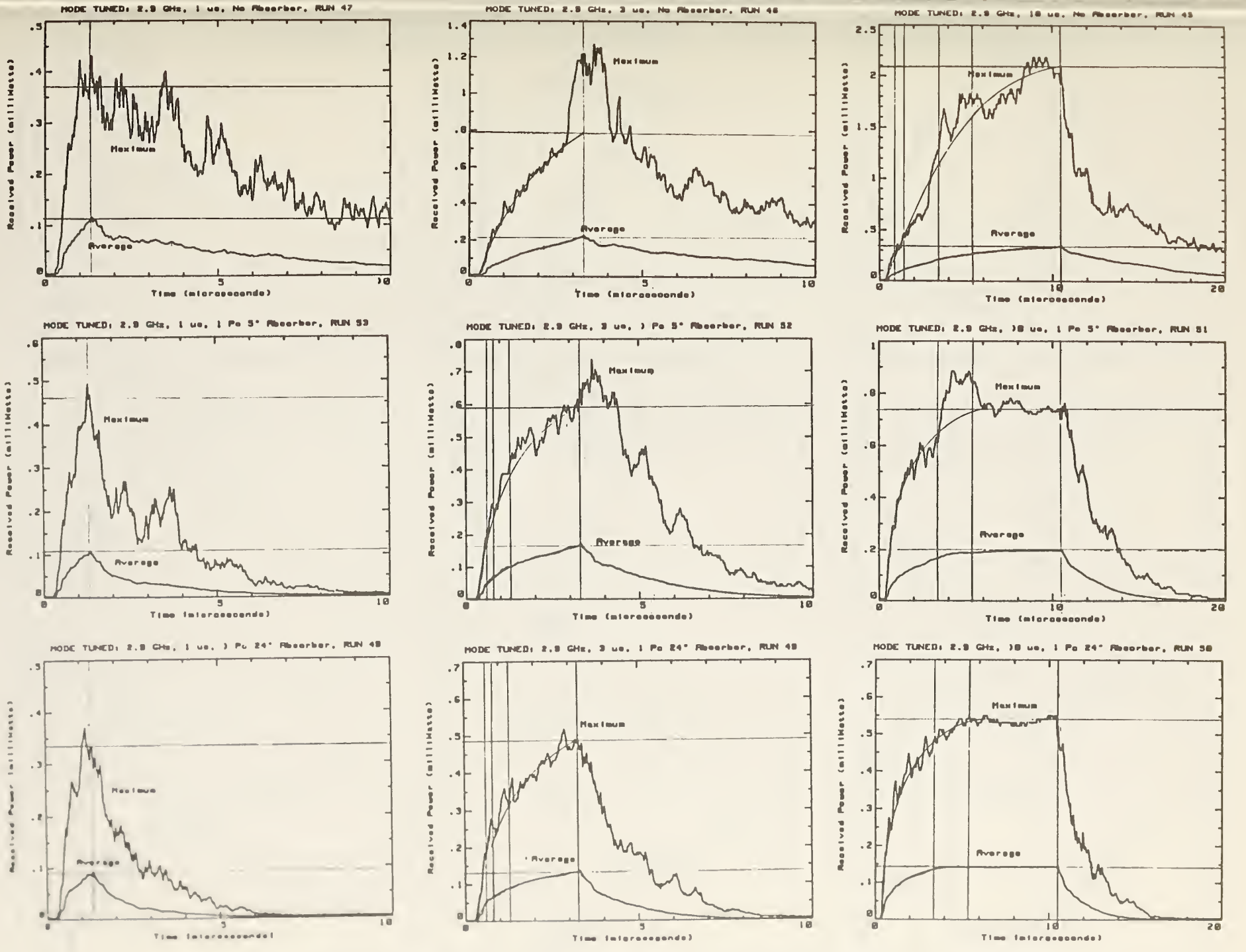

Figure 4.3. Sheet 5 of 10. Frequency = 2.9 GHz, input pulse amplitude is 0.1 W.

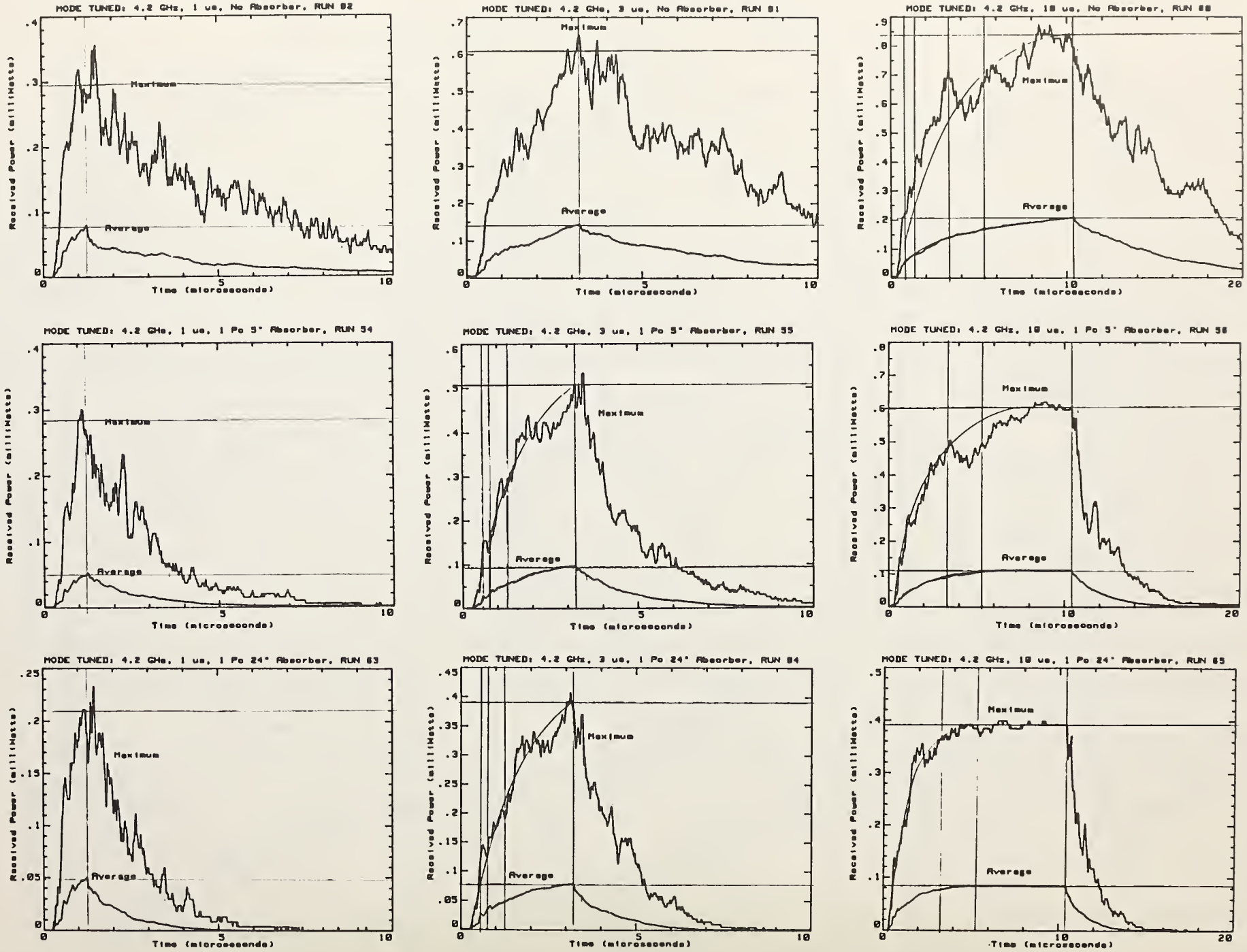

Figure 4.3. Sheet 6 of 10. Frequency = 4.2 GHz, input pulse amplitude is 0.1 W.

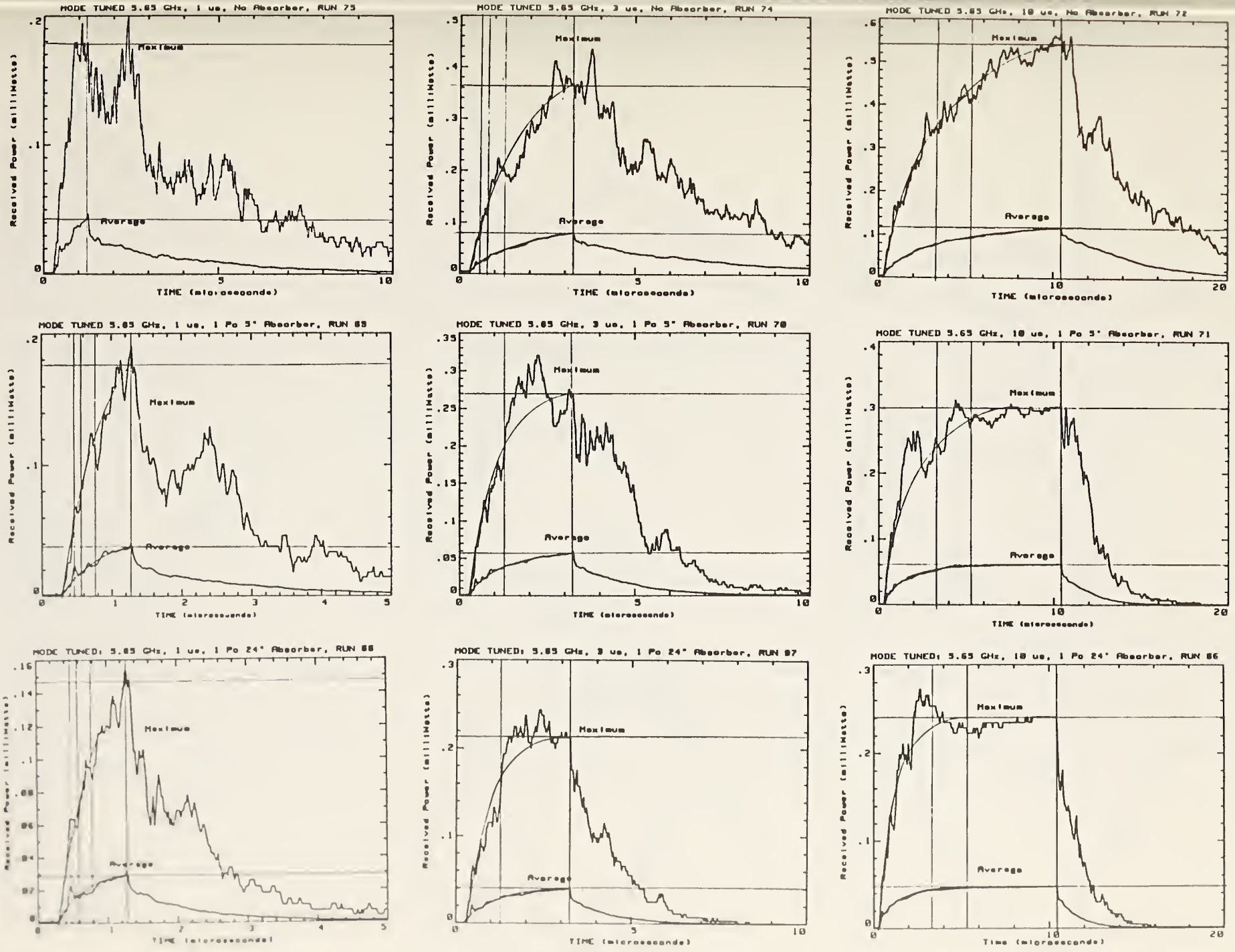

Figure 4.3. Sheet 7 of 10. Frequency = 5.65 GHz, input pulse amplitude is 0.1 W.

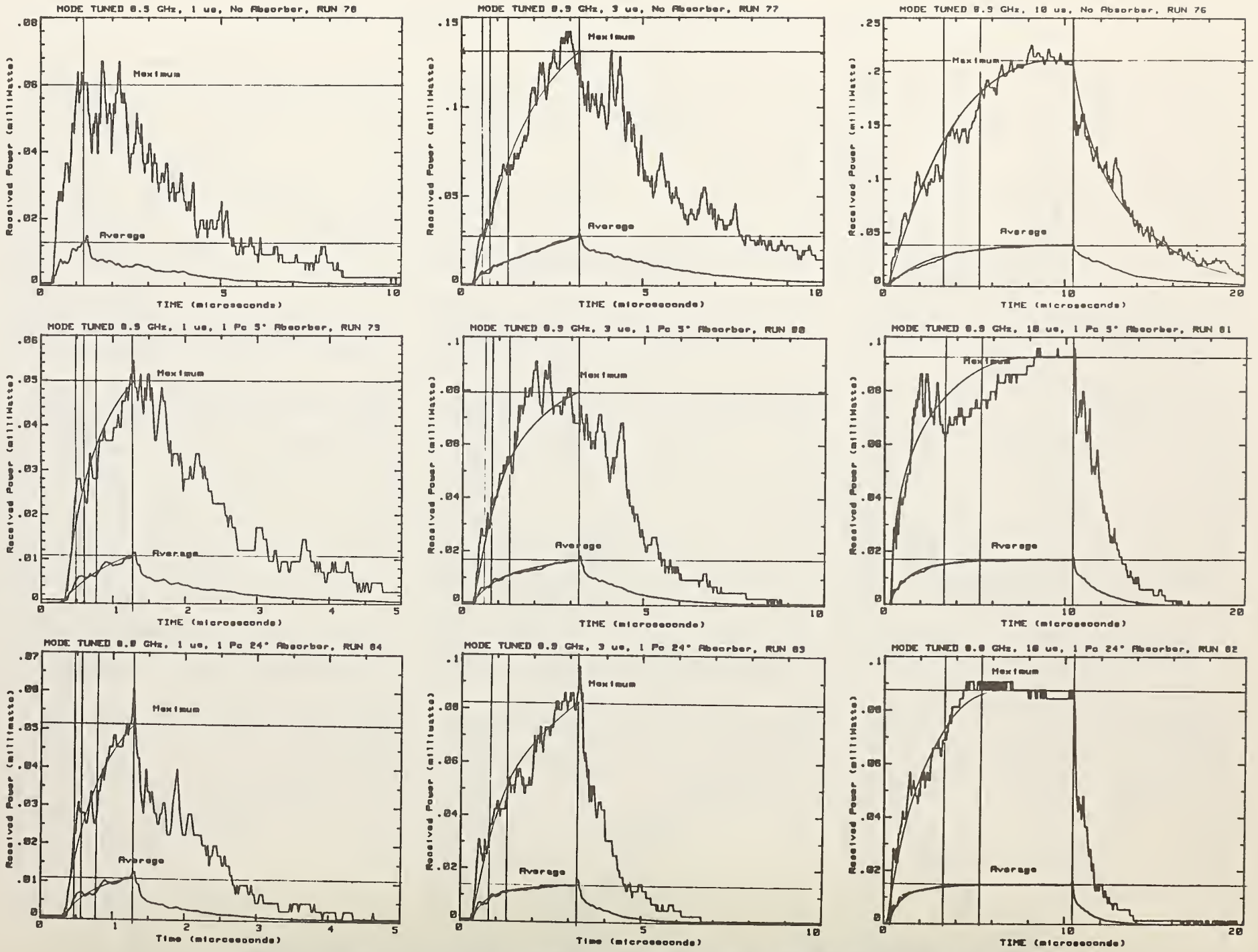

Figure 4.3. Sheet 8 of 10. Frequency = 8.9 GHz, input pulse amplitude is 0.1 W.

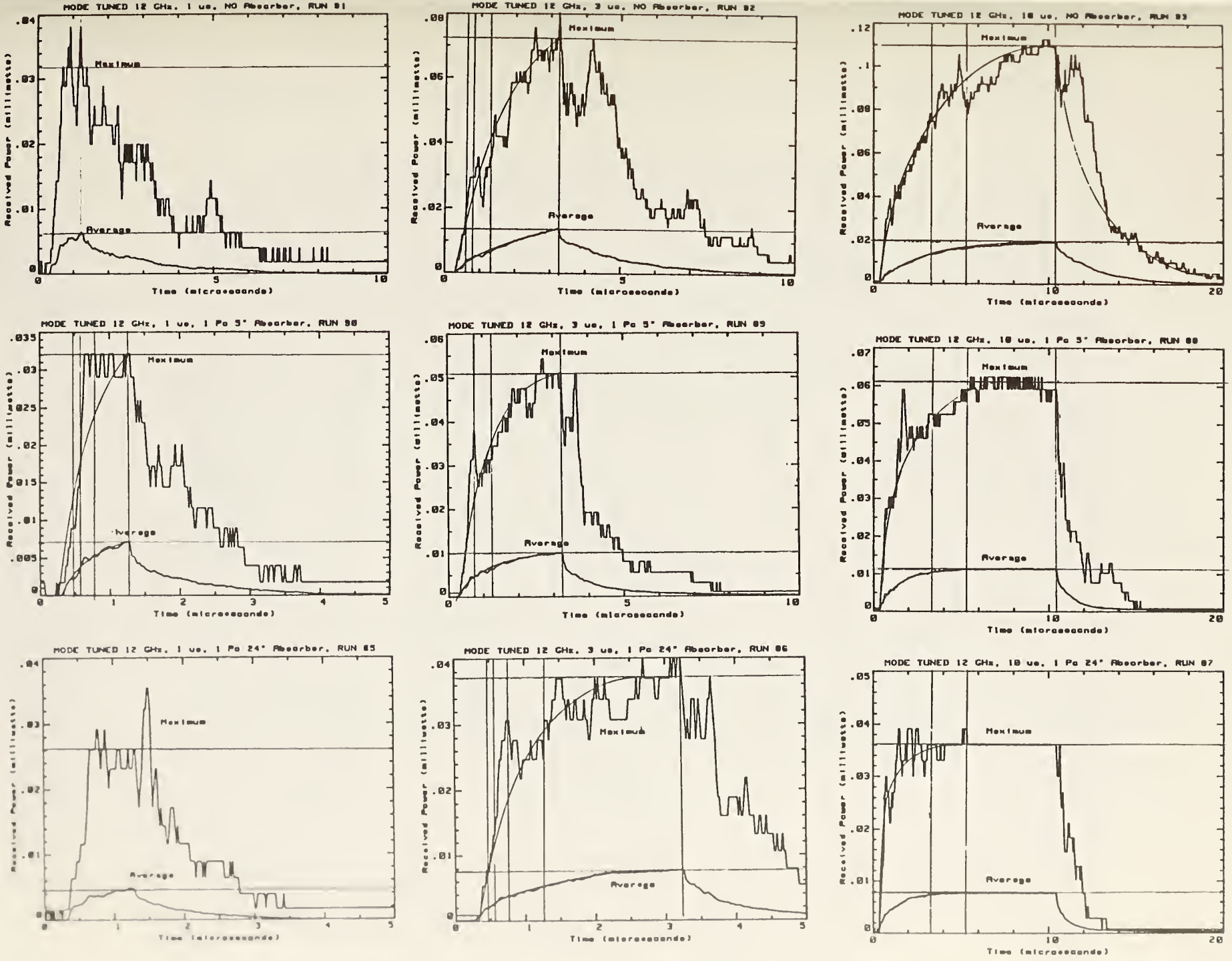

Figure 4.3. Sheet 9 of 10. Frequency = 12.0 GHz, input pulse amplitude is 0.1 W.

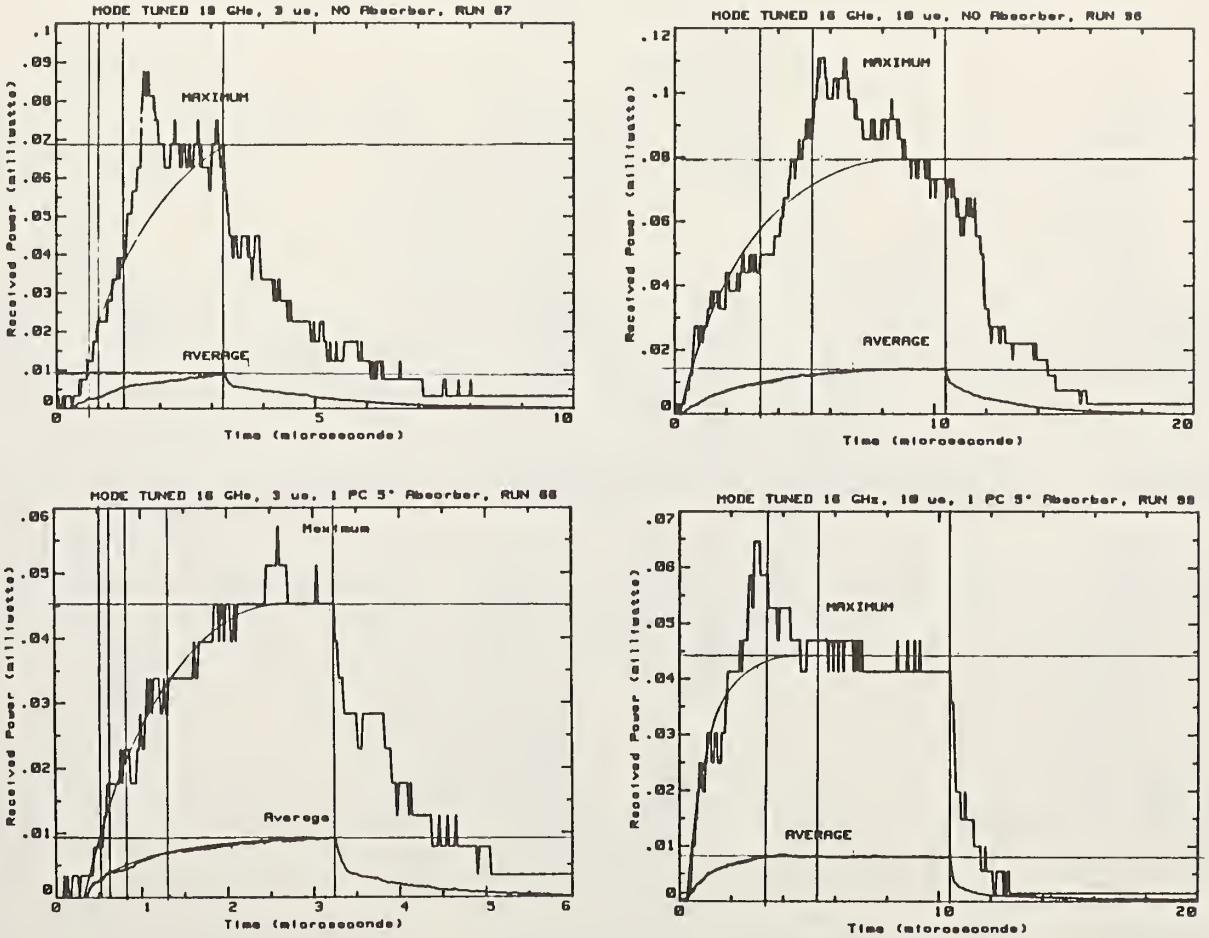

Figure 4.3. Sheet 10 of 10. Frequency = 16.0 GHz, input pulse amplitude is 0.1 W.

Figure 4.3. Statistical amplitude distribution (maximum and average) for rf pulse waveforms obtained inside RADC reverberating chamber at selected frequencies, input pulse widths and absorber loadings.

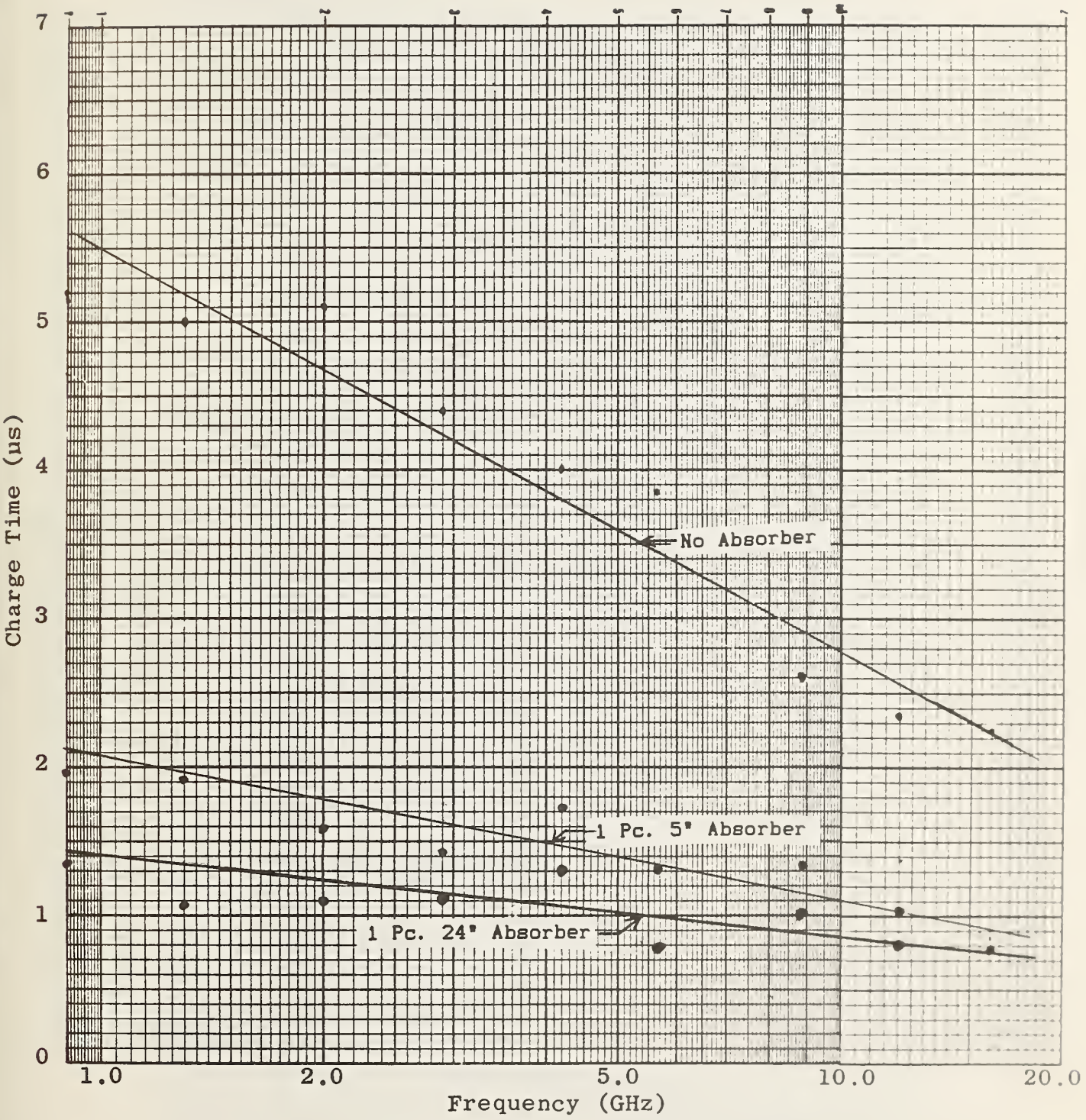

Figure 4.4. Time required for rf signal transmitted into RADC reverberating chamber to rise 63% of steady state amplitude as a function of frequency. Chamber empty (no absorber), with 1 piece of 5" x 24" x 24" rf absorber, and with 1 piece of 24 " x 24" x 24" rf absorber.

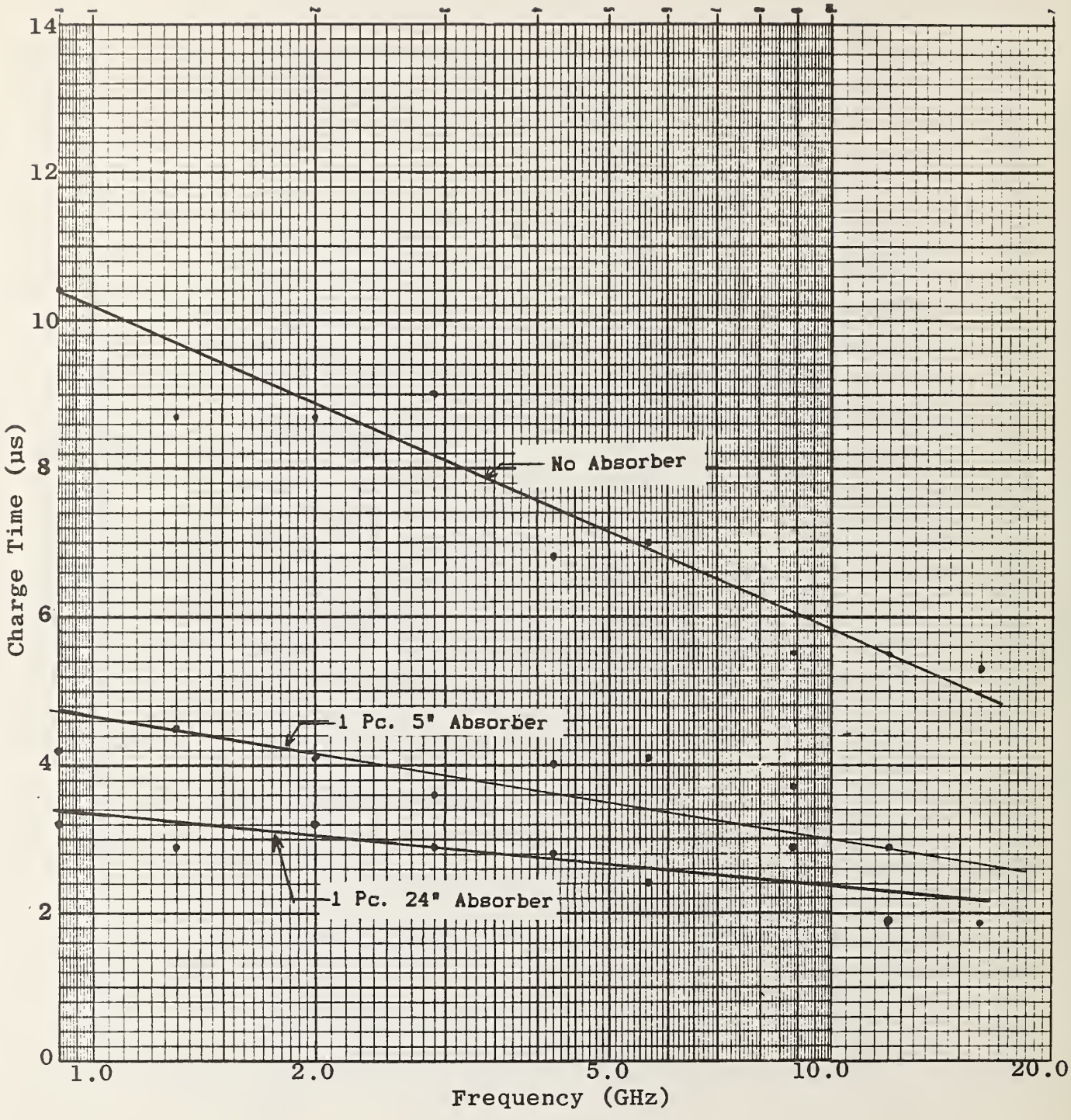

Figure 4.5. Time required for rf signal transmitted into RADC reverberating chamber to rise to 90% of steady state amplitude as a function of frequency. Chamber empty, with 1 piece of 5" x 24" x 24" rf absorber, and with 1 piece of 24" x 24" x 24" rf absorber.

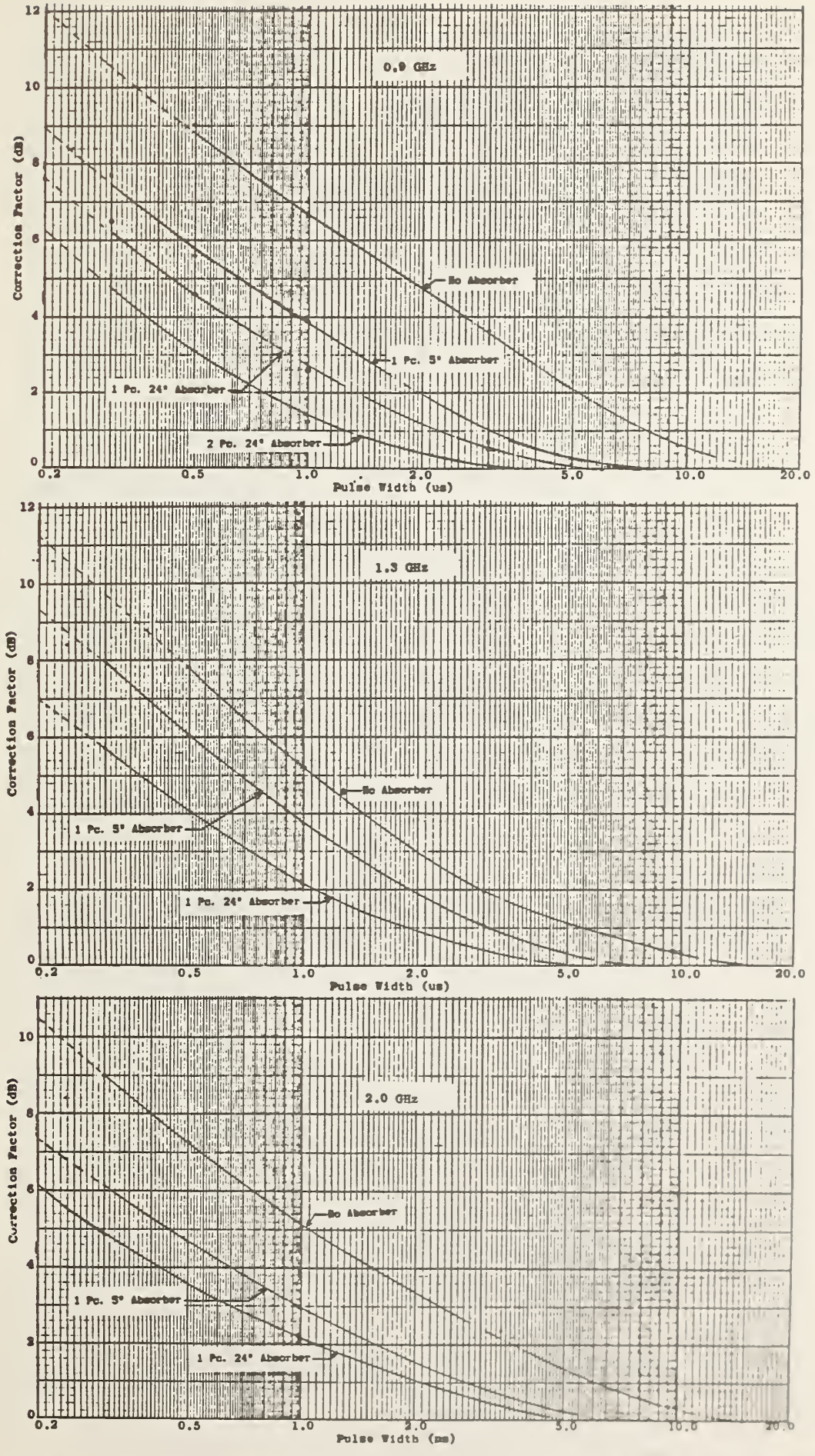

Figure 4.6. Sheet 1 of 3. Frequencies = 0.9, 1.3, and 2.0 GHz.

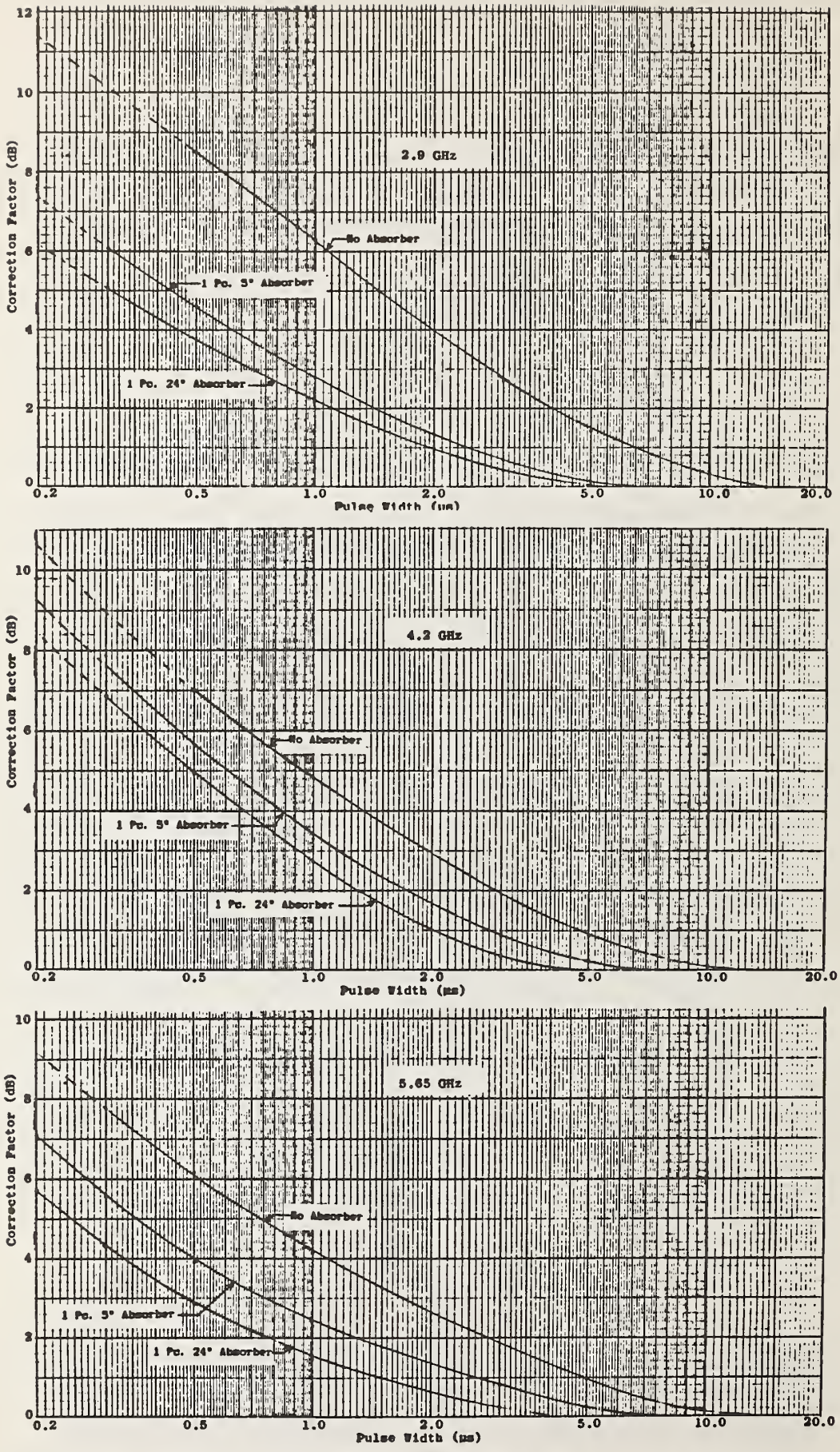

Figure 4.6. Sheet 2 of 3. Frequencies = 2.9, 4.2, and 5.65 GHz.

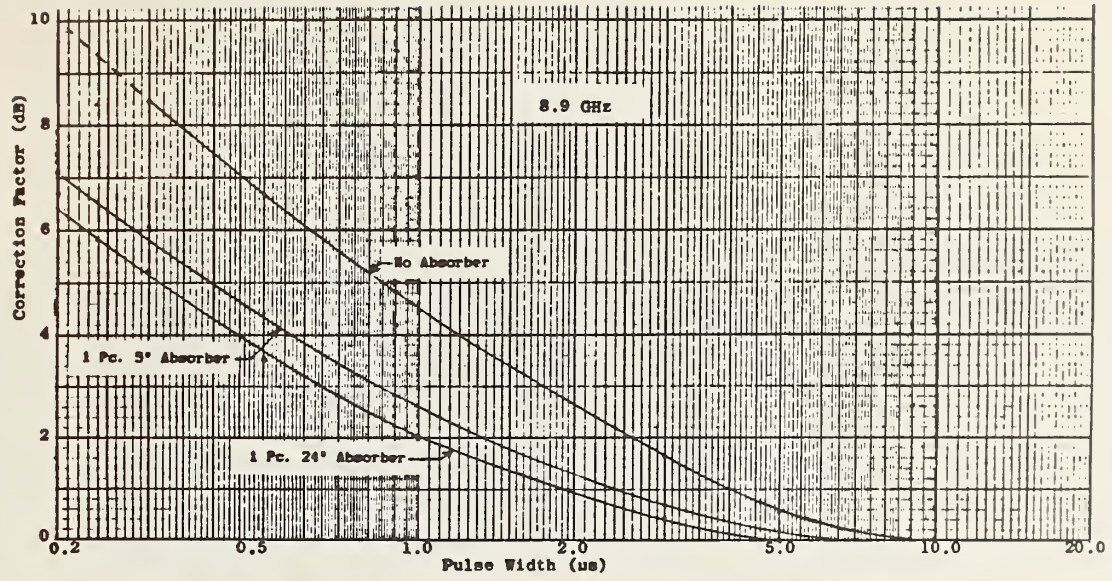

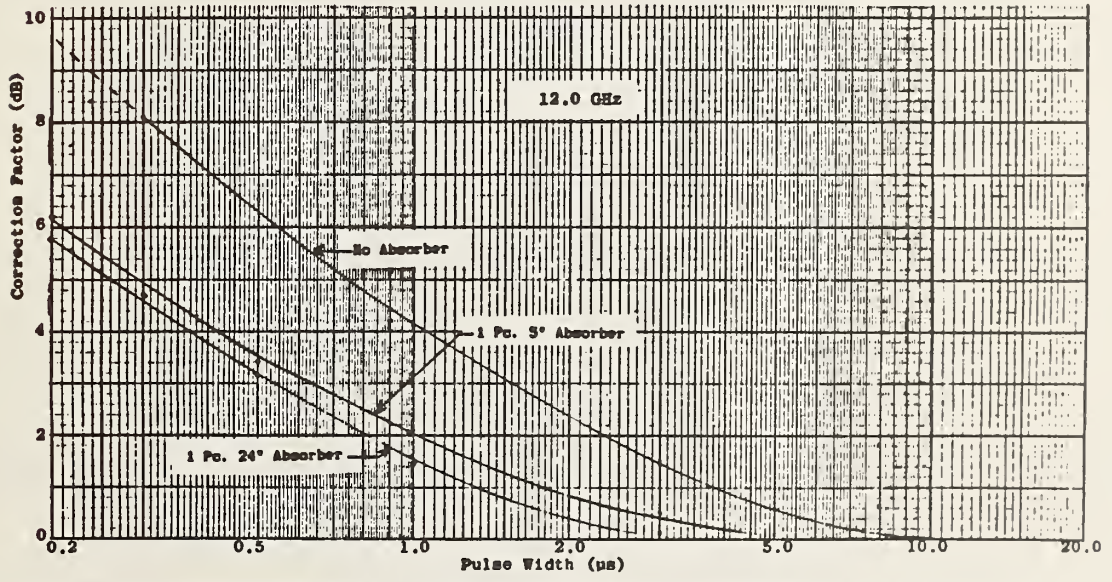

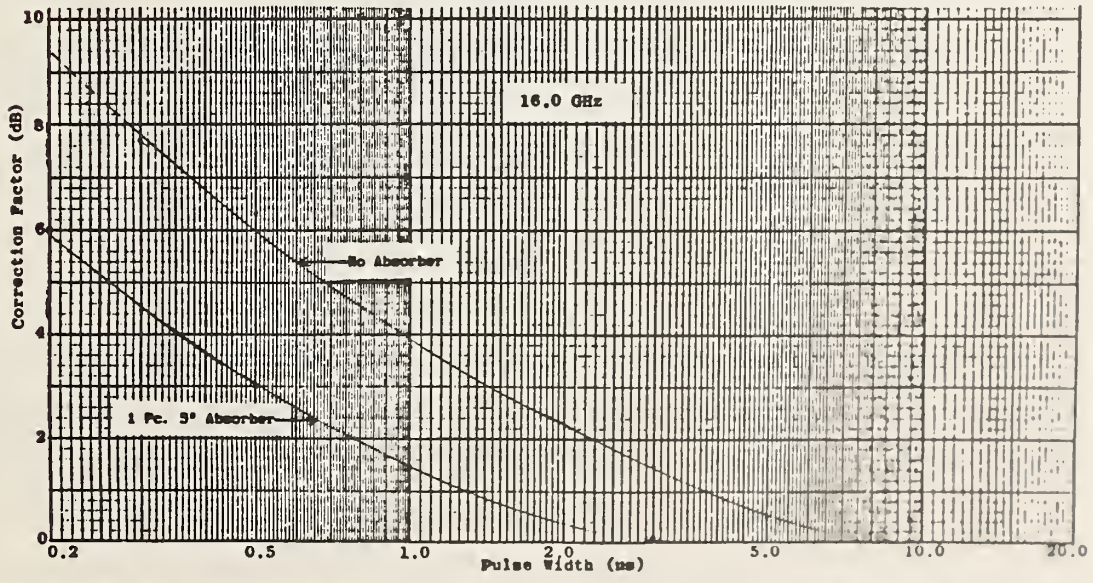

Figure 4.6. Sheet 3 of 3. Frequencies = 8.9, 12.0, and 16.0 GHz.

Figure 4.6. Estimated correction factor for amplitude response of test signal inside RADC reverberating chamber as a function of rf input pulse duration at selected frequencies.

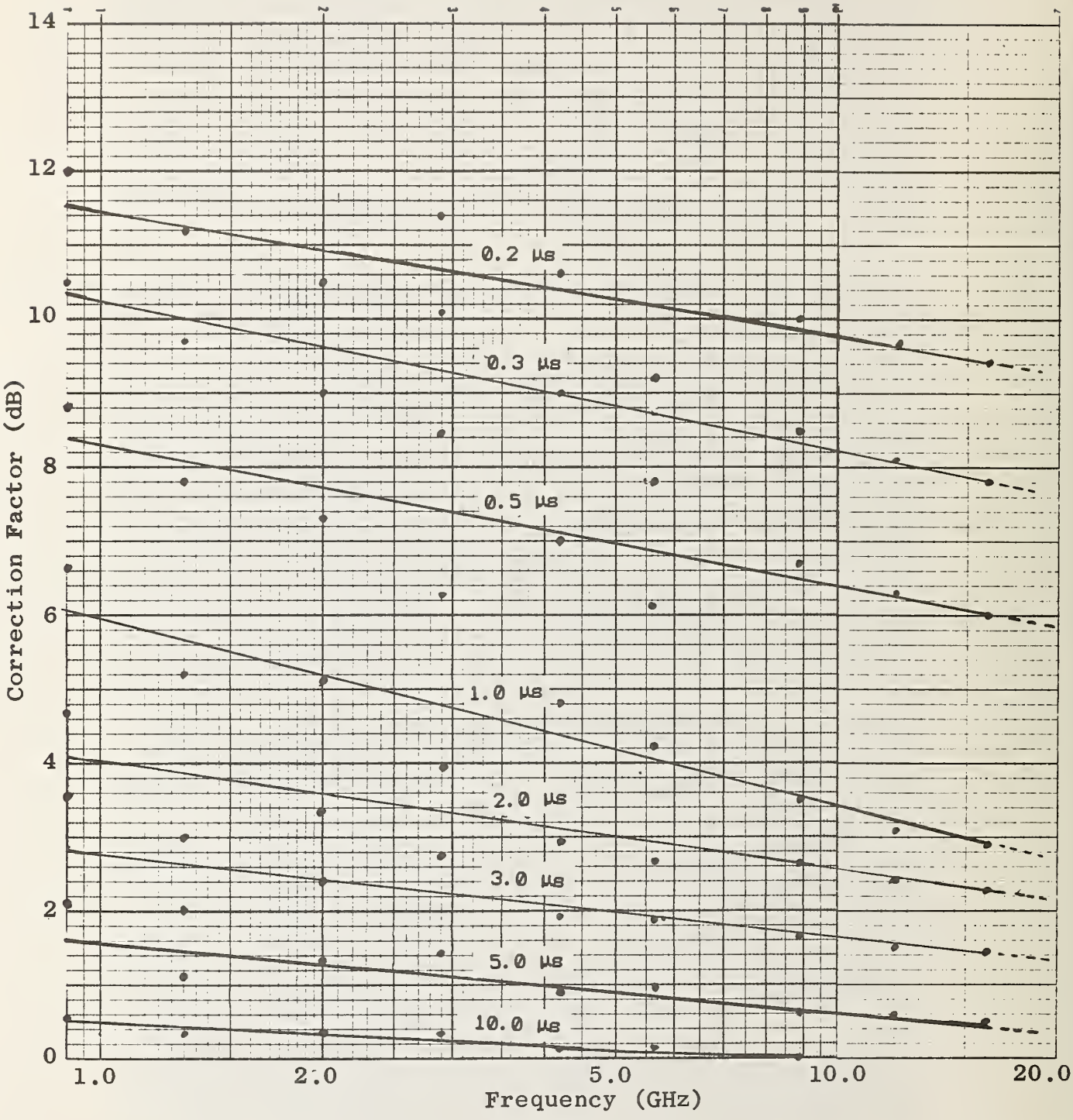

Figure 4.7. Sheet 1 of 3. RADC chamber empty (no absorber).

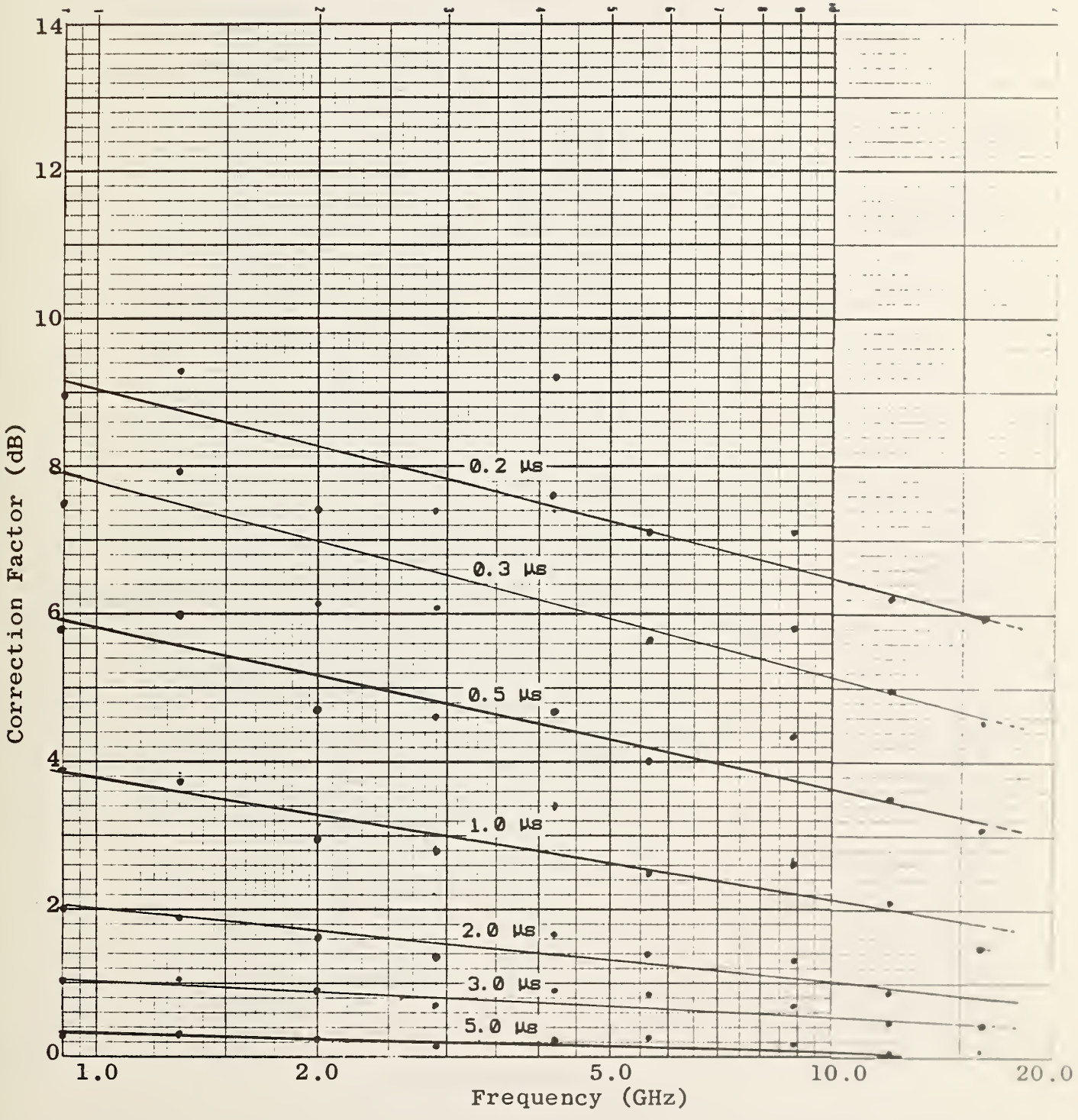

Figure 4.7. Sheet 2 of 3. RADC chamber loaded with 1 piece 5' x 24' x 24' rf absorber.

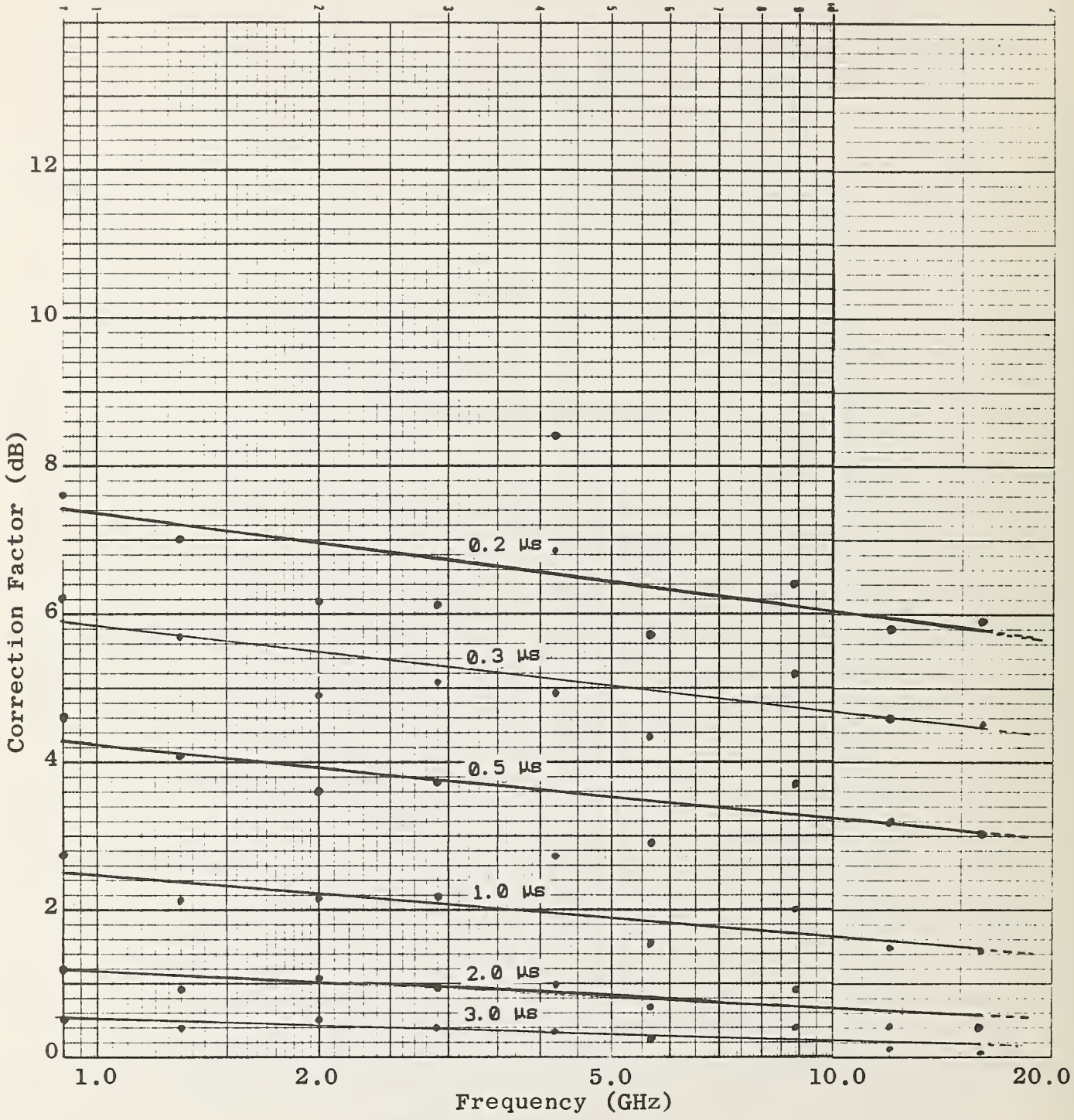

Figure 4.7. Sheet 3 of 3. RADC chamber loaded with 1 piece 24" x 24" x 24" rf absorber.

Figure 4.7. Estimated correction factor for amplitude response of test signal inside RADC reverberating chamber as a function of frequency at selected rf input pulse durations. (Data extracted from figure 4.6).

Table 3.1. Spatial variations in the E-field average and maximum values measured inside the RADC reverberating chamber.

Frequency (GHz)	Variation in E-field (dB)
100	< ± 9.0
150	< ± 6.0
200	< ± 5.0
300	< ± 3.5
500	< ± 3.0
1000	< ± 2.5
2000	< ± 2.0

Table 4.1. Influence of absorber loading on loss, quality factor and charge/decay time of RADC reverberating chamber at 0.9 GHz.

Absorber Loading	Chamber Loss (dB) Ave	Quality Factor $\tilde{Q}$	Charge/Decay *Time μs
none	14.5	28294	10.01
1/2 Pc. 3"	16.6	17445	6.17
1 Pc. 3"	18.5	11264	3.98
1 Pc. 5"	19.1	9811	3.47
1 Pc. 8"	19.8	8350	2.95
1 Pc. 11"	20.3	7442	2.63
1 Pc. 24"	20.5	7107	2.51
2 Pc. 24"	22.1	4917	1.74
4 Pc. 24"	23.5	3562	1.26

* Charge/decay time calculated from $2Q/\omega_0$ and is based upon (1-1/e)A or 63 % of amplitude of steady state field inside chamber after excitation source is turned on or has decayed 63 % from steady state amplitude after source is turned off.

Table 4.2. Comparison of measured and calculated chamber charge/decay times determined from chamber average loss measurements and from data of figure 4.3. Chamber empty, with 1 Pc. 5" x 24" x 24" rf absorber, and with 1 Pc. 24" x 24" x 24" rf absorber.

Frequency (GHz)	Chamber Loss (Ave) (dB)			Quality Factor X 10000			Calculated Charge/Decay time (μs)			Measured Charge/Decay time (μs)		
	Empty	5"	24"	Empty	5"	24"	Empty	5"	24"	Empty	5"	24"
0.9	14.5	19.1	20.5	2.83	0.98	0.71	10.0	3.47	2.51	5.62	2.12	1.43
1.3	18.0	22.1	24.0	3.81	1.48	0.96	9.33	3.63	2.34	5.19	1.97	1.35
2.0	22.0	26.2	27.8	5.52	2.10	1.45	8.79	3.34	2.31	4.69	1.79	1.24
2.9	26.0	30.2	31.8	6.70	2.55	1.76	7.36	2.80	1.93	4.23	1.63	1.15
4.2	29.8	34.1	35.4	8.49	3.15	2.34	6.43	2.39	1.77	3.80	1.48	1.07
5.65	33.0	36.9	38.0	9.89	4.03	3.13	5.57	2.27	1.76	3.46	1.34	1.00
8.9	37.5	41.8	42.9	13.7	5.10	3.96	4.90	1.82	1.41	2.90	1.16	0.89
12.0	40.8	43.1	44.8	15.7	9.26	6.26	4.17	2.46	1.66	2.57	1.03	0.82
16.0	43.9	46.1	46.7	18.3	11.0	9.58	3.63	2.19	1.91	2.24	0.90	0.76

Table 5.1. Summary and estimates of measurement uncertainties for determining cw field strength inside RADC reverberating chamber.
Mode Tuned (100 MHz - 2.0 GHz)

Source of Error	Error (dB) 100 MHz Ave.	Max.	150 MHz Ave.	Max.	200 MHz Ave.	Max.	500 MHz Ave.	Max.	1.0 GHz Ave.	Max.	2.0 GHz Ave.	Max.
1a. Received Power												
Cable Loss	± 0.05		± 0.05		± 0.05		± 0.05		± 0.05		± 0.10	
Attenuator Cal.	± 0.10		± 0.10		± 0.10		± 0.10		± 0.10		± 0.10	
Antenna Efficiency	± 0.05		± 0.05		± 0.05		± 0.05		± 0.05		± 0.10	
Pwr. Meter Cal.	± 0.20		± 0.20		± 0.20		± 0.20		± 0.20		± 0.20	
Sub Total	± 0.40		± 0.40		± 0.40		± 0.40		± 0.40		± 0.50	
Mismatch	-4.1	-8.2	-3.4	-8.2	-3.7	-7.4	-1.5	-4.1	-1.1	-2.8	-1.3	-2.4
1b. E-Field Meas. 1-cm dipole probe	---------- ± 1.0 ----------											
2. Sampling Efficiency Spatial Field Var.	± 9.0		± 6.0		± 5.0		± 3.5		± 2.5		± 2.0	
Limited Sample Size (see [5])	±0.2	±0.5	±0.2	±0.5	±0.2	±0.5	±0.2	±0.5	±0.2	±1.5	±0.3	±1.0
Sub Total	±9.2	±9.5	±6.2	±6.5	±5.2	±5.5	±3.7	±4.0	±2.7	±4.0	±2.3	±3.0
3. Wave Impedance (see [5])	-2.8	-2.8	-2.4	-2.4	-2.0	-2.0	-2.0	-2.0	-2.0	-2.0	-2.0	-2.0
	+2.0	+6.0	+2.0	+6.0	+2.0	+6.0	+2.0	+4.5	+2.0	+3.0	+2.0	+3.0
E-Field Determined By Receiving Ant.												
Total Worst Case Error	-16.5	-20.9	-12.4	18	-11	-15.3	-7.6	-10	-6.2	-9.2	-5.1	-7.9
	+10.6	+14.9	+9.2	+13.9	+8.6	+12.9	+5.6	+8.4	+5.1	+7.4	+4.3	+6.0
RSS Error	-10.5	-12.9	-7.5	-10.7	-6.7	-9.4	-4.5	-6.1	-3.6	-5.3	-3.4	-4.4
	+8.5	+10.4	+7.5	+9.6	+6.5	+8.9	+3.8	+5.3	+3.4	+5.0	+2.7	+3.9
E-Field Determined By Dipole Probe												
Total Worst Case Error	-13.0	-13.3	-9.6	-9.9	-8.2	-8.5	-6.7	-7.0	-5.7	-7.0	-5.3	-6.0
	+12.2	+16.5	+9.2	+13.5	+8.2	+12.5	+6.7	+9.5	+5.7	+8.0	+5.3	+7.0
RSS Error	-9.7	-10	-6.7	-7.0	-5.7	-5.9	-4.3	-4.6	-3.5	-4.6	-3.2	-3.7
	+9.5	+11.3	+6.6	+8.9	+5.7	+8.2	+4.3	+6.1	+3.5	+5.1	+3.2	+4.4

Table 5.2. Summary and estimates of measurement uncertainties for determining cw field strength inside RADC reverberating chamber. Mode Stirred (1.0 GHz - 18.0 GHz).

Source of Error	Error (dB) 1.0 GHz Ave.	Max.	2.0 GHz Ave.	Max.	4.0 GHz Ave.	Max.	8.0 GHz Ave.	Max.	12.0 GHz Ave.	Max.	18.0 GHz Ave.	Max.
1a. Received Power												
Cable Loss	± 0.05		± 0.10		± 0.10		± 0.15		± 0.15		± 0.20	
Atten. Calibration	± 0.10		± 0.10		± 0.15		± 0.15		± 0.20		± 0.20	
Antenna Efficiency	± 0.05		± 0.10		± 0.15		± 0.15		± 0.20		± 0.20	
Spec. Analyzer Cal.	± 1.00		± 1.00		± 1.50		± 1.50		± 1.50		± 1.50	
Sub Total	± 1.20		± 1.30		± 1.90		± 1.95		± 2.05		± 2.10	
Mismatch	-1.3	-3.1	-1.3	-2.4	-0.8	-1.3	-0.4	-0.8	-0.5		-2.3	
1b. E-Field Meas.												
1-cm Dipole Probe	± 1.0		± 1.0		± 1.5		± 1.5		± 2.0		± 2.0	
2. Sampling Efficiency												
Spatial Field Var.	± 2.5		± 1.5		± 1.0		± 0.5		± 0.5		± 0.5	
Limited Sample Size (see [5])	±0.1	±0.2	±0.1	±0.3	±0.2	±0.5	±0.3	±0.7	±0.3	±1.0	±0.3	±1.5
Sub Total	±2.6	±2.7	±1.6	±1.8	±1.2	±1.5	±0.8	±1.5	±0.8	±1.5	±0.8	±2.2
3. Wave Imped ≠ 120π (see [5])	Average < ±2.0, -2.0 < Maximum < +3.0											
4. Input Power Var.	-1.3	-2.4	-1.2	-1.7	-0.8	-1.3	-1.6		-0.5		-1.0	
E-Field Determined By Receiving Ant.												
Total Worst Case Error	-8.4	-11.4	-7.4	-9.2	-6.7	-8.0	-6.8	-7.9	-5.9	-6.6	-8.2	-9.6
	+5.8	+6.9	+4.9	+6.1	+5.1	+6.4	+4.8	+6.5	+4.9	+6.6	+6.9	+7.3
RSS Error	-4.0	-5.3	-3.4	-4.2	-3.2	-3.6	-3.3	-3.6	-3.1	-3.3	-3.9	-4.4
	+3.5	+4.2	+2.9	+3.7	+2.9	+3.9	+2.9	+3.9	+3.0	+3.9	+3.0	+4.3
E-Field Determined By Dipole Probe												
Total Worst Case Error	-6.9	-8.9	-5.8	-6.5	-5.5	-6.3	-5.9	-6.6	-5.3	-6.0	-5.8	-7.2
	+5.6	+6.7	+4.6	+5.8	+4.7	+6.0	+4.3	+6.0	+4.8	+6.5	+4.8	+7.2
RSS Error	-3.7	-4.3	-3.0	-3.3	-2.9	-3.2	-3.1	-3.3	-3.0	-3.2	-3.1	-3.7
	+3.4	+4.2	+2.8	+3.6	+2.8	+3.7	+2.6	+3.7	+2.9	+3.9	+2.9	+4.2

Table 5.3. Estimates of upper limit of impedance mismatch uncertainties for reference antenna's received power measurements for RADC reverberating chamber.

Frequency GHz	VSWR Source Ave	VSWR Source Max	VSWR Load Max	Mismatch Error (dB) Ave	Mismatch Error (dB) Max
0.1	7.5	22.0	1.10	-4.14	-8.17
0.15	6.0	22.0	1.10	-3.40	-8.17
0.2	6.5	18.0	1.10	-3.66	-7.37
0.3	5.0	15.0	1.10	-2.83	-6.67
0.5	3.0	7.5	1.10	-1.46	-4.14
1.0	2.5	5.0	1.10	-1.07	-2.83
1.0	2.5	5.0	1.20	-1.25	-3.10
2.0	2.5	4.0	1.20	-1.25	-2.44
4.0	2.0	2.5	1.20	-0.81	-1.25
8.0	1.5	2.0	1.20	-0.37	-0.81
12.0	1.5	1.5	1.30	-0.48	-0.48
18.0	3.0	3.0	1.50	-2.25	-2.25

NBS-114A (REV. 2-8C)

U.S. DEPT. OF COMM. BIBLIOGRAPHIC DATA SHEET (See instructions)	1. PUBLICATION OR REPORT NO. NBSIR 87-3080	2. Performing Organ. Report No.	3. Publication Date December 1987

4. TITLE AND SUBTITLE

EMR Test Facilities Evaluation of Reverberating Chamber Located at RADC, Griffiss AFB, Rome, New York

5. AUTHOR(S) Myron L. Crawford, Galen H. Koepke, and John M. Ladbury

6. PERFORMING ORGANIZATION (If joint or other than NBS, see instructions)

NATIONAL BUREAU OF STANDARDS
DEPARTMENT OF COMMERCE
WASHINGTON, D.C. 20234

7. Contract/Grant No.

8. Type of Report & Period Covered

9. SPONSORING ORGANIZATION NAME AND COMPLETE ADDRESS (Street, City, State, ZIP)

10. SUPPLEMENTARY NOTES

☐ Document describes a computer program; SF-185, FIPS Software Summary, is attached.

11. ABSTRACT (A 200-word or less factual summary of most significant information. If document includes a significant bibliography or literature survey, mention it here)

This report describes measurement procedures and results obtained from evaluating the reverberating chamber facility located at the Rome Air Development Center (RADC), Griffiss Air Force Base, Rome, New York. The facility was developed by the RADC for use in measuring and analyzing the electromagnetic susceptibility/vulnerability (EMS/V) of weapon systems and the shielding effectiveness of enclosures and shielding materials. A brief description of the facility, including the instrumentation used for performing its evaluation and calibration by the National Bureau of Standards (NBS), is given. Measurements described include: (1) evaluation of the chamber's transmitting and receiving antennas' voltage standing wave ratios; (2) measurement of the chamber's insertion loss or coupling efficiency versus frequency; (3) measurement of the chamber's tuner effectiveness; (4) determination of the E-field uniformity in the chamber's test zones versus frequency; (5) determination of the absolute amplitude calibration of the test E-fields in the chamber based upon the reference antenna's received power measurements and calibrated dipole probe antenna measurements; (6) comparison of reference standard equipment under test (EUT) responses to test fields established inside the RADC reverberating chamber and the NBS anechoic chamber; and (7) evaluation of the performance characteristics of the reverberating chamber excited by pulsed rf at selected discrete frequencies as a function of pulse width (0.2 - 20 μs) and the chamber's quality factor (Q). Conclusions indicate that the chamber can be used at frequencies down to approximately 150 MHz for cw testing, and for rf pulsed immunity testing with pulse widths as short as 0.3 μs by using rf absorber loading. Immunity testing to pulsed rf fields however has some inherent limitations that are discussed in the report. Estimates of the cw measurement uncertainties derived empirically from the test results are given.

12. KEY WORDS (Six to twelve entries; alphabetical order; capitalize only proper names; and separate key words by semicolons)

Key words: electromagnetic radiated susceptibility/vulnerability measurements; reverberating chamber.

13. AVAILABILITY

☒ Unlimited

☐ For Official Distribution. Do Not Release to NTIS

☐ Order From Superintendent of Documents, U.S. Government Printing Office, Washington, D.C. 20402.

☒ Order From National Technical Information Service (NTIS), Springfield, VA. 22161

14. NO. OF PRINTED PAGES 80

15. Price

USCOMM-DC 6043-P80

☆ U.S. GOVERNMENT PRINTING OFFICE: 1988—574-318 85,062 REGION NO 8